Determining the mechanism of microtubule poisons in breast cancer and methods to increase their efficacy

By

Christina M. Scribano

A dissertation submitted in partial fulfilment of the requirements for the degree of

Doctor of Philosophy

(Molecular and Cellular Pharmacology)

at the

UNIVERSITY OF WISCONSIN-MADISON

2021

Date of final oral examination: 09/03/2021

The dissertation is approved by the following members of the Final Oral Committee:

Beth A. Weaver, Associate Professor, Cell and Regenerative Biology

William Bement, Professor, Integrative Biology

Tim Bugni, Professor, School of Pharmacy

Ahna Skop, Professor, Genetics

ACKNOWLEDGEMENTS

First and foremost, I would like to thank my mentor, Beth Weaver. Thank you for allowing me to join your lab and for training me to be become the scientist I am today. Your curiosity is infectious, and you got me excited about my project on day one. I have always admired your fearlessness in asking tough questions and your persistence to see a problem through. Thank you for readily lending your expertise in some contexts and your willingness to learn together in others. I learned so much during my time here and am I so grateful that I had the opportunity to work in your lab.

Thank you to Mark Burkard, Bill Bement, Tim Bugni, and Ahna Skop for serving on my thesis committee. My committee meetings were always comprised of thoughtful questions and fruitful discussions. Your support and guidance along the way was much appreciated. Thank you to the Molecular and Cellular Pharmacology and Cancer Biology programs for their support during my graduate career. I would also like to thank our program coordinator, Kristin Cooper, for helping me navigate the program requirements and graduate school in general.

I would like to thank my friends and colleagues in the Weaver lab, my graduate school experience would not have been the same without them. Thank you to former lab members Eric Britigan, Lauren Zasadil, Jun Wan, Amber Lasek, and Laura Funk for welcoming me into the lab and showing me the ropes when I was just starting out. Thanks for fostering a productive and collaborative work environment and for all the fun we had outside of lab. Thank you to my current lab mates Pippa Cosper, John Tucker, Amber Zhou, Sarah Copeland, Daniel Sam, and Sarah Bonema. Thanks for valuable

scientific discussions and everyday chatter about life. It has been a pleasure to collaborate and work alongside of you all.

Thank you to my previous undergraduate research mentors, Scott Gehler and Sean Georgi. I am not sure if I would have gone into scientific research if it were not for these valuable experiences in undergrad. I would also like to thank my previous teachers and mentors who pushed me inside and outside of the classroom. Thanks to my good friends from college Samantha Krysa, Emily Haskins, Lauren Cornwell, and Chandler Todd for their support and friendship, and for providing an outlet for the stress.

I also need to extend a heartfelt thanks to Mark, and our tripawd Zeke, for their untiring emotional support. Coming home to both of you is my favorite part of the day. Mark, while the grad school experience and road to a PhD is foreign to most, I am thankful to have shared in this experience with you. Thanks for commiserating with me over failed experiments, inconsistent data, and late-night thesis writing sessions. I'm also grateful for all your love, hugs, and smoothies along the way. Thanks for enjoying in life outside of grad school with me too. I'm looking forward to many more hikes, camping trips, volleyball beer leagues, nights out at Genna's, and trips to the dog park with you and little Z. Zeke, thanks for making me the happiest and proudest dog mom. Thank you for demanding that I take breaks from working while I am at home, and thanks for always greeting me with a wagging tail at the end of a long day.

Finally, I would like to thank my family for their unwavering support and encouragement over the years. Thanks to my Dad, Gino, for passing on your inquisitive nature and methodical thinking. To my mom, Michelle, for imparting your patience and grit. Thank you for always believing in me and for getting me through the early days of

tears when it was time to go to school. Thank you both for all the sacrifices you have made for my sisters and I. Our accomplishments are yours as well, we wouldn't be where we are today without you. To my sisters, Jennifer, Brianna, Francesca, and Angelina, I am incredibly lucky to be surrounded by such intelligent, caring, and independent women. I hope we continue to push each other, and I can't wait to see all the great things you will all go on to do. Thanks for all the laughs, and for making home a great place to escape to when life and grad school got to be a little too much. I dedicate this thesis to my parents, my sisters, and my good boy, Zeke.

ABBREVIATIONS

AC- a combination of Adriamycin and cyclophosphamide

ARF- alternate reading frame

APC/C- anaphase promoting complex/cyclosome

CENP-E- centromere associated protein E

Cdc20- cell-division cycle protein 20

Cdk1- cyclin dependent kinase 1

CIN- chromosomal instability

DMSO- dimethyl sulfoxide

DNA- deoxyribonucleic acid

ER- estrogen receptor

FDA- Food and Drug Administration

HER2- Human epidermal growth factor receptor 2

HPLC- High performance liquid chromatography

LC-MS/MS- Liquid chromatography tandem mass spectrometry

Mad1- mitotic arrest deficient 1

Mad2- mitotic arrest deficient 2

MCC- mitotic checkpoint complex

MEF- mouse embryonic fibroblast

Mps1/TTK- monopolar spindle 1

MTOC- microtubule organizing center

NCI- National Cancer Institute

NEB- nuclear envelope breakdown

NuMA- nuclear mitotic apparatus protein

PBD- Polo box domain

PCM- pericentriolar material/matrix

Plk1- Polo-like kinase 1

Plk4- Polo-like kinase 4

USDA- U.S. Department of Agriculture

ABSTRACT

Microtubule poison chemotherapy remains a cornerstone of breast cancer treatment despite the development of targeted therapies and immune checkpoint inhibitors. However, their mechanism of cytotoxicity is poorly understood. It is widely assumed that these drugs cause cell death due to mitotic arrest, as is observed at typically used concentrations in cell culture. We recently showed that both standard-of-care doses of the microtubule stabilizing drug paclitaxel are insufficient to cause mitotic arrest in primary breast cancer. Instead, low nanomolar, clinically relevant concentrations induce multipolar mitotic spindle formation in all patients examined. Thus, we hypothesize that paclitaxel induces cell death as a result of chromosome missegregation on multipolar spindles. We identified a mechanism of paclitaxel resistance, as multipolar spindles focused into bipolar spindles with varying efficiency. Maintaining multipolarity during mitotic transit was necessary to elicit the high rates of chromosomal instability (CIN) necessary to cause paclitaxel-induced cell death. Furthermore, we found that pre-treatment CIN sensitized breast cancer cells and metastatic patients to taxane treatment, suggesting that baseline levels of CIN can be used as a predictive biomarker of response.

Moreover, we found that low nanomolar doses of other clinically used microtubule poisons, like paclitaxel, caused multipolar spindle formation without evidence of mitotic arrest in breast cancer cells. Results from a small clinical trial demonstrated that microtubule poison therapy leads to multipolar spindle formation and not mitotic arrest in metastatic breast cancer patient tumors. These results suggest that

the mechanisms of sensitization and resistance described for paclitaxel may be more broadly applicable to other clinically used microtubule poisons.

Given that multipolar spindle formation supports a uniform mechanism of cytotoxicity, it is now important to understand the cellular processes of multipolar spindle establishment and maintenance. We demonstrate that multipolar spindle formation required Eg5 and Plk1, but not Mps1, CENP-E, gamma-tubulin, pericentrin, or centrin. Surprisingly, multipolar spindle formation exhibited time dependency; reducing mitotic duration reduced multipolar spindles, whereas prolonging mitosis increased multipolarity. Identification of the cellular and temporal requirements for multipolarity induced by paclitaxel, and of agents that increase multipolar spindle maintenance and CIN, may improve the clinical utility of paclitaxel and other microtubule poisons.

TABLE OF CONTENTS

CHAPTER 1: INTRODUCTION

1.1 Mitosis and the mitotic checkpoint

Mitosis is the process by which duplicated chromosomes are divided equally between two daughter cells (McIntosh, 2016). Mitosis begins with prophase, the stage in which chromosomes containing genetic material in the form of DNA begin to condense. During prophase, centrosomes, the main microtubule organizing centers of vertebrate cells, begin to separate and migrate towards opposite ends of the cell. Between prophase and prometaphase, the nuclear envelope breaks down (NEB) in most higher animal and plant cells, allowing the nucleoplasm and cytoplasm to mix (Bakker et al., 2016). Following NEB, centrosomes continue to nucleate microtubules that form the mitotic spindle, and fully condensed chromosomes begin to establish attachments to the spindle via the kinetochore. Metaphase is achieved when all chromosomes are aligned at the spindle equator (also known as the metaphase plate) (McIntosh, 2016). Once all chromosomes have made stable attachments to microtubules, the mitotic checkpoint is satisfied, and the cell can begin its transition into anaphase. During anaphase, the sister chromatid pairs begin to separate, and the spindle subsequently elongates to further aid in chromosome segregation to opposite sides of the cell (McIntosh, 2016). The final stage of mitosis, telophase, is characterized by the de-condensation of DNA, nuclear envelope reformation, and compression of the spindle midzone. Cytokinesis follows mitosis and serves to physically separates the two daughter cells, thereby completing cell division (McIntosh, 2016).

Each daughter cell from this resulting division should receive two copies (a maternal and a paternal copy) of each chromosome. If all chromosomes are segregated properly, both daughter cells should be genetically identical to their parental cell (McIntosh, 2016). The accurate segregation of chromosomes during mitosis is ensured by the mitotic checkpoint. As stated above, the mitotic checkpoint delays the metaphase to anaphase transition. Mitotic checkpoint signaling (reviewed in (Ji et al., 2017)) involves numerous proteins and kinases that generate a signal to delay anaphase onset until all chromosomes have made stable attachments to the spindle microtubules via the kinetochore. The Ndc80 complex, a component of the outer kinetochore and KMN complex (comprised of Knl1, Mis12, and NDC80 complexes), serves as the linker between chromosomes and the spindle microtubules. The kinase Mps1 recognizes unattached kinetochores by directly binding to Ndc80 complexes that are not bound to spindle microtubules (Ji *et al.*, 2017). At kinetochores, Mps1 phosphorylates MELT motifs on Knl1 to recruit the Bub1-Bub3 complex. After a priming phosphorylation on Bub1 S459 by Cdk1, Mps1 phosphorylates Bub1 at T461. The dually phosphorylated Bub1 subsequently binds and recruits the Mad1-Mad2 complex. Then, Mps1 phosphorylates a third substrate, Mad1 at T716, which allows for the recruitment and conversion of open Mad2 (O-Mad2) to closed Mad-2 (C-Mad2), enabling its binding to Cdc20 (Ji *et al.*, 2017). Cdc20 makes two important contacts with mitotic checkpoint proteins: its N-terminal basic tail is bound to the phosphorylated C-terminal domain of Mad1, and its WD40 domain is bound to Phe and KEN boxes of Bub1. In this way, Cdc20 is brought in close proximity to C-Mad2. The miotic checkpoint complex (MCC), formed when the C-Mad2-Cdc20 complex further binds BubR1 and Bub3 (bound to

Bub1 or from the cytosol), binds and inhibits the anaphase promoting complex/cyclosome (APC/C) (Ji *et al.*, 2017). As a result of this signaling cascade, the cell cannot enter anaphase in the presence of unattached kinetochores.

Defects in mitotic checkpoint signaling allow cells to enter anaphase in the presence of improper kinetochore microtubule attachments and result in consequent chromosome missegregation. Alteration of mitotic checkpoint protein stoichiometry, via increasing or decreasing protein levels, or modulation (e.g. increasing or decreasing) activity levels of mitotic checkpoint kinases have been used as mechanisms to weaken mitotic checkpoint signaling and study the consequences of chromosome missegregation in vitro and in vivo (Kops et al., 2005).

Chromosome missegregation can be judged through observation of errors during mitosis. These errors include lagging chromosomes, misaligned chromosomes, chromosome bridges, and multipolar spindles. Lagging chromosomes, thought to be generated by merotelic attachments (Gregan et al., 2011), are chromosomes that lag behind the segregating masses of DNA in anaphase and telophase. Merotelic attachments are formed when a single kinetochore is attached to microtubules emanating from both spindle poles on opposite sides of the cell (Gregan *et al.*, 2011). These differ from proper amphitelic attachments in which each chromatid in a sister chromatid pair is attached to opposite spindle poles. Misaligned chromosomes, another type of mitotic error, occur when chromosomes do not properly congress to the metaphase plate. Polar chromosomes represent a specific case of chromosome misalignment in which chromosomes remain associated with one of the spindle poles. Misaligned and polar chromosomes are characteristic of reduced CENP-E function

(Schaar et al., 1997). Chromosome bridges, as their name implies, form bridge-like structures from chromosomes that stretch between segregating masses of DNA in anaphase and telophase. Finally, multipolar spindles are characterized by the presence of more than two spindle poles per cell.

Defects in mitotic checkpoint signaling, sister chromatid cohesion, kinetochore structure, or the mitotic spindle can lead to chromosome missegregation events (Bakhoum et al., 2014b; Funk et al., 2016). Chromosome missegregation during mitosis can generate numerical aneuploidy, a state in which a cell possesses an abnormal number of chromosomes due to whole chromosome gains or losses. Structural aneuploidies can also be observed in human tumors, which are characterized by the gain or loss of portions of chromosomes. Here we will focus on numerical aneuploidy given that it is the result of whole chromosome missegregation during mitosis. Aneuploidies can be stably maintained in the event that no further chromosome misegregation events occur after the initial missegregation event (Storchova and Pellman, 2004). On the other hand, ongoing rates of chromosome missegregation events on a population level over time generates chromosomal instability or CIN (Lengauer et al., 1997; Thompson and Compton, 2008).

1.2 Aneuploidy and CIN in cancer

Defects in mitosis that are associated with aneuploidy and CIN have been observed in cancer for over 100 years. In 1890, von Honsseman documented various mitotic defects he observed in human tumor tissue including multipolar spindles, lagging chromosomes, and chromosome bridges. Given the prevalence of mitotic errors in

cancerous tissue, early in the 1900s, Theodor Boveri hypothesized that these mitotic defects and aneuploid cells give rise to tumors (Boveri, 1902; 1914). It is well established today that aneuploidy and chromosomal instability are commonly observed in cancer. Recent estimates suggest that 86% of solid tumors are numerically aneuploid and 44% of solid tumors exhibit CIN (Zasadil et al., 2013). In breast cancer, specifically, estimations of CIN are slightly higher at just over 50% (Zasadil *et al.*, 2013).

Numerous genetically engineered mouse models have been developed to test Boveri's hypothesis that aneuploidy and CIN can promote tumorigenesis, with mixed results. Alteration of mitotic checkpoint genes is known to cause chromosome missegregation, aneuploidy, and CIN, and has been a common approach to assess Boveri's hypothesis. For example, heterozygous deletion of Mad1 ($Mad1^{+/-}$) resulted in significantly higher tumor incidence compared to wild type controls (Iwanaga et al., 2007). Similarly, heterozygous deletion of Mad2 ($Mad2^{+/-}$) (Michel et al., 2001) or CENP-$E^{+/-}$ (Weaver et al., 2007) caused an increase in lung, and splenic lymphomas and lung tumors, respectively. Increased tumor incidence was also observed following overexpression of Hec1 (Diaz-Rodríguez et al., 2008). Even so, these tumor phenotypes were observed with incomplete penetrance, in only a subset of tissues, and in late stages of a mouse's life (≥18 months of age). Importantly, not all aneuploid mouse models demonstrated a significant increase in tumor formation. No increased tumor burden was observed in mice expressing hypomorphic alleles of BubR1 ($BubR1^{H/H}$), despite the presence of increased aneuploidy in mouse embryonic fibroblasts (MEFs) with this mutant genotype as compared to wild type controls (Baker et al., 2004). Similarly, heterozygous deletion of Cdc20 ($Cdc20^{+/-}$) increased aneuploidy

in MEFs and splenocytes compared to control littermates; however tumor burden was unaffected (Malureanu et al., 2010). Taken together, these data suggest that low levels of CIN, in some contexts, can be mildly tumor promoting. These single insults to genome stability are thought to promote tumorigenesis by accelerating the loss of tumor suppressor genes or the gain of oncogenes (Burkard and Weaver, 2017). There is also evidence, however, that high levels of CIN can suppress tumors and be used as a potential therapeutic strategy.

1.3 High CIN causes cell death, tumor suppression, and is potentially useful therapeutic strategy

While low levels of CIN can be pro-tumorigenic, several lines of evidence have demonstrated that high rates of CIN can cause cell death and tumor suppression, likely due to the loss of too many chromosomes or both copies of an essential gene (Funk *et al.*, 2016; Kops et al., 2004). In cell culture experiments, combining reduced levels of Mps1 or BubR1, genetic manipulations known to induce CIN, with low nanomolar doses of paclitaxel further increased the severity of chromosome segregation defects and reduced cell viability as measured by a reduction in colony formation (Janssen et al., 2009). Several mouse models have also shown that high CIN can lead to cell death and tumor suppression. Although CENP-E heterozygosity led to an increase in lung and splenic tumors, liver tumors were reduced in size and number compared to wild type controls (Weaver et al 2007). This reduced tumor formation can be explained by the fact that hepatocytes already have low rates of chromosome missegregation at baseline (Putkey…Cleveland 2002). In other experiments, homozygous loss of the tumor suppressor gene ARF, which elevated the rates of chromosome missegregation,

prolonged the survival of mice with CENP-E heterozygosity, suggesting that high CIN can be used as a therapeutic strategy (Weaver *et al.*, 2007). In a more recent study, CENP-E reduction (CENP-$E^{+/-}$) combined with reduction of Mad2 (Mad$2^{+/-}$) showed analogous results. Cells that were heterozygous for both genes displayed higher rates of chromosome missegregation than cells heterozygous for either gene alone. When looking at tumor burden in these mice, doubly heterozygous animals showed reduced splenic lymphomas and lung adenomas compared to singly heterozygous mice (Silk et al., 2013). Similarly, combining overexpression of Mad2 with conditional mouse models of a Kras activating mutation ($Kras^{G12D}$) or Her2 overexpression in the adult mammary gland increased mitotic errors, karyotypic complexity, and delayed tumor onset compared to $Kras^{G12D}$ or Her2 expression alone (Rowald et al., 2016). Overall, these results suggest that in contexts with low baseline levels of CIN, increasing CIN to higher levels suppresses tumor formation and may be used therapeutically to improve patient outcomes.

In patients, several studies have demonstrated that high levels of CIN are associated with improved prognosis. Specifically, stratifying ovarian, gastric, non-small cell lung, and ER- breast cancer patients based on a gene expression signature of CIN revealed that patients with a high CIN gene expression signature had improved recurrence-free or distant metastasis-free survival compared to patients with lower expression levels of this CIN gene signature (Birkbak et al., 2011). Likewise, high CIN in ER- breast cancer patients, measured by inter-cellular heterogeneity of chromosome copy numbers by fluorescence in situ hybridization (FISH), was associated with improved long-term survival (Jamal-Hanjani et al., 2015; Roylance et al., 2011).

Therefore, data from numerous mouse models and human datasets support the premise that increasing CIN may be a viable therapeutic strategy. Whether baseline levels of CIN may be used as a potential predictive biomarker for chemotherapy agents remains to be determined. Data discussed in Chapter Two suggest that patients that exhibit CIN may be particularly sensitive to increasing CIN with microtubule poison (taxane) therapy.

1.4 Microtubule poisons as antimitotic chemotherapy agents

Microtubules are protein filaments comprised of α-tubulin and β-tubulin heterodimers that make up part of the cytoskeleton of eukaryotic cells (Jordan and Wilson, 2004). During interphase, microtubules extend throughout the cell and play a role in the maintenance of cell shape, cell movement, and the intracellular transport of vesicles and organelles. The microtubule network is completely reorganized upon entry into mitosis, during which the tubulin subunits are reassembled to ultimately form the mitotic spindle (Prosser and Pelletier, 2017). This reorganization requires that microtubules are dynamic and can undergo rapid cycles of assembly and disassembly. Individual microtubules exhibit periods of growth, shrinkage, and pause, collectively referred to as dynamic instability (Mitchison and Kirschner, 1984). Dynamic instability also plays an important role throughout mitosis, as the mitotic spindle again changes in shape and structure to physically separate sister chromatids to the daughter cells.

Cancer cells exhibit uncontrolled cell division and are known to proliferate at higher rates than most normal tissues (Inwald et al., 2013; Urruticoechea et al., 2005). Since microtubules play an essential role in mitosis, they are an attractive target for anti-

cancer drugs. Anti-mitotic chemotherapy agents called microtubule poisons target microtubules and disrupt their dynamics. Multiple drugs belonging to this family, with diverse chemical structures and tubulin binding sites, have demonstrated clinical efficacy and are approved for use in the treatment of various cancers (Jordan and Wilson, 2004). Despite the development of new therapies in recent decades, including targeted therapies and immune checkpoint inhibitors, microtubule poisons remain a cornerstone of cancer treatment and are some of the most profitable anti-cancer drugs to date.

Despite their long history of clinical use and success in the clinic, microtubule poisons, like all chemotherapy drugs, come with a host of undesirable side effects. As anti-mitotic chemotherapy agents, microtubule poisons not only affect rapidly dividing tumor cells, but also other rapidly dividing, non-cancerous tissue. Common side effects include alopecia (hair loss) and nausea from the detrimental effects of these drugs on the rapidly dividing cells in the hair and gut, respectively (Markman, 2003). Neutropenia, or the presence of abnormally low neutrophils (a type of white blood cell), is another potentially life-threatening side effect associated with microtubule poison therapy related to its cytotoxic effects on rapidly dividing white blood cells (Gidding et al., 1999; Markman, 2003). Another significant negative side effect of these drugs is peripheral neuropathy, which is characterized by a numbness or tingling in the extremities. Peripheral neuropathy can significantly diminish quality of life and can remain permanent even after patients are taken off these drugs. Although the exact cause of peripheral neuropathies is incompletely understood, it is thought to arise after microtubule poison treatment due to impaired microtubule transport along axons

(Quasthoff and Hartung, 2002). Consequently, the extremities might be most severely affected since they are innervated by the longest axons in the body. While multiple microtubule poisons are used in the clinic and have similar toxicity profiles, these drugs have been historically subdivided into two main subgroups: microtubule destabilizers and microtubule stabilizers.

The vinca alkaloids are one class of microtubule destabilizers. These drugs were isolated from the Madagascar periwinkle plant and are classically defined as microtubule destabilizers due to the fact that they inhibit microtubule polymerization and decrease microtubule polymer mass at high concentrations. Three vinca alkaloids have been approved for clinical use in the United Sates including vinblastine, vincristine, and the semi-synthetic derivative vinorelbine (Moudi et al., 2013). Vinblastine, vincristine, and vinorelbine bind to the interface between the α and β-subunit of tubulin dimers at the plus ends of microtubules at the so called “vinca alkaloid binding domain” (Jordan and Wilson, 2004). Another drug belonging to the family of microtubule destabilizers is eribulin. Eribulin is synthetic analogue of Halochondrin B, a naturally occurring compound isolated from the marine sponge Halichondria okadai (Shetty and Gupta, 2014). It was approved by the FDA for the treatment of metastatic breast cancer in 2010 and is now approved in 40 countries worldwide. Similar to other microtubule poisons, eribulin inhibits microtubule polymerization, but it has little to no effect on microtubule shortening rate (Dybdal-Hargreaves et al., 2015). Experimental and modeling data suggest that eribulin binds to microtubules in a distinct manner compared to the vinca alkaloids by binding to exposed β-subunits at the microtubule plus end (Bai et al., 2011; Cortes et al., 2018). Mechanistically, microtubule destabilizers have been proposed to

induce mitotic arrest due to activation of the spindle assembly checkpoint following microtubule depolymerization (Jordan et al., 1991; Jordan and Wilson, 2004; Ngan et al., 2001).

On the other hand, microtubule stabilizers promote microtubule polymerization at high concentrations (Jordan and Wilson, 2004; Schiff et al., 1979). The first agent to be identified in this class was paclitaxel (Taxol™). Isolated from the bark of the Pacific yew tree, paclitaxel was identified as part of a collaborative plant screening program between the National Cancer Institute (NCI) and the United Stated Department of Agriculture (USDA) to identify naturally occurring compounds with anti-cancer activity (Weaver, 2014). In 1992, the Food and Drug Administration (FDA) approved paclitaxel for the treatment of ovarian cancer, and for the treatment of breast cancer in 1994 (Weaver, 2014). Other clinically used drugs belonging to this family include docetaxel, a semi-synthetic analog of paclitaxel, and the epothilones (Jordan and Wilson, 2004). Epothilones A and B were isolated from culture broth of the myxobacterium *Sorangium cellulosum* (Lee and Swain, 2008). Replacement of the lactone oxygen atom with nitrogen in epothilone B resulted in the synthesis of aza-epothilone B, also known as ixabepilone (Lee et al., 2001). Ixabepilone is the most clinically developed of the epothilones, and was FDA approved in 2007 (Cobham and Donovan, 2009). Paclitaxel, docetaxel, and the epothilones bind along the interior surface of the microtubule at the β-subunit (Jordan and Wilson, 2004; Nogales et al., 1995). However, the epothilones are structurally dissimilar to taxanes and have a different mode of binding to β-tubulin (Nettles et al., 2004). Similar to the microtubule destabilizing drugs, microtubule stabilizers are thought to work by arresting cells in mitosis due to an inability to satisfy

the mitotic checkpoint, as evidenced by the presence of Mad2 at kinetochores (Waters et al., 1998).

The classification of microtubule poisons as microtubule stabilizers and destabilizers is a misleading overgeneralization. Like all drugs, microtubule poisons exhibit concentration dependent effects. While it is certainly true that microtubule stabilizers increase microtubule polymer mass and microtubule destabilizers decrease microtubule polymer mass at some concentrations, different effects are observed at very low and very high concentrations of drug. For example, very high concentrations (μM) of microtubule destabilizers increase the affinity of tubulin for itself and consequently cause the formation of tubulin paracrystals and increased microtubule polymer mass (Bensch and Malawista, 1968; Bensch et al., 1969; Na and Timasheff, 1982). On the other hand, low (nM) concentrations of both microtubule stabilizers and destabilizers disrupt microtubule dynamic instability and kinetically stabilize microtubules (Castle et al., 2017; Jordan and Wilson, 2004). This observation of overlapping function at low doses may offer a unifying explanation for why these two classes of drugs with seemingly antagonistic actions both demonstrate clinical utility. Therefore, the clinically used microtubule poisons could exhibit similar mechanisms of cytotoxicity dependent on their ability to kinetically stabilize microtubules at concentrations that are too low to significantly alter microtubule polymer mass.

1.5 Examining the predominant paradigm: microtubule poisons cause mitotic arrest

For the past several decades, the predominant hypothesis has been that microtubule poisons kill tumor cells as a consequence of unresolved mitotic arrest. Early studies using vinca alkaloids found that inhibition of cell proliferation coincided with an arrest of cells in a metaphase-like state of the cell cycle (Jordan *et al.*, 1991; Sweeney et al., 1978; Tucker et al., 1977). A similar mitotic arrest phenotype was observed when cultured cells were treated with paclitaxel (Jordan et al., 1993; Milas et al., 1995; Schiff and Horwitz, 1980). Mitotic arrest induced by these drugs results from activation of the mitotic checkpoint or spindle assembly checkpoint from unattached kinetochores (Jordan and Wilson, 2004; Waters *et al.*, 1998). Mitotic arrest either results in death during mitosis or mitotic slippage, an abnormal exit from mitosis without chromosome segregation to form a tetraploid G1 cell. The striking effects of high concentrations of microtubule poisons on mitotic arrest and induction of cell death led to the hypothesis that the mechanism of cytotoxicity of these drugs was related to their ability to arrest cells in mitosis.

Because mitotic arrest was observed at typically used concentrations of microtubule poisons in cell culture, it was widely assumed that mitotic arrest was responsible for their clinical efficacy in patients. However, numerous drugs aimed at inducing mitotic arrest, targeting Aurora A, CENP-E, Eg5/KSP, and Plk1, failed clinical trials due to an inadequate therapeutic window (Komlodi-Pasztor et al., 2012). Moreover, a pre-clinical study in mice (Milross et al., 1996), and studies in human breast cancer patients (Symmans et al., 2000) found that mitotic arrest induced by paclitaxel did not correlate with response to the drug. The lack of efficacy of other drugs developed to arrest cells in mitosis, coupled with evidence that mitotic arrest does not

correlate with tumor response to paclitaxel, suggests that the therapeutic action of paclitaxel and other microtubule poisons might occur through a mechanism outside of mitotic arrest.

1.6 Clinically relevant concentrations of paclitaxel cause chromosome missegregation on multipolar spindles

In order to better understand the mechanism of cytotoxicity of paclitaxel in human cancer, our lab enrolled six female patients with newly diagnosed, HER2 negative, locally advanced, treatment naive breast cancer into a clinical trial. Enrolled patients were treated with single agent, neoadjuvant 175 mg/m^2 paclitaxel therapy followed by Adriamycin and cyclophosphamide (AC) and/or surgery, per physician discretion. Research biopsies were obtained prior to the initiation of paclitaxel and 20 hours after the patient's first dose of paclitaxel. The 20-hour timepoint was selected because cultured cells mount a robust mitotic arrest in response to high concentrations of paclitaxel, showing a ≥15-fold increase in mitotic index compared to untreated control cells (Zasadil et al., 2014). The mitotic index, a measurement of the percent of cells in mitosis, was quantified in pre-treatment and post-paclitaxel treatment patient samples. If the mechanism of cytotoxicity of paclitaxel were dependent on its ability to induce a mitotic arrest, we would expect to see substantial increases in the mitotic index following paclitaxel treatment. However, we found that the change in mitotic index between the pre- and post-treatment biopsies ranged from a slight decrease to an increase of only a few percent (Zasadil *et al.*, 2014). These subtle changes in the mitotic index are inconsistent with a strong mitotic arrest phenotype.

To determine patient response, the longest tumor diameter was measured by mammogram, ultrasound, or both before treatment (at baseline) and after completion of paclitaxel therapy (and before AC or surgery). Tumor response was evaluated according to Response Evaluation Criteria for Solid Tumors (RECIST) 1.1 guidelines (Eisenhauer et al., 2009), which defines a partial response as a ≥30% decrease in the largest tumor diameter. Although two patients in this trial exhibited increases in mitotic index in response to paclitaxel (albeit by only a few percent), these patients only displayed minimal tumor regression and did not meet the partial response RECIST 1.1 criteria (Zasadil *et al.*, 2014). These data suggested that mitotic arrest is not required for response to paclitaxel and there is likely an alternate mechanism of cytotoxicity. While uniform changes in the mitotic index were not observed across patients following paclitaxel, paclitaxel treatment induced an increase in multipolar mitotic cells in all patient tumors examined. These data led us to hypothesize that multipolar spindles are important for the cytotoxicity of paclitaxel.

Patient samples were also obtained to measure the plasma and intratumoral concentrations of paclitaxel. The concentration of paclitaxel measured within patient tumors ranged from 1-9 μM, which was higher than the plasma levels in all patients (80-280 nM), consistent with cell culture experiments demonstrating intracellular accumulation of paclitaxel. To better study the effects of paclitaxel on mitosis and cell death, determination of the appropriate dose with which to treat cultured cells to mimic the clinically relevant concentration of paclitaxel achieved in patient tumors was needed. To this end, intracellular drug levels were measured by High Performance Liquid Chromatography (HPLC). We determined that low nanomolar doses of (5–10 nM for

MDA-MB-231 and 10–50 nM for Cal51) resulted in clinically relevant intracellular concentrations of 1–9 μM (Zasadil *et al.*, 2014).

Importantly, while supraphysiological doses of paclitaxel caused breast cancer cells to arrest in mitosis, clinically relevant doses did not. Instead, at clinically relevant concentrations of paclitaxel, we observed that cells proceeded through mitosis in the presence of multipolar spindles with a relatively brief delay (Zasadil *et al.*, 2014). Reassuringly, this mimicked the multipolar spindle phenotype observed in patient tumor biopsies following paclitaxel treatment, demonstrating consistency between our in vitro and in vivo models. Multipolar mitoses result in improper segregation of chromosomes. Instead of equal DNA division into two daughter cells that was observed in control cells, chromosomes were often segregated in three, four, or five different directions in the presence of paclitaxel. Multipolar spindle clustering coupled with cytokinesis failure resulted in cell divisions that oproduced two or three daughter cells with improper genetic content (Zasadil *et al.*, 2014). Taken together, this data led us to hypothesize that paclitaxel causes cell death in patient tumors due to chromosome missegregation that results from cell division on multipolar spindles.

Whether multipolar spindles are observed in patients receiving the other standard of care paclitaxel therapy (a lower, but equally clinically effective dose) remains an important outstanding question. In addition, since paclitaxel induces cell death due to chromosome misseggreation, it remains to be determined if patients with higher baseline levels of chromosomal instability (CIN) are more likely to receive a therapeutic benefit from paclitaxel. These topics are further investigated in Chapter Two. Additionally, whether chromosome missegregation on multipolar spindles is a relevant

mechanism of cytotoxicity of other clinically-used microtubule poisons is examined in Chapter Three.

1.7 Efforts toward identification of biomarkers for microtubule poison response

Despite their long history of clinical use, there is still no clinically used biomarker to identify which patients will experience positive therapeutic effects from microtubule poison therapy. This may, in part, be due to an incomplete understanding of their mechanism of cytotoxicity in patients. Studies in cell culture have found that upregulation of multidrug transporters can mediate in vitro resistance to microtubule poisons (Beck, 1984; Mechetner et al., 1998). However, expression of multidrug transporters was not found to correlate with response in patients (Roque et al., 2013). Moreover, clinical trials have demonstrated that combination treatment with p-glycoprotein inhibitors does not significantly improve patient outcomes (Leonard et al., 2003; Samuels et al., 1997; Toppmeyer et al., 2002). Altered expression of tubulin isotypes has also been suggested as a predictive biomarker of microtubule poison therapy. In vitro, overexpression of the β-tubulin III isotype conferred resistance to paclitaxel in Chinese Hamster Ovary cells (Hari et al., 2003). Although, in a separate study, overexpression of β-tubulin III in prostate cancer cells did not confer resistance to paclitaxel or vinblastine (Ranganathan et al., 2001). In non-small cell lung cancer patients, high levels of the β-tubulin III isoform were associated with worse response to paclitaxel/carboplatin; however, patients with high expression of β-tubulin III showed the greatest tumor response to cisplatin/vinorelbine (Rosell et al., 2003). Therefore, expression of β-tubulin III has been shown to correlate with diverse response outcomes

and future studies are required to evaluate it as a predictive biomarker for microtubule poison therapy.

While previous studies have shown that increasing CIN can be a useful therapeutic strategy, it is currently unknown whether baseline levels of CIN affect response to paclitaxel and other microtubule poisons. If microtubule poison therapy causes cell death due to chromosome missegregation on multipolar spindles, patients with higher baseline levels of CIN may be poised to better respond to microtubule poison therapy, as treatment of this patient cohort with these drugs will further exacerbate chromosome missegregation and push their cells towards excessive chromosome loss and cell death. We found that pre-existing CIN correlated with taxane response in our metastatic breast cancer patient cohort (Chapter Two), suggesting that baseline levels of CIN can be used as a predictive biomarker of taxane response. If other clinically used microtubule poisons have similar mechanisms of cytotoxicity, pre-existing CIN may be a general biomarker for this family of drugs. Identification of a biomarker to predict patient response would substantially improve patient outcomes and reduce effective treatment delays and unwanted side effects associated with microtubule poison therapy in non-responding patients.

1.8 Maintaining spindle integrity: mechanisms of bipolar and multipolar mitotic spindle formation and maintenance

The establishment and maintenance of spindle bipolarity is essential for the accurate segregation of chromosomes during mitosis (Prosser and Pelletier, 2017). The mitotic spindle contains two centrosomes, each comprised of a pair of centrioles embedded in pericentriolar material (PCM). Centrosomes are the canonical microtubule

organizing centers (MTOCs) in vertebrate cells. Microtubules that make up the mitotic spindle nucleate from the gamma tubulin ring complexes within the PCM. The presence of two centrosomes helps to ensure the bipolar nature of the mitotic spindle and promote bi-orientation of chromosomes that results the in equal segregation of duplicated chromosomes into two daughter cells (Prosser and Pelletier, 2017).

Cells with more than the normal number of two mitotic spindle poles are termed multipolar. One mechanism that can lead to spindle multipolarity is the presence of too many centrosomes (Maiato and Logarinho, 2014). Centrioles within centrosomes normally replicate exactly once per cell cycle. However, if this process is dysregulated, centrioles may be over duplicated, resulting in supernumerary centrosomes. Over-expression of Polo-like kinase 4 (Plk4), the master regulator of centriole duplication, is one mechanism of induced centrosome amplification (Holland et al., 2012). Centrosome amplification can also arise from abnormal mitotic exit such as mitotic slippage or cytokinesis failure. In these cases, centrosomes and chromosomes are not properly segregated into each daughter cell. Instead, a single cell is formed, leading to both centrosome amplification and tetraploidy.

Multipolar spindles can also form in the absence of extra centrosomes through centriole disengagement, PCM fragmentation, or the formation of additional acentriolar microtubule nucleating foci (Maiato and Logarinho, 2014). Centriole disengagement occurs when the paired centrioles are separated due to defects in centriole cohesion. A disruption in centrosome structural integrity can result in PCM fragmentation and the formation of acentriolar fragments capable of nucleating microtubules. We observed multipolar spindles in paclitaxel breast cancer patients without evidence of centrosome

amplification (Zasadil *et al.*, 2014). However, exactly how and why paclitaxel and other microtubule poisons induce multipolar spindle formation at low nanomolar doses remains an important outstanding question. To begin to understand this, the molecular and temporal requirements for microtubule poison induced multipolar spindle establishment and maintenance are explored further in Chapter Four.

Several proteins have been implicated in bipolar spindle formation that may also play a role in multipolar spindle formation. One such protein is Eg5/Kif11/kinesin-5. Eg5 is a tetrameric plus end-directed kinesin with two anti-parallel homodimers. Localized to the mitotic spindle, Eg5 cross links and slides anti-parallel microtubules within the spindle. Each homodimer exerts plus-end directed forces on microtubules and as a result of its antiparallel orientation, effectively pushes spindle poles apart (Kapitein et al., 2005). Inhibition of Eg5 with a small molecule inhibitor, monastrol, inhibits the forces generated by Eg5 to push the spindle poles apart and results in the collapse of the normal bipolar spindle down to a monopolar spindle (Maliga et al., 2002). Whether Eg5 plays a role in multipolar spindle formation in response to microtubule poisons remains unknown and is assessed in Chapter Four.

Polo-like kinase 1 (Plk1) is a mitotic kinase that plays diverse roles throughout mitosis, including roles in mitotic entry, centrosome maturation, formation of a bipolar mitotic spindle, chromosome segregation, and cytokinesis (Barr et al., 2004). The N-terminal domain of Plk1 contains the catalytic kinase domain, while the C-terminal domain contains two Polo box domains (PBDs). Plk1 interacts with its substrates via its PBD, a phosphopeptide binding domain that requires substrates to be previously phosphorylated (“priming phosphorylation”). After PBD binding, Plk1 then

phosphorylates its substrates to carry out its diverse biological functions. While hundreds of Plk1 substrates have been identified, the functional consequence of phosphorylation on many of these substrates is not well defined (Santamaria et al., 2011). Regarding its role in bipolar spindle assembly, Plk1 is known to participate in signaling required for Eg5 loading (van Ree et al., 2016). Chemical inhibition of Plk1 can be achieved with BI2536, an ATP competitive inhibitor (Steegmaier et al., 2007). High concentrations of BI2536 also result in a loss of bipolar spindle integrity and a monopolar spindle phenotype (Lera and Burkard, 2012). However, the effects of Plk1 inhibition on multipolar spindle formation caused by microtubule poison treatment remain untested.

Mps1, or monopolar spindle 1, was first identified in the budding yeast *Saccharomyces cerevisiae*. *mps1* mutants underwent monopolar mitoses due to a lack of spindle pole body (the functional equivalent of the centrosome in higher eukaryotes) duplication (Fisk et al., 2004). However, whether human Mps1 plays a role in centrosome duplication remains controversial. One study did not find human Mps1 localization at centrosomes and failed to identify a role for it in centrosome duplication in a multi-faceted analysis that included antibody microinjection, siRNA knockdown, and overexpression of wild type and kinase dead Mps1 (Stucke et al., 2002). Conversely, a separate study using distinct Mps1 antibodies observed Mps1 centrosomal localization (Fisk et al., 2003). In their study, overexpression of human Mps1 caused centrosome reduplication, while siRNA mediated knockdown and overexpression of a dominant negative kinase dead mutant hindered centrosome duplication (Fisk *et al.*, 2003). Given its potential function in centrosome duplication in

human cells and previously described role in bipolar spindle formation in budding yeast, we tested whether Mps1 might affect the formation of multipolar spindles (Chapter Four), as this role has not been assessed thus far.

Centromere associated protein E (CENP-E) is a kinesin like protein that is responsible for chromosome congression, or the alignment of chromosomes at the spindle equator/metaphase plate. It is a plus-end directed motor that powers chromosome alignment by attaching to spindle microtubules at its N-terminus and to kinetochores of chromosomes at its C-terminus, walking misaligned chromosomes to the metaphase plate (Kim et al., 2008). Accordingly, pharmacological inhibition of CENP-E with GSK923925 results in polar and misaligned chromosomes (Wood et al., 2010). The forces generated by CENP-E for chromosome alignment must be appropriately counteracted to maintain spindle pole integrity and prevent multipolar spindles (Logarinho et al., 2012). As such, some studies have reported a small number of multipolar spindles formed upon inhibition of CENP-E (McEwen et al., 2001; Yao et al., 2000). In Chapter 4, we determined if CENP-E is required for microtubule poison-induced multipolar spindle formation.

While the molecular requirements for multipolar spindle formation remain understudied, evidence suggests there is a temporal requirement for the induction of multipolarity. We found that accelerating transit through mitosis through two mechanisms, by overexpression of Mad1 or inhibition of Mps1, led to a reduction in paclitaxel induced multipolar spindle maintenance (Chapter Two). Conversely, increasing mitotic duration has been shown to increase multipolarity induced by CSAG1 depletion (Sapkota et al., 2020). The exact mechanism underlying the

temporal requirement for the formation of multipolar spindles is still unknown. Data discussed in Chapter Four evaluates the role of Eg-5, Plk1, Mps1, and CENP-E in microtubule poison-induced multipolar spindle establishment and maintenance. Moreover, the temporal requirements for microtubule poison-induced multipolarity are assessed. Determining the molecular and temporal requirements for microtubule poison induced will aid in our understanding of how and why multipolar spindles are formed in response to these drugs. These findings may also lead to the identification of new molecular biomarkers for microtubule poison response. Mechanistic insight regarding how multipolar spindles are formed and maintained in mitosis may also lead to the development of novel methods to increase multipolarity and improve the clinical efficacy of microtubule poisons.

CHAPTER 2: CHROMOSOMAL INSTABILITY SENSITIZES PATIENT TUMORS TO MULTIPOLAR DIVISIONS INDUCED BY PACLITAXEL.

Christina M. Scribano, Jun Wan, Karla Esbona, John B. Tucker, Amber Lasek, Amber S. Zhou, Lauren M. Zasadil, Ryan Molini, Jonathan Fitzgerald, Angela M. Lager, Jennifer J. Laffin, Kayla Correia-Staudt, Kari B. Wisinski, Amye J. Tevaarwerk, Ruth O'Regan, Stephanie M. McGregor, Amy M. Fowler, Richard J. Chappell, Tim S. Bugni, Mark E. Burkard, and Beth A. Weaver

*The work in this chapter was accepted for publication at *Science Translational Medicine*.

Abstract

Paclitaxel (Taxol) is a cornerstone of cancer treatment. However, its mechanism of cytotoxicity is incompletely understood and not all patients benefit. We discovered that breast cancer patients did not accumulate sufficient intratumoral paclitaxel to induce mitotic arrest. Instead, clinically relevant concentrations induced multipolar mitotic spindle formation. However, the extent of early multipolarity did not predict patient response. While multipolar divisions frequently led to cell death, multipolar spindles focused into bipolar spindles prior to division at variable frequency, and maintaining multipolarity throughout mitosis was critical to induce the high rates of chromosomal instability necessary for paclitaxel to elicit cell death. Increasing multipolar divisions in paclitaxel resulted in improved cytotoxicity. Conversely, decreasing paclitaxel-induced multipolar divisions reduced paclitaxel efficacy. Moreover, we discovered that pre-existing chromosomal instability sensitized breast cancer cells to paclitaxel. Both genetic and pharmacological methods of inducing chromosomal instability were sufficient to increase paclitaxel efficacy. In patients, pre-treatment chromosomal instability directly correlated with taxane response in metastatic breast cancer, such that patients with a higher rate of pre-existing chromosomal instability showed improved response to taxane. Together, these results support the use of baseline rates of chromosomal instability as a predictive biomarker for paclitaxel response. Furthermore, they suggest that agents that increase chromosomal instability or maintain multipolar spindles throughout mitosis will improve the clinical utility of paclitaxel.

Introduction

Paclitaxel is the founding member of the taxane family of microtubule stabilizing drugs, and is used clinically as anti-mitotic chemotherapy to treat a variety of cancers, including breast, ovarian, and lung (Huang and Campbell, 2012). In breast cancer, paclitaxel is a cornerstone of treatment and is used for primary and metastatic tumors of all subtypes (Crown et al., 2004). Paclitaxel can be administered preoperatively (neoadjuvant) or postoperatively (adjuvant) and is delivered as a single agent prior or subsequent to anthracycline chemotherapy (Zaheed et al., 2019). There are two standard-of-care dosing regimens for patients with primary breast cancer receiving paclitaxel therapy. Patients either receive four doses of 175 mg/m^2 paclitaxel every other week or 12 weekly doses of 80 mg/m^2 paclitaxel. The results of a large clinical trial (SWOG S0221) suggested that both regimens are equally effective (Budd et al., 2015). Similar doses and schedules are used in the metastatic cancer setting. However, only about 50% of breast cancer patients display tumor regression following paclitaxel treatment (Fountzilas et al., 2009). There is currently no clinically used biomarker to predict patient response to paclitaxel, underscoring the importance of further mechanistic studies.

Despite the long history of paclitaxel use, its mechanism of therapeutic response remains controversial (Komlodi-Pasztor et al., 2013). A range of paclitaxel concentrations have been tested in cell culture, with most studies focusing on high concentrations that cause cell death due to mitotic arrest resulting from activation of the mitotic checkpoint [also known as the spindle assembly checkpoint (Waters *et al.*, 1998)]. It was widely assumed that mitotic arrest was necessary for the therapeutic

action of paclitaxel; however, other drugs developed to cause mitotic arrest have been largely ineffective in patients due to an inadequate therapeutic window, including drugs targeting Aurora kinase A, Eg5/kinesin spindle protein, and Polo-like kinase 1 (Komlodi-Pasztor *et al.*, 2013). Moreover, paclitaxel-induced mitotic arrest does not correlate with tumor response in preclinical allograft studies in mice (Milross *et al.*, 1996) or in human breast cancer patients (Symmans *et al.*, 2000). These observations suggest that paclitaxel exerts antitumor effects through mechanisms other than unresolved mitotic arrest.

We recently discovered that breast cancer patients receiving 175 mg/m^2 paclitaxel have intratumoral concentrations of paclitaxel too low to cause mitotic arrest in patient tumors or cell models (Zasadil *et al.*, 2014). High doses of paclitaxel (5 μM) cause supraphysiological intracellular drug concentrations and mitotic arrest, and increase the mitotic index ≥15 fold over baseline. In contrast, low nanomolar, clinically relevant concentrations of paclitaxel do not cause mitotic arrest and only increase the mitotic index ~3 fold (Zasadil *et al.*, 2014). In all primary breast tumors examined, paclitaxel increased the percentage of multipolar, as distinct from normal bipolar, mitotic spindles (Zasadil *et al.*, 2014). In cell culture, mitotic divisions on multipolar spindles resulted in a relatively brief mitotic delay, chromosome missegregation, aneuploid daughter cells, and increased cell death (Ganem et al., 2009; Zasadil *et al.*, 2014). Thus, we proposed that paclitaxel exerts its anti-cancer effects by causing chromosome missegregation on multipolar spindles. In this study we address whether low-dose, weekly paclitaxel also induces multipolar spindles without mitotic arrest. Verifying this

mechanism provides crucial insight necessary to elucidate why some tumors respond to paclitaxel, whereas others are resistant.

About 50% of breast tumors exhibit chromosomal instability, an ongoing rate of chromosome missegregation that generates heterogenous aneuploid cells (Denu et al., 2016; Zasadil *et al.*, 2013). The rate of chromosomal instability dictates cell viability (Godek et al., 2016; Laucius et al., 2019; Silk *et al.*, 2013; Weaver *et al.*, 2007). Low rates of chromosomal instability can be advantageous to tumor cells, since ongoing changes in genomic content provide variable karyotypes that allow cells to survive under various selective pressures (Rutledge et al., 2016; Selmecki et al., 2009; Zasadil *et al.*, 2013). However, high rates of chromosomal instability cause cell death and tumor suppression, likely due to loss of both copies of an essential chromosome (Funk et al., 2020; Kops *et al.*, 2004) or the antiproliferative effects of aneuploidy-induced stress (Chunduri and Storchová, 2019). In patients, high rates of chromosomal instability are associated with improved prognosis (Birkbak *et al.*, 2011; Jamal-Hanjani *et al.*, 2015; Roylance *et al.*, 2011). Since 175 mg/m^2 paclitaxel induces multipolar spindles without mitotic arrest, and multipolar spindles elevate chromosomal instability (Ganem *et al.*, 2009; Zasadil *et al.*, 2014), we propose that paclitaxel exerts its anti-cancer effects by increasing chromosomal instability over a maximally tolerated threshold. Moreover, breast cancers that exhibit chromosomal instability prior to therapy may be poised to respond to the increase in chromosomal instability caused by paclitaxel.

Results

Both 80 mg/m^2 and 175 mg/m^2 paclitaxel result in similar intratumoral concentrations in primary breast cancers

To determine whether multipolar mitotic spindles without mitotic arrest were fundamental for the efficacy of paclitaxel and were therefore caused by 80 mg/m^2 as well as 175 mg/m^2 paclitaxel, we enrolled patients in an ongoing clinical trial in which patients with newly diagnosed primary breast cancer were treated with standard-of-care weekly low-dose (80 mg/m^2) paclitaxel as a single agent. Enrolled patients were female with treatment naïve HER2-negative breast cancer, and consented to have timed research biopsies and blood tests. Patients with HER2-positive tumors were excluded from this study to eliminate the confounding variable of concurrent therapy with a HER2-targeted antibody. Data from the first 15 patients enrolled are reported here (ages 37-62, median 50; table 2.S1). One patient withdrew from the study and three patients were evaluated for a subset of endpoints due to insufficient biopsy material (2) or deviation from treatment protocol (1).

The trial design is depicted in Figure 2.1A. After diagnostic core needle biopsy, tumors were measured by ultrasound before patients received 12 weekly doses of 80 mg/m^2 paclitaxel infused over 1 hour. A second core biopsy and blood draw were obtained 20 hours after initiation of the first infusion of paclitaxel. This timepoint was selected because cultured breast cancer cells mount a robust mitotic arrest to high doses of paclitaxel at 20 hours, showing ≥15 fold increase in mitotic index as compared to vehicle-treated cells (Zasadil *et al.*, 2014). Therefore, we expected that mitotic arrest would also be evident in patient tumors at 20 hours. After 12 doses of 80 mg/m^2 paclitaxel, tumors were measured again by ultrasound. Tumor response was evaluated

by measurement of the largest tumor diameter at baseline and after paclitaxel therapy, according to Response Evaluation Criteria in Solid Tumors (RECIST) 1.1 guidelines (Eisenhauer *et al.*, 2009). After paclitaxel treatment and tumor imaging, patients received 4 cycles of the DNA damaging drugs Adriamycin/doxorubicin and cyclophosphamide (AC) and surgery, with the order at the discretion of the treating physician.

Quantification of paclitaxel concentrations in patient samples revealed that intratumoral concentrations ranged from 0.34 to 3.43 μM 20 hours after the first dose of 80 mg/m^2 paclitaxel, which extends the lower limit of the clinically relevant range measured after 175 mg/m^2 paclitaxel [1.1-9.0 μM; Table 2.1, (Zasadil *et al.*, 2014)]. Plasma concentrations of paclitaxel 20 hours after the first infusion ranged from 0.011 to 0.094 μM in our patient cohort (Table 2.1), in agreement with previous measurements (Hertz et al., 2018) and similar to what was observed after 175 mg/m^2 paclitaxel (Zasadil *et al.*, 2014). The degree of intratumoral accumulation of paclitaxel ranged from 9- to 172-fold (Table 2.1), consistent with its known uptake variability.

Mimicking the appropriate intratumoral concentration in cell lines was complicated by the fact that paclitaxel accumulates intracellularly to varying extents depending on the cell type and concentration used (Jordan et al., 1996; Yvon et al., 1999; Zasadil *et al.*, 2014). Therefore, identifying the concentration of paclitaxel with which to treat cells in order to achieve a clinically relevant intracellular concentration required measurements over a range of concentrations in each cell line. Liquid chromatography followed by tandem mass spectrometry (LC-MS/MS) was used to identify clinically relevant ranges of paclitaxel in MDA-MB-231 triple negative breast

cancer cells and MCF10A nontransformed breast epithelial cells, as well as in commonly used cellular models including HeLa cervical cancer cells and h-TERT immortalized retinal pigmented epithelial (RPE-1) cells (table 2.S2). As expected based on previous results (Jordan *et al.*, 1996; Yvon *et al.*, 1999; Zasadil *et al.*, 2014), the degree of intracellular paclitaxel concentration varied from 32-fold to 1360-fold based on cell type and the dose of paclitaxel administered. Low nanomolar doses of paclitaxel recapitulated clinically relevant intracellular paclitaxel concentrations in each of these cell lines (table 2.S2).

Paclitaxel induces multipolar spindles without mitotic arrest in primary breast cancer

To determine whether 80 mg/m^2 paclitaxel induces mitotic arrest or, like 175 mg/m^2 paclitaxel, multipolar mitotic spindles without mitotic arrest, tumor core biopsies acquired before and after paclitaxel therapy were analyzed by immunofluorescence (Figure 2.1B). Before paclitaxel therapy, the majority of mitotic cells displayed a normal bipolar mitotic spindle (Figure 2.1, B top and C). At 20 hours after 80 mg/m^2 paclitaxel treatment there was a substantial increase in multipolar mitotic cells in all patient cancers examined (Figure 2.1, B bottom and C), with increases ranging from 25-60% (Figure 2.1C, paired *t* test $p \leq 0.001$). This substantial increase in multipolar spindles was accompanied by only modest effects on the percentage of cells in mitosis (mitotic index; Figure 2.1D). Thus, both standard doses of paclitaxel induce multipolar spindles without mitotic arrest in patient tumors.

Multipolar spindles induced by paclitaxel focus into bipolar spindles with variable frequency

Division of duplicated chromosomes into >2 daughter cells on a multipolar spindle typically results in massive chromosome missegregation and inviable progeny (Ganem *et al.*, 2009). However, multipolar spindles often focus into bipolar spindles prior to chromosome segregation, which reduces chromosome missegregation rates and increases cell viability (Ganem *et al.*, 2009). Because spindle pole focusing could not be assessed in patient samples, which are fixed specimens that contain an insufficient observed number of cells in late stages of mitosis for accurate analysis, the propensity of paclitaxel-induced multipolar spindles to focus into bipolar spindles was assessed in MDA-MB-231 and Cal51 cells. These cells were selected because they are human triple negative breast cancer cell lines that lack expression of the estrogen receptor (ER) and progesterone receptor (PR) and do not overexpress human epithelial growth factor receptor 2 (HER2). Treatment with 10 nM paclitaxel resulted in a clinically relevant intracellular concentration in both MDA-MB-231 and Cal51 cells [as well as in MCF10A, RPE1 and HeLa cells; table 2.S2; (Zasadil *et al.*, 2014)]. Henceforth, all experiments using paclitaxel are at clinically relevant concentrations unless otherwise noted.

Consistent with the effects in patient tumors, 10 nM paclitaxel caused a substantial increase in multipolar spindles without inducing the peak mitotic index caused by higher concentrations of drug in all 5 cell lines (Figure 2.1E and F, 2.S1A to G). However, these cell lines differed in their ability to maintain paclitaxel-induced multipolar spindles (Figure 2.1G, 2.S1H to M). The percentage of spindle multipolarity

increased as cells progressed from early stages of mitosis (prometaphase and metaphase) to later stages (anaphase and telophase) in MDA-MB-231 cells (Figure 2.1G) and remained largely unchanged in RPE1 and HeLa cells (Figure 2.S1L and M). Whereas MDA-MB-231 (as well as RPE1 and HeLa) cells maintained multipolar spindles throughout division, Cal51 and MCF10A cells appeared to focus paclitaxel-induced multipolar spindles during mitotic transit (Figure 2.1G, 2.S1K).

Timelapse microscopy confirmed the propensity of Cal51 cells to focus paclitaxel- induced multipolar spindles (fig 2.S1 H and I). Cal51 cells expressing fluorescent α-tubulin and histone H2B (from transgenes or after CRISPR-mediated tagging of endogenous loci) to visualize microtubules and chromosomes respectively, were observed in the presence or absence of 10 nM paclitaxel. Whereas control Cal51 cells had bipolar spindles at anaphase onset and formed two daughter cells, in the presence of a clinically relevant dose of paclitaxel, most cells exhibited a transient multipolar spindle in the early stages of mitosis and approximately 40% of cells had a multipolar spindle at anaphase onset (Figure 2.S1H and I). Although over a third of cells entered anaphase with a multipolar spindle, continued spindle focusing coupled with partial cytokinesis failure produced two daughter cells in 95 ± 2% (range 93-96%) of divisions. While control-treated Cal51 cells showed the typical striking spindle elongation during anaphase, multipolar spindle elongation in the presence of paclitaxel was often quite abbreviated and/or followed by rapid spindle focusing, impeding identification of multipolar anaphase and telophase cells in fixed analysis. Thus, though fixed analysis underestimates anaphase/telophase multipolarity, timelapse analysis

confirms that, unlike MDA-MB-231 cells, Cal51 cells readily focus paclitaxel-induced multipolar spindles into bipolar spindles.

Persistent multipolarity causes paclitaxel-induced cell death

Next, we performed timelapse microscopy to track the fate of paclitaxel-treated cells. We noted that mitotic arrest, which is followed by death during mitosis or mitotic slippage to produce a tetraploid G1 cell, occurred very rarely in cells treated with clinically relevant concentrations of paclitaxel. Of all cells observed here, mitotic slippage occurred in 4 of 1060 (0.38%), death from mitosis in 17 of 1060 (1.6%), and mitotic arrest with an unknown fate in 7 of 1060 (0.67%), while the remaining cells successfully transited mitosis and divided their chromosomes in anaphase after a relatively brief mitotic delay.

Given that the vast majority of cells successfully completed mitosis, we tracked the fate of daughter cells resulting from these divisions in DMSO-treated controls and in clinically relevant concentrations of paclitaxel using 72-hour timelapse microscopy. We categorized cells based on whether they exhibited only a normal bipolar spindle or at least transient multipolarity. Cells with multipolar spindles, whether transient or persistent, showed a higher frequency of daughter cell death than cells with only bipolar spindles (Figure 2.1H). In order to determine if multipolar persistence led to cell death, cells with multipolar spindles were further subdivided based on the duration the multipolar spindle was maintained. Cells with the most persistent multipolar spindles maintained multipolarity throughout mitosis and produced three or more daughter cells. These divisions resulted in higher frequencies of daughter cell death than cells with a

multipolar spindle that persisted until anaphase onset, but produced two daughter cells as a result of spindle pole focusing after anaphase onset and/or partial cytokinesis failure (Figure 2.1H). These divisions resulted in higher frequencies of cell death than divisions with the lowest degree of multipolar persistence, which had a multipolar spindle in prometaphase that was subsequently focused into a bipolar spindle prior to anaphase onset and remained bipolar throughout anaphase and telophase to produce two daughter cells. Overall, multipolar divisions resulted in more cell death than bipolar divisions in both cell lines (Figure 2.1H), although multipolar divisions were rarer in Cal51 cells compared to MDA-MB-231 cells due to their increased propensity to cluster multipolar spindles.

To disentangle the contributions of persistent multipolarity from the effects of a delayed mitosis on cytotoxicity, we treated MDA-MB-231 and Cal51 breast cancer cell lines and non-transformed breast epithelial MCF10A cells with concentrations of paclitaxel that yielded similar mitotic delays (Figure 2.S2A). We found no significant difference in the duration of divisions that resulted in death of at least one daughter cell as compared to divisions that produced only viable daughter cells (Figure 2.S2 B to D). When comparing multipolar spindle persistence and cell fate under these conditions, we again observed that multipolar divisions resulted in more cell death than bipolar divisions in all three cell lines (Figure 2.S2E to G). Moreover, we found that multipolar spindles that were maintained longer in mitosis led to a higher rate of cell death compared to cells that focused multipolar spindles into bipolar spindles earlier in mitosis (Figure 2.S2E to G). These data support the conclusion that persistent multipolarity that

causes high rates of chromosome missegregation, rather than mitotic delay, is responsible for paclitaxel cytotoxicity.

Increasing multipolar divisions improves paclitaxel efficacy in breast cell lines

If chromosome division on multipolar spindles is important for the efficacy of paclitaxel, increasing paclitaxel-induced multipolar divisions should increase paclitaxel cytotoxicity. Two methods were used to increase multipolar divisions in Cal51 breast cancer cells, which readily cluster paclitaxel-induced multipolar spindles (Figure 2.1G, 2.S1, H and I). First, an inhibitor of the kinesin-like protein HSET/KifC1, which functions in spindle pole clustering in cells with and without centrosome amplification (Kleylein-Sohn et al., 2012; Kwon et al., 2008), was used. Though Cal51 cells did not overexpress HSET (Figure 2.S1J), inhibition of HSET activity with CW-069 (Watts et al., 2013) in the presence of paclitaxel was sufficient to increase multipolar spindles in late stages of mitosis without affecting early mitotic spindle polarity (Figure 2.2, A to C, 2.S3, A and B). Moreover, this combination substantially decreased cell viability and increased cell death when compared to cells treated with paclitaxel alone (Figure 2.2, D and E, 2.S3, C and D). Similar results were achieved with a second inhibitor of HSET, AZ82 (Figure 2.S3, E to H).

As a second approach to increase multipolar divisions in paclitaxel, we genetically introduced centrosome amplification, which is known to induce at least transient multipolar spindles (Ganem *et al.*, 2009). For these experiments, we used nontransformed breast epithelial MCF10A cells, which have a low basal rate of centrosome amplification. Centrosome amplification was accomplished by tetracycline

(tet)-inducible overexpression of Polo-like kinase 4 (Plk4), the master regulator of centriole duplication (Godinho et al., 2014; Habedanck et al., 2005). Overexpression of Plk4 produced centrosome amplification in a majority of cells over at least 10 days (Figure 2.S4, A and B). In fixed cells, Plk4 overexpression increased multipolar spindles early in mitosis, but these had largely focused into bipolar spindles in anaphase and telophase cells (Figure 2.S4, C to F). However, in a subclinical dose of paclitaxel (1 nM), centrosome amplification substantially increased the incidence of multipolar spindles both before and after anaphase onset, as compared to paclitaxel treatment alone (Figure 2.S4, C to F). Timelapse analysis of MCF10A cells expressing histone H2B-mNeonGreen and mScarlet-tubulin (Figure 2.3, A and B) revealed that compared to paclitaxel treatment alone, centrosome amplification increased the incidence of multipolar spindles and the number of poles per spindle before (Figure 2.S4, G and H), after (Figure 2.S4I), and at (Figure 2.3C, 2.S4J) anaphase onset. Importantly, death of cells treated with paclitaxel was dramatically increased by Plk4 overexpression and the resulting increase in multipolarity (Figure 2.3, C to E). Although overall mitotic duration did not predict cell fate (Figure 2.S4K), cells that spent more time after anaphase onset with multipolar spindles than bipolar spindles were particularly likely to die (Figure 2.3E). Consistent with this, centrosome amplification substantially reduced the metabolic viability of parental MCF10A cells treated with a subclinical dose of paclitaxel (Figure 2.S4L). Thus, increasing multipolar divisions via HSET inhibition or centrosome amplification sensitizes cells to paclitaxel.

Reducing multipolar divisions reduces paclitaxel cytotoxicity

If chromosome division on multipolar spindles is important for the efficacy of paclitaxel, reducing paclitaxel-induced multipolar divisions should decrease paclitaxel cytotoxicity. To test this, we used two strategies to reduce paclitaxel-induced spindle multipolarity in MDA-MB-231 human breast cancer cells, a majority of which underwent multipolar divisions when treated with clinically relevant concentrations of paclitaxel (Figure 2.1G). The first strategy involved chemical inhibition of the kinase Monopolar spindles 1 (Mps1; also known as TTK). Multiple clinical trials aimed at determining whether Mps1 inhibition increases the efficacy of paclitaxel in solid tumors are currently ongoing (NCT03411161, NCT03328494, NCT02366949), providing a rationale to mechanistically examine this combination treatment. A pharmacological inhibitor of Mps1, reversine (Santaguida et al., 2010), reduced mitotic timing both in the absence and presence of paclitaxel (Figure 2.S5A). Reversine treatment did not affect establishment of bipolar spindles in control cells or multipolar spindles in paclitaxel-treated cells (Figure 2.4, A and B, 2.S5B). However, inhibition of Mps1 substantially reduced the incidence of multipolar spindles in late stages of mitosis (Figure 2.4A and C, 2.S5C), suggesting that reversine impaired the maintenance of paclitaxel-induced multipolarity, permitting cells to form bipolar spindles. Timelapse microscopy of MDA-MB-231 cells expressing GFP-tubulin and RFP-histone H2B confirmed that Mps1 inhibition substantially reduced the number of spindle poles in MDA-MB-231 cells entering anaphase (Figure 2.4D). Spindle poles continued to focus after initial chromosome separation at anaphase onset (Figure 2.S5D), resulting in a substantial decrease in the number of daughter cells formed (Figure 2.4E), including an increase in the formation of a single daughter cell from divisions in the combined treatment of

paclitaxel and reversine (Figure 2.4E). These single daughter cells almost exclusively resulted from spindle pole focusing after anaphase onset and/or cytokinesis failure, rather than from mitotic slippage, which was observed in only 2 of 224 (0.89%) of cells. Consistent with a reduction in multipolar divisions and in chromosome missegregation, reversine treatment increased metabolic survival and decreased cell death in cells treated with paclitaxel (Figure 2.4, F and G). Whole genome doubling as a result of single daughter cell formation may contribute to the buffering of chromosome missegregation in the combination treatment. A second Mps1 inhibitor, AZ3146 (Hewitt et al., 2010), also increased metabolic survival and colony-forming ability in cells treated with paclitaxel (Figure 2.S5, E and F), decreasing the likelihood that the reduction in paclitaxel efficacy was due to off-target effects of reversine.

A second method of reducing paclitaxel-induced multipolar divisions involved upregulation of the mitotic checkpoint protein Mitotic Arrest Deficient 1 (Mad1), which is frequently observed in breast cancer and is associated with poor patient prognosis (Ryan et al., 2012). We generated MDA-MB-231 breast cancer cells stably expressing tet-inducible Mad1-YFP (Wan et al., 2019). 24 hour tet treatment induced uniform, clinically relevant Mad1 upregulation [Figure 2.S6, A and B, (Ryan *et al.*, 2012; Wan *et al.*, 2019)], which decreased the duration of mitosis (Figure 2.S6C), without affecting the incidence of early mitotic spindle multipolarity in cells treated with paclitaxel (Figure 2.5, A and B, S6D). However, Mad1-YFP expression substantially decreased the incidence of multipolar anaphase and telophase spindles in MDA-MB-231 cells treated with 10 nM paclitaxel (Figure 2.5A and C, 2.S6E) and reduced the number of daughter cells formed (Figure 2.5D). While most divisions in MDA-MB-231 cells treated with paclitaxel

produced 3 daughter cells, in paclitaxel-treated cells expressing Mad1-YFP most divisions resulted in 2 daughter cells (Figure 2.5D). Although these divisions sometimes resulted in a single daughter cell, these single daughters exclusively resulted from spindle pole focusing after anaphase onset and/or cytokinesis failure, rather than from mitotic slippage, which was observed in 0 of 203 cells analyzed. Hence, Mad1 upregulation had no impact on multipolar spindle formation early in mitosis but reduced the maintenance of multipolar spindles in MDA-MB-231 cells, resulting in fewer multipolar divisions and reduced chromosomal instability. Importantly, when treated with 10 nM paclitaxel, cells expressing Mad1-YFP showed decreased cell death (Figure 2.5E) and increased metabolic viability and colony formation (Figure 2.5F and 2.S6F) as compared to isogenic MDA-MB-231 cells without Mad1 upregulation.

Consistent with these results in cell culture, expression of Mad1-YFP reduced the paclitaxel sensitivity of orthotopic MDA-MB-231 tumors in athymic nude mice treated with a clinically relevant dose of paclitaxel every other day for 5 days once tumors reached a minimum volume of 75 mm^3 (1.19-2.28 μM after iv injection of 30 mg/kg paclitaxel; Figure 2.5G, 2.S6G). Tumors expressing Mad1-YFP were resistant to paclitaxel as compared to isogenic parental MDA-MB-231 cells with endogenous Mad1 expression. Whereas tumors expressing Mad1-YFP shrank by 31% over a period of 14 days and then grew to their original size by 18 days, parental tumors shrank by 53% over a period of 25 days and did not recover to their initial size given a period of 44 days (Figure 2.5H, 2.S6, H and I). Thus, reducing paclitaxel-induced multipolar divisions in MDA-MB-231 cells reduced chromosomal instability and decreased the cytotoxicity of paclitaxel in vitro and in vivo.

Pre-anaphase multipolarity is not predictive of paclitaxel patient response

Although cell culture experiments demonstrated that the maintenance of multipolar spindles in late stages of mitosis was critical for paclitaxel efficacy, patient samples cannot be assessed for multipolar spindle maintenance due to a lack of observed anaphase and telophase cells. In all patient samples, a large majority of mitotic cells identified both before and after paclitaxel treatment were in stages of mitosis prior to anaphase onset (96 +/- 4%, mean +/- SD, range 88%-100%). This precludes determination of the prevalence of multipolar spindle focusing in fixed biopsy specimens.

In our analysis of predominately pre-anaphase mitotic cells, neither the overall incidence of spindle multipolarity achieved in response to paclitaxel nor the percent increase in multipolar spindles were predictive of patient response (Figure 2.S7, A to D), likely because these spindles in early stages of mitosis could be subsequently focused into bipolar spindles with varying efficiency. As in our previous patient cohort treated with 175 mg/m^2 paclitaxel (Zasadil *et al.*, 2014), response did not correlate with the intratumoral concentration of paclitaxel (Figure 2.S7E). Ki67, which is used clinically as a measure of the proliferative ability of tumors, correlated with mitotic index (Figure 2.S7F). However, neither pre-treatment Ki67 nor mitotic index before or after treatment correlated with tumor response (Figure 2.S7, G to I) suggesting that, though a minimum amount of proliferation is likely necessary for paclitaxel response, above a minimal threshold of proliferation, additional factors dictate patient outcome. Thus, these

characteristics are not sufficient to predict the response of individual tumors to paclitaxel and an additional metric(s) is necessary.

Chromosomal instability sensitizes breast cancer cells to paclitaxel

To test whether other mechanisms of chromosomal instability sensitize cells to paclitaxel, we increased chromosomal instability in Cal51 cells, which typically focus paclitaxel-induced multipolar spindles such that a majority of cells undergo bipolar divisions (Figure 2.1G, 2.S1, H and I), via two mechanisms. First, we inducibly upregulated Mad1-mNeonGreen (Figure 2.S8, A to B). Whereas expression of Mad1 decreased chromosomal instability in paclitaxel-treated MDA-MB-231 cells by reducing the high percentage (>89%) of cells that underwent multipolar divisions (Figure 2.1G, 2.5C), the incidence of multipolar divisions in paclitaxel-treated Cal51 cells was relatively low and unaffected by expression of Mad1-mNeonGreen (Figure 2.6, A to C, 2.S8, C and D). Although upregulation of Mad1 did not impact multipolar divisions in this cell type, it impaired mitotic checkpoint signaling which reduced mitotic timing and increased mitotic errors consistent with chromosome missegregation in the absence of paclitaxel, as expected (Figure 2.6D, 2.S8E). Expression of Mad1-mNeonGreen also increased mitotic defects indicative of chromosomal instability in the presence of paclitaxel in Cal51 cells (Figure 2.6D). Defects during anaphase and telophase primarily occurred on bipolar spindles (Figure 2.S8, F to H). This increase in chromosomal instability increased paclitaxel sensitivity; Cal51 cells expressing Mad1-mNeonGreen had decreased metabolic viability and colony forming ability and increased cell death in paclitaxel as compared to cells without Mad1-mNeonGreen (Figure 2.6, E and F, 2.S8, I

and J). Similar results were observed in DLD1 cells, which also primarily exhibited bipolar divisions when treated with paclitaxel (Figure 2.S8, K to M).

We also induced chromosomal instability by inhibition of the plus-end directed kinesin CENtromere associated Protein E (CENP-E) with GSK923295 *(Wood et al., 2010).* Timelapse microscopy of cells with endogenously labeled histone H2B-mScarlet and α-tubulin-mNeonGreen (Figure 2.6, G to O) revealed that, as expected, control cells typically underwent a normal division (Figure 2.6G), while CENP-E inhibition alone caused a substantial increase in misaligned chromosomes at or near spindle poles (Figure 2.6H). 80% +/- 8.0% (mean +/- SEM) of cells treated with GSK923295 alone initially displayed misaligned chromosomes, though many of these ultimately aligned prior to anaphase onset (Figure 2.6H and J to L). CENP-E inhibition did not affect the propensity of Cal51 cells to focus paclitaxel-induced multipolar spindles (Figure 2.6M and N). It did, however, substantially increase the frequency with which cells entered anaphase with misaligned chromosomes, as well as the number of misaligned chromosomes at anaphase onset, which increased chromosomal instablility over paclitaxel treatment alone (Figure 2.6I and J to L). In addition to increased chromosomal instability, treatment of cells with GSK923295 and paclitaxel also increased cell death (Figure 2.6O). *Importantly,* a formal Chou-Talalay synergy test (Chou, 2010) confirmed that CENP-E inhibition is synergistic with clinically relevant doses of paclitaxel (table 2.S3). Thus, two mechanisms of increasing chromosomal instability (Mad1 upregulation and CENP-E inhibition) increased sensitivity to paclitaxel.

Pre-treatment chromosomal instability sensitizes metastatic breast cancer to taxane treatment

To investigate the effect of chromosomal instability on the sensitivity of patient cancers to paclitaxel, we followed these promising results in cell culture with a retrospective analysis of patient samples. We identified 37 cases of metastatic breast cancer with measurable disease and available archived tissue that were treated with single agent taxane therapy. Patients either received paclitaxel (16 cases), albumin-bound paclitaxel (nab-paclitaxel; 17 cases), or the paclitaxel analog docetaxel (4 cases). Patient characteristics are summarized in table 2.S4. Response to taxane therapy was evaluated according to RECIST 1.1 guidelines [Figure 2.7, A to C; (Eisenhauer *et al.*, 2009)]. Rates of chromosomal instability prior to treatment were measured with interphase fluorescence in situ hybridization (FISH) using centromeric probes for 6 different chromosomes. Chromosomal instability was quantified by calculating the average percentage of non-modal chromosomes [Figure 2.7D, supplementary methods, (Denu *et al.*, 2016)]. Taxane response did not correlate with breast cancer receptor subtype (Figure 2.7C) or several variables previously suggested to influence taxane sensitivity, including β-tubulin III and phospho-glycoprotein 1 (P-gp1) expression (Figure 2.S9). Samples from metastatic tumors were available in 21 cases, 11 of which also had matching tissue from the primary site. Only primary tumor samples were available in 16 cases. When including both primary and metastatic samples, we observed a direct correlation between pre-treatment chromosomal instability and taxane response, such that cancers with higher rates of chromosomal instability before therapy responded preferentially to taxane treatment (Figure 2.7E). This correlation plot yielded a slope of -0.71%, meaning for every percent increase in non-modal chromosomes, response to

therapy improved by 0.71%. Removal of the cases containing samples from only primary tumors reduced the sample size but yielded a stronger correlation with a slope of -0.93% (Figure 2.7F). These results demonstrate that, in this cohort, metastatic breast cancers with higher baseline rates of chromosomal instability experienced greater tumor shrinkage in response to taxane therapy.

Discussion

Paclitaxel remains a cornerstone of breast cancer treatment, even with the introduction of targeted therapy and immune checkpoint inhibitors. Prior to our work, it was largely accepted that paclitaxel exerts its anti-cancer effects by causing mitotic arrest, as it does at typically used concentrations in cell culture. It is now clear that neither standard-of-care paclitaxel treatment regimen produces an intratumoral concentration that is sufficient to arrest breast cancers in mitosis. Instead, contrary to the expectation of the last several decades, the anti-cancer effects of both doses of paclitaxel are due to chromosome missegregation on multipolar spindles and not mitotic arrest.

Our data further demonstrated that clustering of multipolar spindles represents a major mechanism of paclitaxel resistance, while drug efflux pumps do not. Paclitaxel accumulated in all tumor samples at 9- to 172-fold the concentration found in plasma (Table 2.1) and induced multipolar spindles in all samples (Figure 2.1C). No correlation was observed between intratumoral paclitaxel concentration and patient response (Figure 2.S7E). These data support the conclusion that resistance is due to multipolar spindle focusing rather than reducing the intratumoral concentration of paclitaxel. Tumor cells exhibit varying capacities to focus paclitaxel-induced multipolar spindles (Figure

2.1G and 2.S1H to M). Previous experiments have established that daughter cells arising from multipolar divisions that produce more than two cells are often inviable and rarely continue to proliferate (Ganem *et al.*, 2009; Kwon *et al.*, 2008). Paclitaxel-induced multipolar spindles can be focused into bipolar spindles throughout mitosis (Fig 2.1H, 2.S2). However, increasing the duration of spindle multipolarity, particularly after anaphase onset, increased the likelihood of chromosome missegregation and cell death (Figure 2.1H, 2.2 and 2.3, 2.S2). Conversely, decreasing the time spindles spend in a multipolar state increased cell survival and decreased paclitaxel efficacy (Figure 2.1H, 2.4, 2.5, 2.S2). These data support the conclusion that multipolar spindle persistance contributes substantially to paclitaxel cytotoxicity. Consistent with this, down-regulation of the MTUS1 gene, which was associated with complete response to neoadjuvant chemotherapy that included taxane in three cohorts of breast cancer patients, increased the incidence of multipolar spindles in low-dose paclitaxel (Rodrigues-Ferreira et al., 2019). Thus, treatments that prevent cells from focusing paclitaxel-induced multipolar spindles into bipolar spindles are likely to improve paclitaxel efficacy. In cells, inhibition of HSET increased multipolar spindle persistence and paclitaxel efficacy (Figure 2.2, 2.S3), but HSET inhibitors suitable for in vivo use are not yet available. Low amounts of replication stress have also been shown to increase the incidence of paclitaxel-induced multipolar divisions in cell culture, suggesting this may be a method of potentiating paclitaxel efficacy translatable to patient tumors (Wilhelm et al., 2019).

Although efforts have been made to identify a biomarker for paclitaxel, none have been implemented in the clinic, in part due to a limited – and erroneous – understanding of the mechanism of paclitaxel. The importance of paclitaxel-induced multipolar spindles

is their ability to induce chromosomal instability. Genetic or pharmacological insults that each cause low, tolerated rates of CIN can be combined to increase the rate of CIN over a maximally tolerated threshold (Funk *et al.*, 2016; Godek *et al.*, 2016; Laucius *et al.*, 2019; Silk *et al.*, 2013; Weaver *et al.*, 2007). Multipolar divisions result in missegregation of multiple chromosomes, typically more than bipolar divisions with lagging or misaligned chromosomes (Ganem *et al.*, 2009). However, in cells that focused paclitaxel-induced multipolar spindles into bipolar spindles, further increasing the rate of chromosomal instability effectively increased sensitivity to paclitaxel (Fig 2.6, table 2.S3). Importantly, pre-treatment chromosomal instability correlated with response to taxane in metastatic breast cancer, even without determining the ability of individual tumors to focus paclitaxel-induced multipolar spindles (Fig 2.7). Thus, these data strongly support the utility of pre-treatment chromosomal instability as a predictive biomarker for paclitaxel response and suggest that treatments that increase the rate of chromosomal instability will increase response to paclitaxel.

Surprisingly, inhibition of Mps1 – which abrogates the mitotic checkpoint and causes chromosomal instability in otherwise unmanipulated cells – decreased chromosomal instability and cell death in MDA-MB-231 cells treated with clinically relevant concentrations of paclitaxel due to a decrease in multipolar divisions (Figure 2.4, 2.S5). Previous preclinical studies, which typically used high concentrations of paclitaxel we now recognize to be above the clinically relevant range, have found that Mps1 inhibition sensitizes cells to paclitaxel (Jemaà et al., 2013; Wengner et al., 2016). Based on this, clinical trials aimed at determining whether Mps1 inhibition increases the efficacy of paclitaxel in solid tumors are ongoing (NCT03411161, NCT03328494,

NCT02366949). It is possible that Mps1 inhibition will sensitize cancer cells that focus paclitaxel-induced multipolar spindles by increasing the rate of chromosomal instability on bipolar spindles, similar to what we observed with Mad1 upregulation in Cal51 and DLD1 cells and CENP-E inhibition in Cal51 cells (Figure 2.6, 2.S8, table 2.S3). However, the variability in spindle focusing among cancers may present an unexpected challenge when combining Mps1 inhibitors with paclitaxel that prevents this approach from being uniformly successful.

We previously showed that Mad1 upregulation causes resistance to high concentrations of microtubule poisons, including paclitaxel, that cause mitotic arrest (Ryan *et al.*, 2012). We now understand that these concentrations are supraphysiological. At clinically relevant doses of paclitaxel, the differential impact of Mad1 upregulation on paclitaxel sensitivity in Cal51 and MDA-MB-231 cells was initially surprising. The differing ability of these cell lines to focus paclitaxel-induced multipolar spindles offers a unifying explanation, in which Mad1 upregulation increases chromosomal instability in paclitaxel-treated Cal51 cells but decreases chromosomal instability in paclitaxel-treated MDA-MB-231 cells (Figure 2.5, 2.6). Discovery of the cell-intrinsic mechanisms used to focus paclitaxel-induced multipolar spindles is an important area for future research that will permit further mechanistic insight.

There are several limitations to our study. Our primary cohort is relatively young (median age 50), in part due to a relatively high proportion of triple negative patients, and consists of predominately white, non-Hispanic or Latino patients. The retrospective metastatic study was underpowered to validate a predictive biomarker and chromosomal instability does not explain all of the patient-to-patient variation in

response in this cohort. We have considered three possible explanations. First, this may be because of modifying roles of other factors, including proliferation rate, p-glycoprotein, and b-tubulin III expression, though we did not find that these correlated with response in our dataset (Figure 2.S9). Multipolar spindle clustering is likely to be a key additional factor in determining taxane response that could be used to improve a chromosomal instability-based biomarker. Given that centrosome amplification increased maintenance of paclitaxel-induced multipolar spindles in MCF10A cells (Figure 2.3), centrosome amplification prior to therapy may impair focusing of paclitaxel-induced multipolar spindles and provide an additional predictor of response. Our recently developed method to quantitate centrosome amplification in circulating tumor cells from metastatic breast cancer patients (Singh et al., 2020) may be useful in this regard. Second, FISH is limited by sampling errors, sectioning artifacts, and analysis of only a subset of chromosomes. In the future, more comprehensive measures of cell-to-cell variation in chromosomes, like single-cell sequencing, may provide more accurate measures of chromosomal instability. Third, in this retrospective study, we were unable to control for prior treatments, site of biopsy, type of taxane used, and other sources of biologic variation such as breast cancer subtype or hormone receptor status. Therefore, we regard this as proof-of-principle that chromosomal instability relates to taxane reponse which accords with the laboratory experiments and mechanistic insights obtained from timed tumor biopsies after paclitaxel. Future studies of a larger homogenous cohort of patients will permit a more robust test of chromosomal instability as a predictive biomarker.

In conclusion, paclitaxel uniformly increases multipolar spindles in breast cancers. Focusing of paclitaxel-induced multipolar spindles is a major mechanism of paclitaxel resistance, and identification of agents that maintain paclitaxel-induced multipolarity is of high priority to improve the clinical utility of paclitaxel. Cancers with a pre-existing rate of chromosomal instability are more sensitive to taxanes than chromosomally stable cancers, and our findings provide support that pre-treatment chromosomal instability can be used as a predictive biomarker of paclitaxel response. Such a biomarker would substantially improve patient outcomes by sparing non-responders paclitaxel-associated toxicities and reducing delays in receiving effective treatment.

Materials and Methods

Study Design

This is an ongoing study of the mechanism of paclitaxel in human breast cancer. The objectives were to determine clinically relevant paclitaxel concentrations and their effects on mitosis, chromosomal instability, cell proliferation, and response to treatment. These objectives were addressed by measurement of intratumoral and intracellular paclitaxel concentrations, immunofluorescence analysis of patient biopsies and cell lines treated with clinically relevant concentrations of paclitaxel (unless otherwise noted), orthotopic studies, FISH, and quantification of patient response according to RECIST 1.1 guidelines (Eisenhauer *et al.*, 2009). All data presented here have been replicated in three mice (six tumors) or in 2-5 biological replicates for cell culture experiments. The patient sample size was selected to provide a sufficient number of

biopsies for sampling intratumoral drug concentrations, effects on mitosis, cell-to-cell variation in chromosome copy number, and patient response. Fixed data analysis was blinded by concealment of slide labels. Cell samples and mice were assigned randomly to experimental groups. Data collection for each experiment is detailed in the respective figures, figure legends, and methods. Data for experiments where $n < 20$ are included in data file S1.

80 mg/m^2 paclitaxel study

Patients who volunteered to participate in the 80mg/m^2 paclitaxel study were enrolled in a prospective trial at the UW Carbone Cancer Center specifying the treatment, biopsy, and analysis plan. The protocol was approved by UW Health Sciences Institutional Review Board, ID 2016-1489, assigned UWCCC protocol number UW16106, conducted in accordance with the ethical standards established in the 1964 Declaration of Helsinki and registered on clinicaltrials.gov (NCT03096418). Patients were enrolled if they had previously untreated locally advanced breast cancer for which neoadjuvant chemotherapy was indicated. Subjects received four cycles of 80 mg/m^2 paclitaxel, per standard-of-care, with biopsy and treatment as outlined in Figure 2.1A. A research biopsy was obtained 18–22 hours after start of the first infusion. After four cycles of paclitaxel, follow-up ultrasound imaging was performed to assess response to therapy and patients continued with surgery and anthracycline-based chemotherapy, per physician discretion. Data analysts were blinded from patient response information until the study was completed and all data had been collected. Patient response was evaluated by an independent board-certified breast imaging radiologist who was blinded

from the results of the study objectives. One patient withdrew and 3 patients were excluded from specific endpoints because of insufficient sample collected by biopsy (2) or deviation from treatment protocol (1). There were no major complications from protocol-mandated research biopsy.

Metastatic taxane study

We identified patients who were treated with a taxane-based regimen for metastatic breast cancer and then identified those with measurable disease. For these cases, response to taxanes was assessed by manual review of CT imaging following RECIST 1.1 criteria (Eisenhauer *et al.*, 2009). Next, all cases with available archived tissue were identified and selected for analysis of potential biomarkers of paclitaxel as described. The protocol was approved through waiver of consent by UW Health Sciences Institutional Review Board, ID 2015-1584, assigned UWCCC protocol number UW15089, and conducted in accordance with the ethical standards established in the 1964 Declaration of Helsinki.

Statistical Analysis

Statistical analysis was performed using GraphPad Prism, R, or Mstat 6.4.2 software (http://www.mcardle.wisc.edu/mstat/index.html). Student's *t*-tests (two-tailed) were used to assess significance, unless otherwise noted. The Sen-Adichie test for parallelism was used for MTT assay growth curves (Figure 2D, 4F, 5F, 6E and S4L) and mouse orthotopic growth curves (Figure 5H, S6H-I), Wilcoxon rank sum test was used in Figure 3E, a Mann-Whitney test was used in Figure S8J, and simple linear regression

was used for correlation plots (Figure S7C-I). The lines in Figure 7 and S9 were fit using least squares regression in the R computing language, version 3.6.3. Other statistical parameters including the number of cells analyzed and the number of replicates are reported in the respective figure legends.

Acknowledgments

We thank Heather Green in the UWCCC 3P lab core facility and Cameron Scarlett in the School of Pharmacy mass spectrometry facility for their assistance with paclitaxel measurements, Jessica Muszynski in the BRMS core for performing orthotopic experiments, Toshi Kinoshita in the Translational Research Initiatives in Pathology (TRIP) lab for histology services, Dr. Duane Compton for NuMA antibody, Dr. David Pellman for the inducible Plk4 MCF10A cell line, Dr. Theodorus Gadella for mScarlet (Bindels et al., 2017), our patients for their participation in this research, and members of the Weaver, Burkard, and Suzuki laboratories for insightful discussions.

Funding

This work was supported, in part, by University of Wisconsin Carbone Cancer Center Support Grant P30 CA014520, the Department of Pathology and Laboratory Medicine, Department of Defense grants W81XWH-16-1-0049 (B.A.W.) and W81XWH-16-1-0050 (M.E.B.), National Institutes of Health grants R01CA234904 (B.A.W., M.E.B.), R01GM104192 (T.S.B.), T32 CA009135 (C.M.S.), T32 GM008688 (J.F., A.S.Z.), Amerian Cancer Society Research Scholar Grant RSG-15-006-01-CCG (B.A.W.), and American Heart Association fellowship 16PRE29650011 (J.W.).

Author contributions

C.M.S., T.S.B., M.E.B., B.A.W. conceived and designed experiments. C.M.S., K.E., J.B.T., A.L., A.S.Z., L.M.Z., R.M., J.F., A.M.L., J.J.L., K.C-S., S.M.M., A.M.F. performed experiments, collected, and analyzed data. J.W. generated cell lines. K.B.W, A.J.T., R.O'R., and M.E.B enrolled patients. C.M.S., and R.J.C. performed statistical analysis. C.M.S. and B.A.W. wrote the manuscript. All authors reviewed the manuscript.

Competing interests

M.E.B. declares the following: Medical advisory board of Strata Oncology; Research funding from Abbvie, Genentech, Puma, Arcus, Apollomics, Loxo Oncology/Lilly, and Elevation Oncology.

Figure 2.1. Clinically relevant concentrations of paclitaxel cause multipolar spindles without mitotic arrest in breast cancer patients and cells.

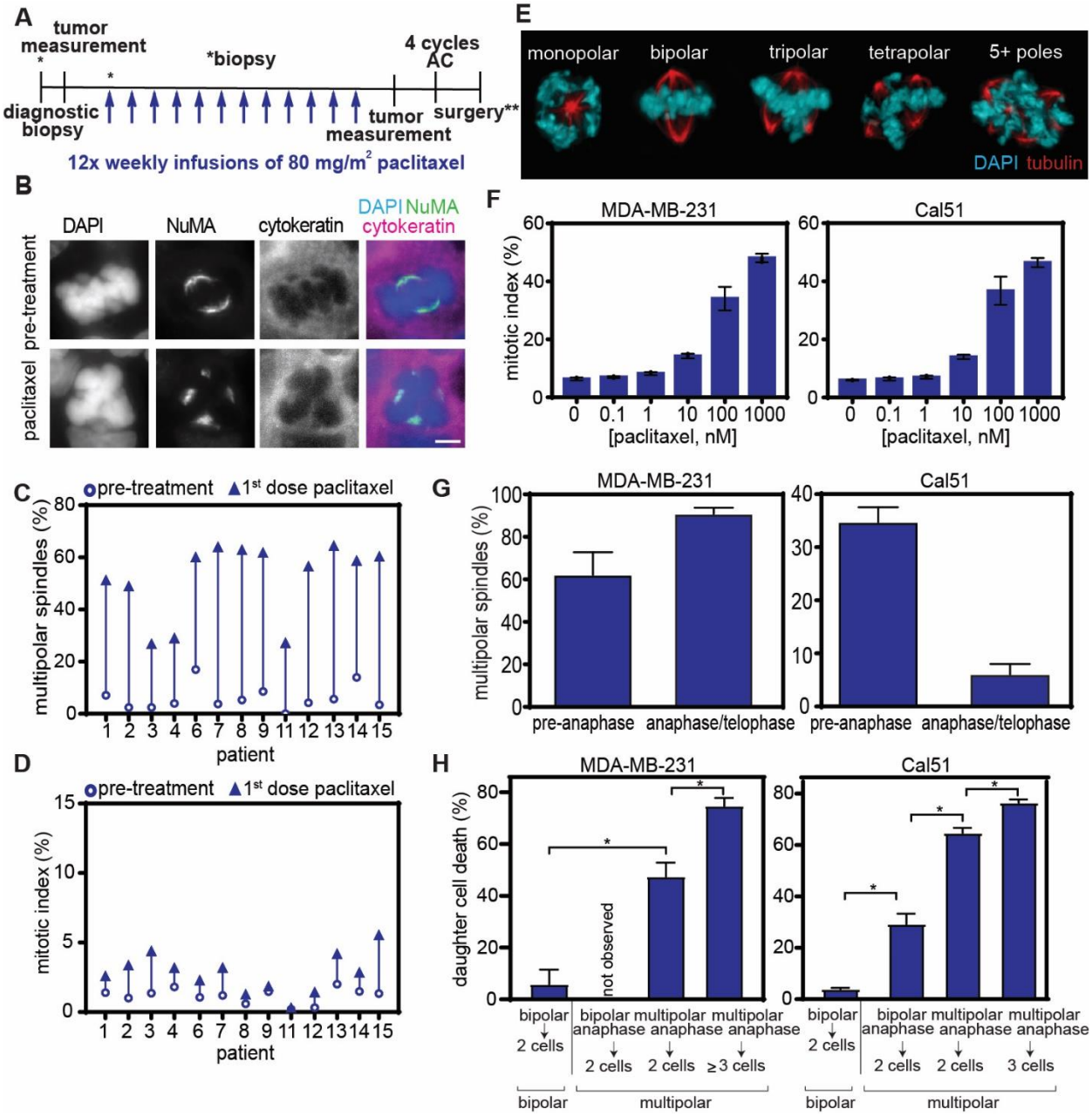

Figure 2.1. Clinically relevant concentrations of paclitaxel cause multipolar spindles without mitotic arrest in breast cancer patients and cells. **A**) Schematic showing trial design. Research biopsies were obtained prior to paclitaxel treatment and 20 hours after the first dose of paclitaxel. AC = Adriamycin and cyclophosphamide. **indicates that surgery could occur before or after AC, per physician recommendation. **B**) Representative images of bipolar (top) and multipolar (bottom) mitotic cells in patient tumors before and after paclitaxel treatment. Mitotic cells were identified based on DNA morphology and the presence of a mitotic spindle, labeled by Nuclear Mitotic Apparatus protein (NuMA), which localizes to spindle poles. Pan-cytokeratin was used to discriminate between breast epithelial (tumor) cells and stroma. Scale bar, 5 μm. **C-D**) Mitotic effects of 80 mg/m^2 paclitaxel treatment in primary breast cancer patients. Quantification of (**C**) multipolar mitotic spindles, defined as containing >2 NuMA foci, and (**D**) mitotic index before (open circle) and after (arrowhead; the direction indicates increase or decrease) paclitaxel treatment. D, n≥500 cells. For assessment of multipolar spindles in C, mitotic cell sample sizes for patients are 113, 41, 100, 101, 106, 79, 75, 35, 6, 24, 106, 86, and 116 cells, respectively, pre-treatment and 109, 100, 104, 103, 108, 103, 27, 63, 11, 30, 110, 102 and 101 cells, respectively, after treatment. Samples from patients 5 and 10 could not be analyzed due to insufficient tumor tissue collected by biopsy and withdrawal of consent, respectively. **E)** Images of mitotic spindles with the indicated number of poles in MDA-MB-231 cells after treatment with 10 nM paclitaxel. **F**) Quantification of mean mitotic index +/- SEM. n≥300 cells from each of 3 independent experiments. **G)** Quantification of multipolar spindles (mean +/- SD) in Cal51 and MDA-MB-231 cells prior to anaphase onset (n≥100 cells in each of 3 replicates) and in

anaphase and telophase (n≥50 cells in each of 3 replicates) in response to 10 nM paclitaxel. **H**) Quantification of percent daughter cell death from long term timelapse microscopy. n≥50 daughter cells in each of 2 replicates. *P<0.05.

Figure 2.2: Elevating the incidence of multipolar divisions in paclitaxel via HSET inhibition increases cytotoxicity.

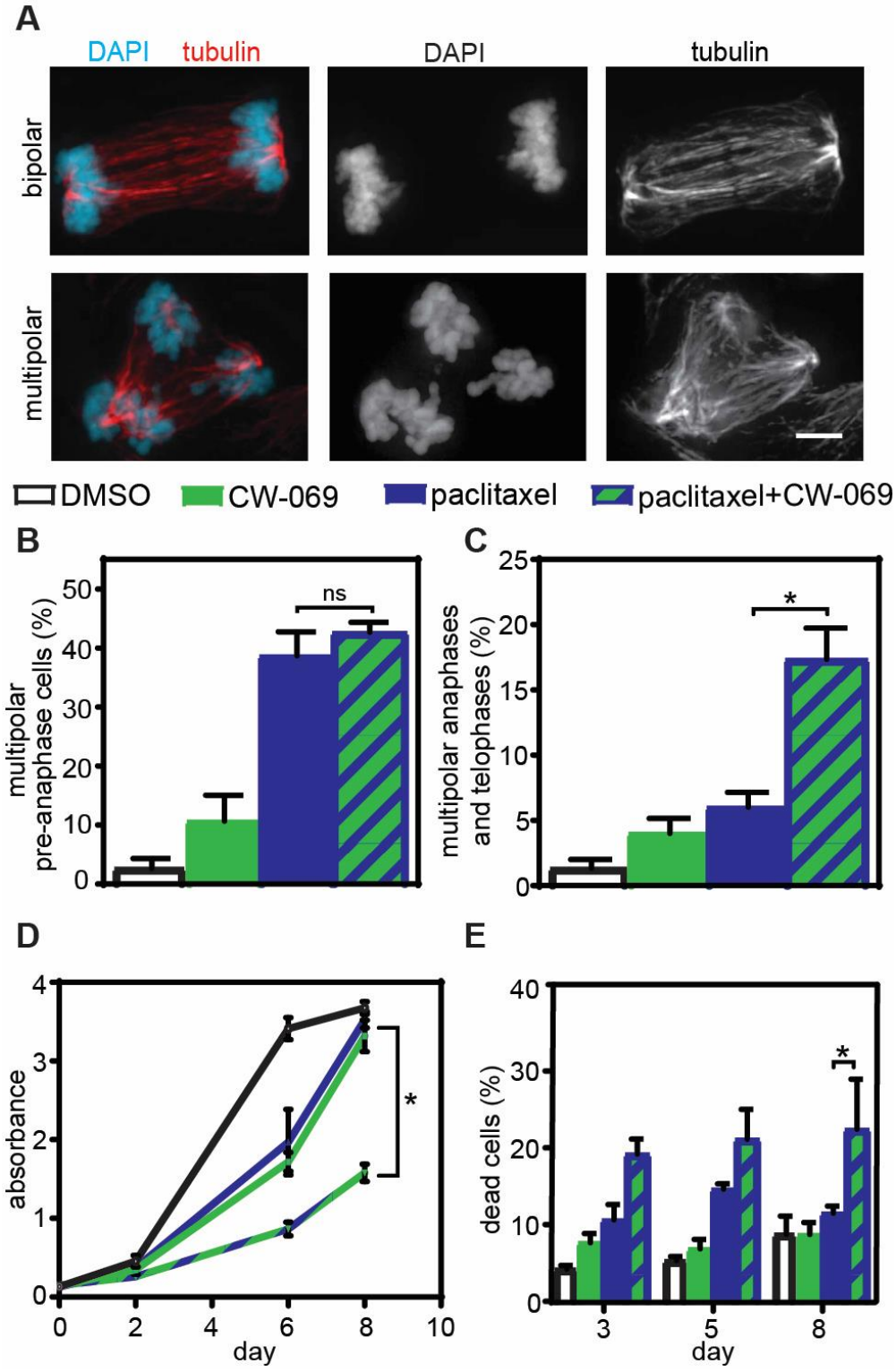

Figure 2.2: Elevating the incidence of multipolar divisions in paclitaxel via HSET inhibition increases cytotoxicity. A) Images of bipolar (top) and multipolar (bottom) anaphase cells. Scale bar, 5 μm. **B-C**) Percent of multipolar pre-anaphase, and anaphase/telophase spindles in Cal51 cells following treatment with paclitaxel and the HSET inhibitor CW-069. Mean percentage +/- SEM of mitotic cells with multipolar spindles prior to anaphase (B, n≥ 100 cells in each of 3 replicates) and after anaphase onset (**C**, n≥ 50 anaphase and telophase cells in each of 3 biological replicates). **D-E**) MTT absorbance and percentage of dead cells after treatment of Cal51 cells with paclitaxel and CW-069. **D**) Mean absorbance +/- SEM from MTT viability assays with 10 nM paclitaxel and 50 μM CW-069. n=3. **E**) Mean percentage +/- SEM of dead cells measured by trypan blue exclusion assay. n=3. *P<0.05. ns=not significant.

Figure 2.3: Increasing the incidence of multipolar divisions through Plk4-induced centriole amplification increases paclitaxel cytotoxicity.

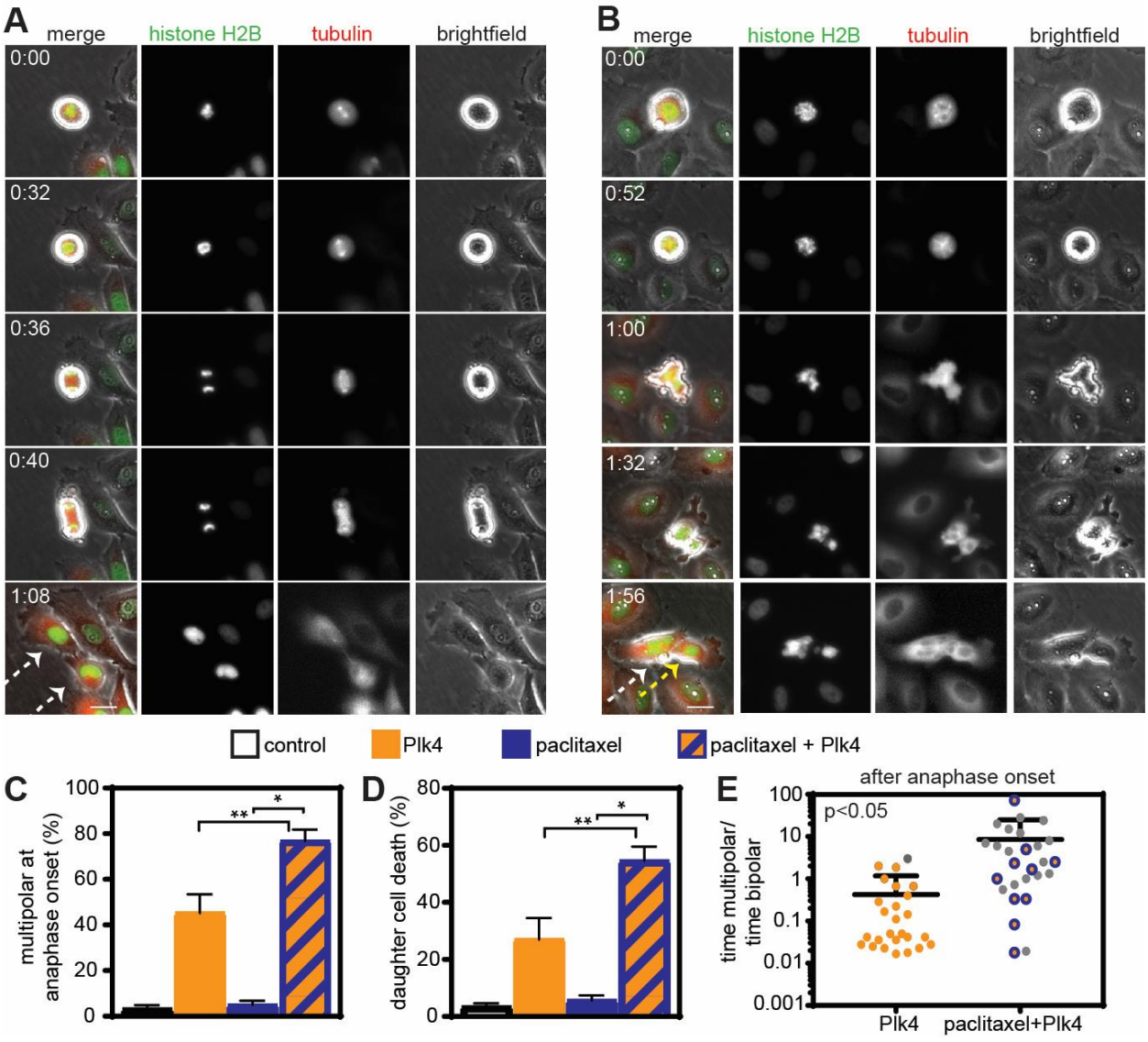

Figure 2.3: Increasing the incidence of multipolar divisions through Plk4-induced centriole amplification increases paclitaxel cytotoxicity. 72-hour timelapse analysis of Plk4 inducible MCF10A cells expressing histone H2B-mNeonGreen and mScarlet-tubulin. **A-B**) Still images of (**A**) control cell undergoing bipolar division which produces two viable daughter cells and (**B**) Plk4 inducible cell undergoing a multipolar division in the presence of paclitaxel with eventual pole focusing, resulting in the formation of two daughter cells, one of which subsequently dies. Arrows indicate daughter cells formed after division. White arrows indicate viable daughter cells. Yellow arrow indicates daughter cell that dies after division. Time is indicated in hours:minutes. Scale bar, 5 μm. **C-D**) Quantification of cells observed by timelapse microscopy. **C**) Mean percentage +/- SEM of cells with multipolar spindles at anaphase onset. n=91 control, n=86 paclitaxel, n=95 +doxycycline (Plk4), and n=83 paclitaxel+doxycycline (Plk4) cells from four independent replicates. **D**) Mean percentage of cell death +/- SEM during timelapse. n=167 control, n=111 paclitaxel, n=176 +doxycycline (Plk4), and n=146 paclitaxel+doxycycline (Plk4) daughter cells from four independent replicates. **E**) Ratio of time spent after anaphase onset with a multipolar versus bipolar spindle. Each dot represents a single cell. Gray dots indicate daughter cells that died during the imaging period. *P<0.05. **P<0.001.

Figure 2.4: Reducing multipolar divisions by Mps1 inhibition decreases the cytotoxicity of paclitaxel.

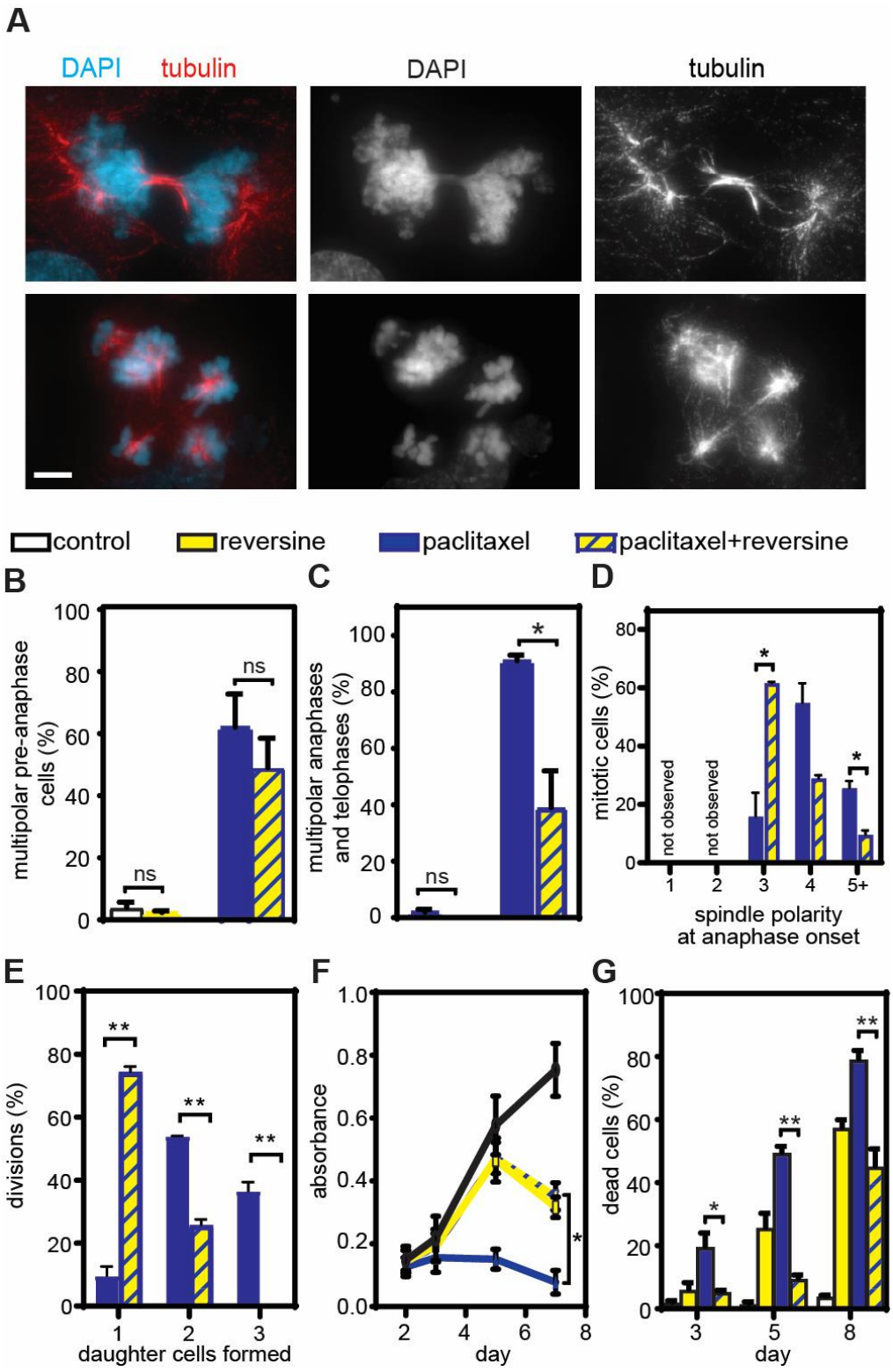

Figure 2.4: Reducing multipolar division by Mps1 inhibition decreases the cytotoxicity of paclitaxel. A) Representative images of bipolar (top) and multipolar (bottom) telophase cells. Scale bar, 5 μm. **B**) Percentage (mean +/- SD) of pre-anaphase cells with multipolar spindles in MDA-MB-231 cells upon Mps1 inhibition and paclitaxel tretment. n≥100 cells in each of 3 independent replicates. **C**) Mean percentage +/- SEM of anaphase and telophase cells with multipolar spindles in MDA-MB-231 cells upon Mps1 inhibition and paclitaxel treatment. n≥50 anaphase and telophase cells from each of 3 independent replicates. **D-E**) Quantification of 24 hour timelapse analysis of MDA-MB-231 cells stably expressing RFP-histone H2B and GFP-tubulin at 3 minute intervals. (**D**) Spindle polarity at anaphase onset. Data represent mean +/- SEM of two movies. n=65 and 68 cells in paclitaxel and paclitaxel+reversine conditions, respectively. (**E**). Number of daughter cells formed following mitosis in MDA-MB-231 cells after paclitaxel and reversine treatment. Data represent mean +/- SEM of three movies. n=101 and n=94 divisions in paclitaxel and paclitaxel+reversine conditions, respectively. **F**) Mean absorbance +/- SEM from MTT metabolic viability assay. n=3. **G**) Cell death (mean +/- SEM) in MDA-MB-231 cells following treatment with reversine and paclitaxel, as measured by trypan blue exclusion assay. n=4. *P<0.05. **P<0.001. ns=not significant.

Figure 2.5: Reducing multipolar divisions by upregulating Mad1 in MDA-MB-231 cells decreases the cytotoxicity of paclitaxel in vitro and in vivo.

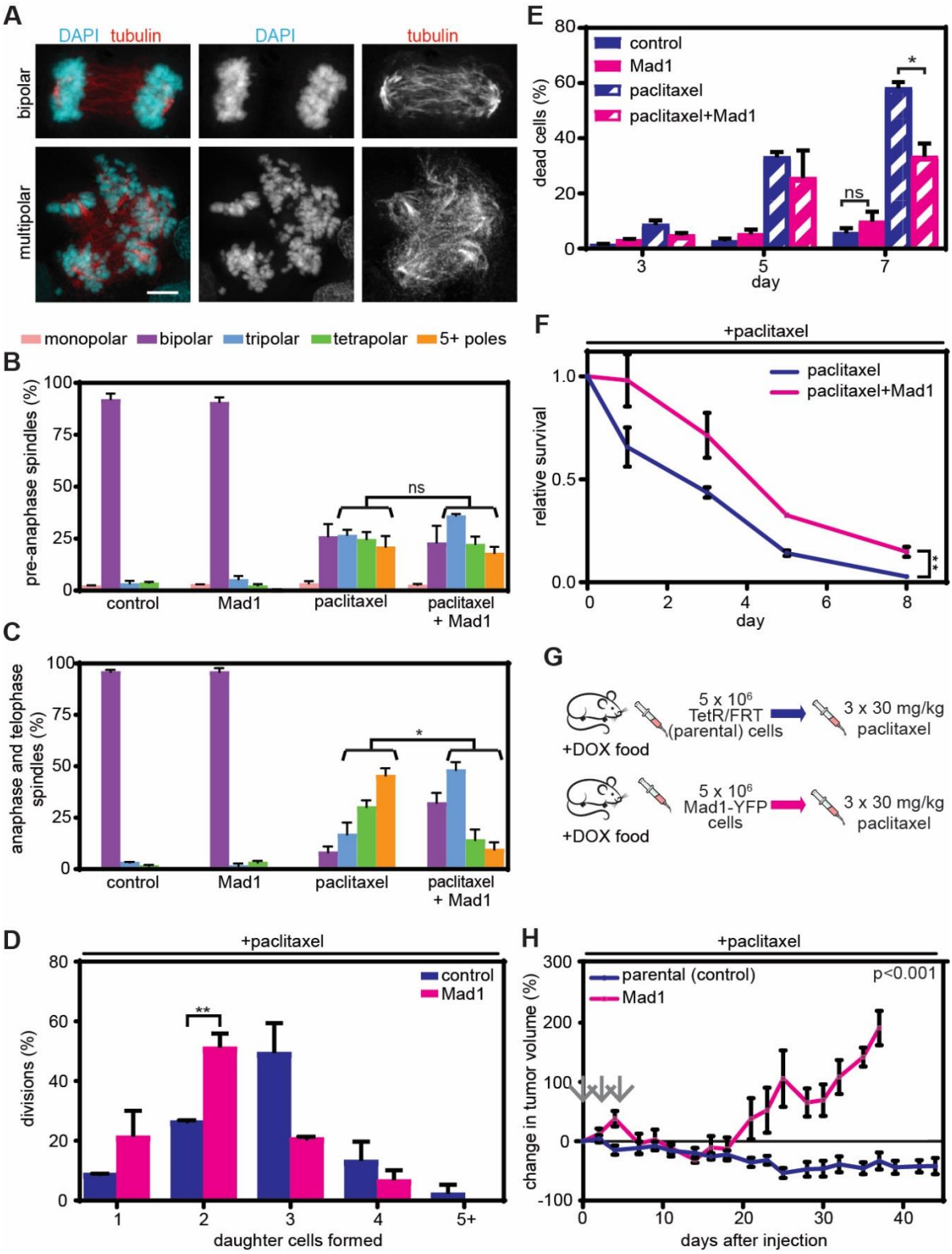

Figure 2.5: Reducing multipolar division by upregulating Mad1 in MDA-MB-231 cells decreases the cytotoxicity of paclitaxel in vitro and in vivo. A) Representative images of bipolar (top) and multipolar (bottom) anaphase cells. Scale bar, 5 μm. **B-C**) Cells were treated with vehicle, tet to induce Mad1, 10 nM paclitaxel, or tet and paclitaxel. **B**) Mean +/- SEM of the number of spindle poles in pre-anaphase cells. n≥100 cells from each of 3 replicates. **C**) Mean +/- SEM of spindle pole number in anaphase and telophase cells. n≥50 anaphase and telophase cells in each of 3 independent experiments. **D**) Quantification of the number of daughter cells formed after mitotic division in 10 nM paclitaxel, with and without Mad1 upregulation, assessed by bright-field timelapse microscopy. Data represent the mean +/- SD of two movies. n=65 divisions for paclitaxel alone and n=83 divisions for paclitaxel + Mad1 upregulation. **E**) Mean +/- SEM of cell death, as assessed by trypan blue exclusion assay. n=4. **F**) Relative MTT survival assay (mean +/- SD) over 8 days. n=3. **G**) Schematic of orthotopic experiment. Mice injected with parental or Mad1-YFP inducible MDA-MB-231 cells were treated with 30 mg/kg paclitaxel (gray arrows) every other day for five days once tumors reached a minimum volume of 75 mm^3. **H**) Percent change (mean +/- SEM) in tumor volume after paclitaxel treatment (arrows). n=6 tumors per treatment condition. *=$p<0.05$. **=$p<0.001$. ns=not significant.

Figure 2.6: Increasing chromosomal instability sensitizes Cal51 cells to paclitaxel in vitro.

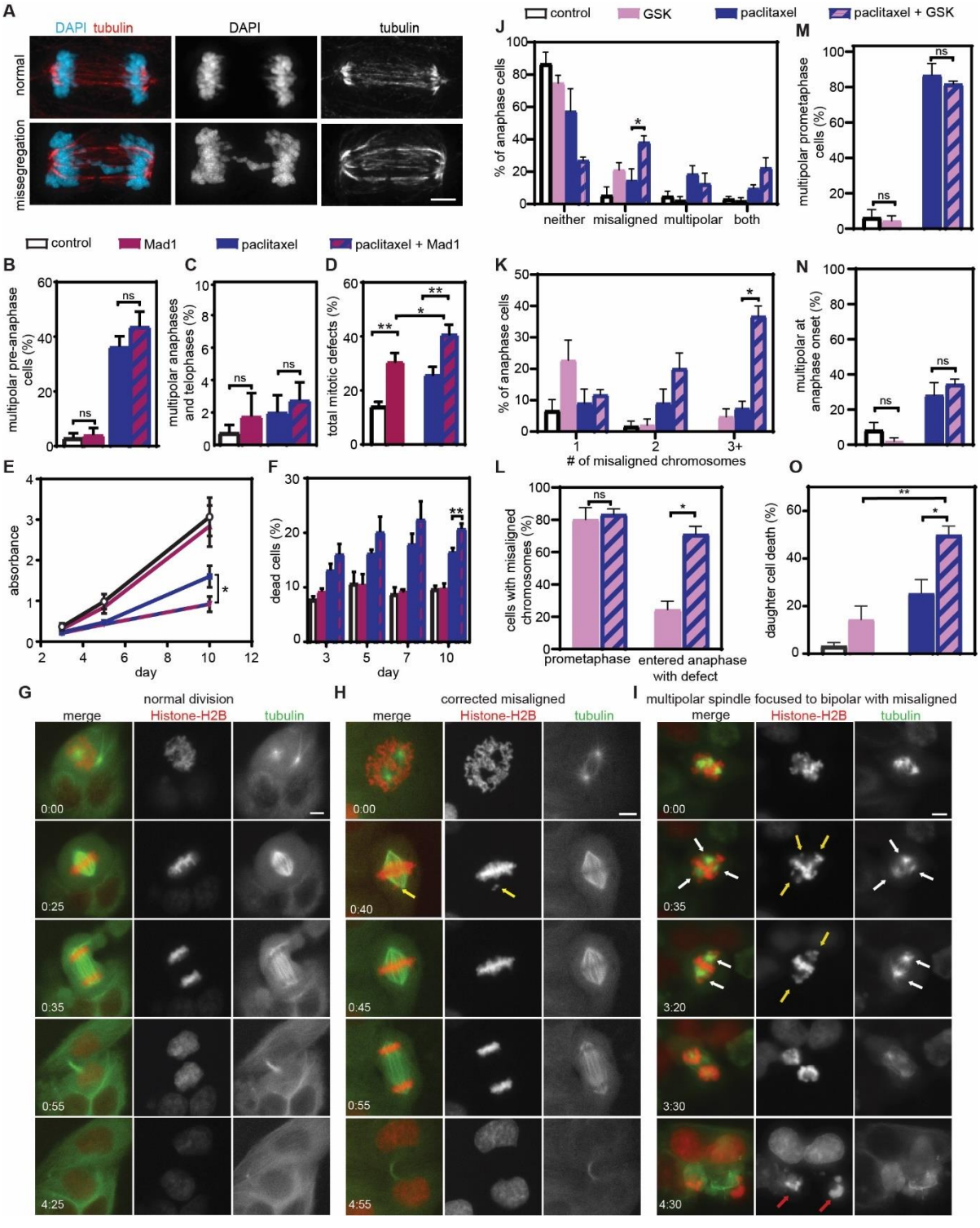

Figure 2.6: Increasing chromosomal instability sensitizes Cal52 cells to paclitaxel in vitro. A) Representative images of a normal bipolar anaphase (top) and a bipolar anaphase with evidence of chromosome missegregation (lagging chromosome, bottom). Scale bar, 5 μm. **B-F**) Cells were treated with vehicle, tet to induce Mad1, 10 nM paclitaxel, or tet and paclitaxel. Mean percentage +/- SEM of multipolar spindles prior to anaphase (**B**, n≥100 cells in each of three biological replicates) and after anaphase onset (**C**, n≥ 50 anaphase and telophase cells in each of three biological replicates). **D**) Quantification of the incidence of total mitotic defects observed by fixed analysis. n≥50 anaphase and telophase cells in each of five biological replicates. **E**) MTT survival assay. Data represent the mean +/- SEM from three biological replicates. **F**) Cell death (mean +/- SEM), measured using trypan blue exclusion assays. n=3. **G-O)** Cal51 cells treated with vehicle, CENP-E inhibitor GSK923295, 5 nM paclitaxel, or both. **G-I**) Still images from timelapse analysis of Cal51 cells with fluorescent chromosomes and microtubules due to endogenous tagging of histone H2B with mScarlet and α-tubulin with mNeonGreen, respectively. Time is indicated in hours:minutes. Scale bar, 5 μm. **G**) Normal bipolar division. **H**) Division in GSK923295, in which a misaligned chromosome, indicated by a yellow arrow, aligns prior to anaphase onset. **I**) Division in combination of 5 nM paclitaxel and 50 nM GSK923295 in which the prometaphase spindle contains multiple spindle poles (indicated by white arrows), focuses into a bipolar spindle prior to anaphase onset (time 3:20) and enters anaphase in the presence of multiple misaligned chromosomes (yellow arrows). Both daughter cells die by 4:30 (red arrows). **J-N**) Quantitation of mitotic defects at anaphase onset (**J**), number of misaligned chromosomes at anaphase onset (**K**), percentage of cells with misaligned

chromosomes in prometaphase and at anaphase onset (**L**), and spindle polarity before (**M**) and at (**N**) anaphase onset. **O**) Percent daughter cell death. Data represent the mean (+/- SEM) from 3 48-hour movies. *P<0.05. **P<0.001. ns=not significant.

Figure 2.7: Pre-treatment chromosomal instability directly correlates with taxane response in metastatic breast cancer patients.

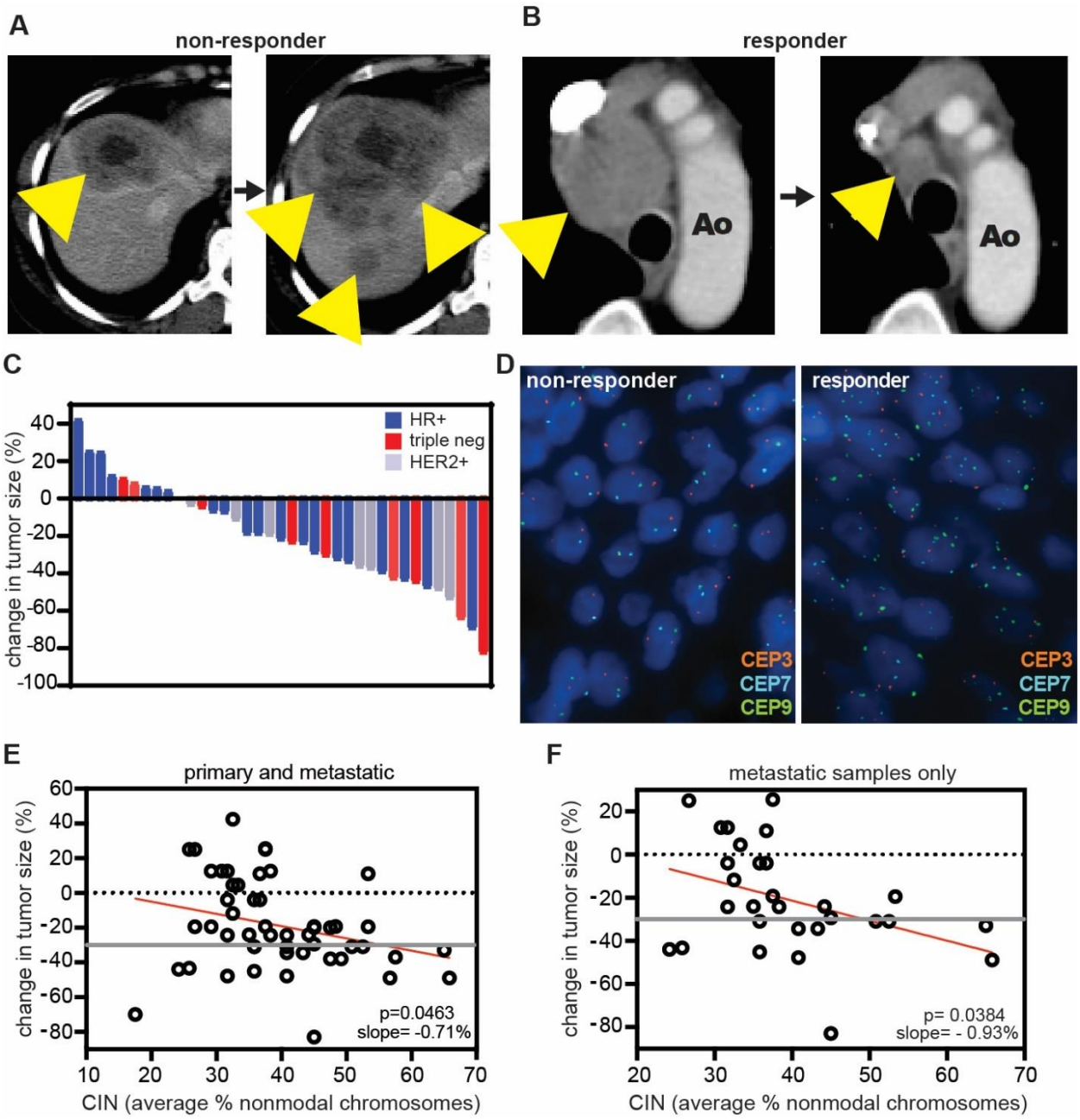

Figure 2.7: Pre-treatment chromosomal instability directly correlates with taxane response in metastatic breast cancer patients. A-B) Representative patient tumor responses to paclitaxel. Yellow arrows indicate tumors. **A**) Progression of a hormone receptor-positive liver metastasis. **B**) Marked improvement of a mediastinal lymph node. **C**) Waterfall plot showing treatment response to taxane therapy in a cohort of 37 metastatic breast cancer patients treated with single-agent taxane. Color indicates breast cancer receptor subtype; hormone receptor positive (HR+), triple negative (triple neg), or human epithelial growth factor receptor 2 positive (HER2+). **D**) Representative FISH images showing probes for centromeres 3, 7, and 9. The average percent non-modal chromosomes was used as a measure of chromosomal instability. **E-F**) Correlation of pre-treatment chromosomal instability with response to taxane treatment. Response cutoff was determined by RECIST 1.1 criteria (Eisenhauer *et al.*, 2009), and is indicated by a gray line. **E**) Data from primary as well as metastatic tumor (51 total) sites. Slope = -0.71%, meaning per percent increase in non-modal chromosomes, tumor size was reduced by an estimated 0.71%. **F**) Data from 29 exclusively metastatic sites. Slope = -0.93%.

Table 2.1: Paclitaxel concentration measurements in patient tumors.

Patient	[plasma paclitaxel, μM]	[Intratumoral paclitaxel, μM]	Degree of concentration
1	0.023	1.07	47x
2	0.040	0.34	9x
3	0.030	0.80	27x
4	0.027	0.57	21x
5	0.031	ND	-
6	0.020	3.43	172x
7	0.013	1.55	119x
8	0.011	0.53	48x
9	0.020	0.63	32x
11	0.038	0.57	15x
12	0.040	ND	-
13	0.094	1.67	18x
14	0.048	0.52	11x
15	0.035	1.20	34x

Intratumoral and plasma paclitaxel concentrations were measured by HPLC analysis 20 hours after the first dose of paclitaxel. Paclitaxel was quantified per tumor volume. Paclitaxel was not determined (ND) in the tumor biopsies for patients 5 and 12 due to insufficient tumor tissue collected by biopsy. Patient 10 withdrew consent.

Supplementary Materials:

Supplementary Materials and Methods

Cell culture

MDA-MB-231, Cal51 and DLD1 cell lines were grown in DMEM supplemented with 10% (vol/vol) FBS, 2 mM L-glutamine, and 50 µg/mL penicillin/streptomycin at 37°C and 5% CO_2. RPE1 cells were grown in DMEM/F12 supplemented with 10% (vol/vol) FBS, 2 mM L-glutamine, and 50 µg/mL penicillin/streptomycin at 37°C and 5% CO_2. MCF10A cells were grown in DMEM/F12 supplemented with 5% (vol/vol) horse serum, 20 ng/mL hEGF, 0.5 mg/mL hydrocortisone, 100 ng/mL cholera toxin, 10 µg/mL insulin, and 50 µg/mL penicillin/streptomycin at 37°C and 5% CO_2. Paclitaxel (LC Laboratories) was diluted in DMSO and used at the indicated final concentrations. CW-069 (MedChem Express, 50 µM), reversine (Sigma-Aldrich, 1 µM), AZ3146 (Selleck Chemicals,1 µM), AZ82 (Cayman Chemical, 1.25 µM), and GSK923295 (AdooQ Bioscience, 50 nM) used in cell culture experiments were dissolved in DMSO. In the inducible Mad1 and Plk4 experiments, 2 µg/mL tet or doxycycline (dox) was added for 24 hours or 48 hours prior to the addition of paclitaxel, respectively.

Orthotopic experiments

All animal studies were performed in compliance with all relevant ethical regulations for animal testing and research. The study was approved by the Institutional Animal Care and Use Committee of the University of Wisconsin-Madison. $5x10^6$ cells were injected orthotopically into the inguinal mammary fat pads of 5-week-old female

athymic nude mice. Three mice were injected with parental MDA-MB-231 cells and three mice were injected with MDA-MB-231 cells that inducibly express Mad1-YFP on both sides (2 tumors per mouse). All mice were started on dox chow (Teklad TD.120769, containing 625 mg/kg dox) the day before cell injection. Tumor size was measured every 2-3 days using calipers. Tumor volumes were calculated using the formula $V = \text{width}^2 \times \text{length}/2$. Mice were treated with sterile saline or 30 mg/kg paclitaxel iv every other day for 5 days once tumors reached a minimum volume of 75 mm^3.

Cell viability assays

Metabolic cell viability was determined using an MTT assay (VWR) . Briefly, cells were counted and plated in 6 well plates. On the day(s) of measurement, cells were incubated with 1 mg/mL MTT reagent (3-(4,5 dimethylthiazol-2-yl)-2,5diphenyltetrazolium bromide) for 3 hours. Viable cells contain NADH oxidoreductase enzymes which convert the MTT substrate to formazan. Formazan was liberated from cells by adding 800 µL of DMSO and 100 µL Sorenson's glycine buffer (0.1M glycine, 0.1M NaCl, pH:10.5 with 0.1M NaOH) to each well, followed by a 10 min incubation at 37°C. 3 x100 µL of solution was transferred to 3 wells in 96 well plates for triplicate measurements of each condition. Formazan, an indirect measure of metabolic cell viability, was colorimetrically detected by measuring absorbance on a plate reader at 540 nm.

Colony formation assays were performed by plating MDA-MB-231 or Cal51 cells at a density of 400 or 600 cells/well, respectively, in 6 well plates. Cells were allowed to

attach overnight, and drugs were added the following day. After 14 days, cells were stained with crystal violet and the number of colonies were counted.

For cell counting assays to quantify live and dead cells, 25,000 cells were plated in 6 cm dishes. Cells were allowed to attach overnight, and drugs were added the following day. On days selected for timepoint analysis, media and PBS rinse were collected in addition to trypsinized cells. Cells were pelleted, resuspended, and diluted in trypan blue before counting on a hemocytometer. Live and dead cells were counted to determine the percent dead cells.

Immunofluorescence in cells and primary patient cohort

Cellular immunofluorescence was performed as in (Ryan *et al.*, 2012). Staining was performed with antibodies to α-tubulin (YL 1/2; Bio-Rad, MCA77G), pericentrin (Abcam, ab4448) diluted 1:1000 or centrin (Millipore Sigma, 04-1624) diluted 1:5000 for one hour at room temperature. For patient immunohistochemistry, 5 μm sections of formalin-fixed, paraffin-embedded tissue sections were subjected to antigen retrieval in citrate buffer, serum-blocked overnight, and stained with rabbit anti-NuMA antibody (a kind gift from Duane Compton), mouse anti-γ-tubulin (Sigma, T6557), and pan-cytokeratin (to mark epithelial cells; Novus Biologicals, NBP2-33200AF647) antibodies diluted 1:100 overnight at 4°C. Alexa Fluor-conjugated secondary antibodies (Invitrogen) were used at 1:200 for one hour at room temperature. DNA was stained using DAPI. Ki67 visual estimate performed by a fellowship-trained subspecialist in surgical pathology of the breast (S.M.M), according to standard clinical practice.

Imaging response criteria

Baseline imaging was performed by ultrasound as part of a complete diagnostic imaging evaluation including mammography. All imaging was performed as closely as possible to the beginning of treatment. Tumors were again evaluated by ultrasound within two weeks of completion of paclitaxel chemotherapy, and prior to any additional chemotherapy or surgery. A single board-certified breast imaging radiologist with seven years of experience (A.M.F,) retrospectively reviewed the reports and saved images from the prospectively performed ultrasound exams. Imaging response was evaluated using RECIST 1.1 criteria (Eisenhauer *et al.*, 2009) and the single longest dimension measured on the baseline and post-paclitaxel ultrasounds. Three patients were excluded from this analysis due to the inability to accurately determine tumor measurements (1), deviation from treatment protocol (1), or withdrawal of patient consent (1).

Paclitaxel measurements

Cells in 6 cm dishes were treated with the indicated concentrations of paclitaxel in 3 mL total volume once they reached 90-100% confluence. After 20 hours, media was collected, and cells were pelleted and resuspended in 1 mL ddH_2O. Both cell and media samples were stored at -20°C until the day of analysis. Cell resuspensions were thawed and sonicated immediately before sample preparation for LC-MS/MS. For solid phase extraction, cell and media samples were applied to an Ostro plate (Waters,186005518). Prior to extraction, deuterium-labeled internal standard paclitaxel-d5 (Toronto Research Chemicals; P132502) was added via diluent to facilitate quantification of sample recovery. Samples were eluted using acetonitrile +1% formic

acid with positive pressure (30-50 psi) of nitrogen into a collection plate. LC-MS/MS analysis was performed using a LC-UV-MS/MS system (QTrap 5500; ABSciex) equipped with a Waters Acquity UPLC System binary pump). A Phenomenex Kinetex C18 column (30 mm × 2.1 mm × 2.6 µm) was used with a gradient of acetonitrile/water/formic acid of 65:35:0.1 (v/v/v) to 100:0:0.1 at 0.35 mL/min flow rate. To monitor and quantify the concentrations of paclitaxel and paclitaxel-d5, a multiple-reaction monitoring (MRM) method was developed with signature ion fragments for each molecule. Calibration curves were obtained using paclitaxel at 0.2, 1, 5, 10, 50, 100, 250, 500, and 1000 ng/mL. Quantification was carried out based on peak area of the MRM transition and the linear calibration curve for each compound.

Patient tissue core biopsies were analyzed as in (Zasadil *et al.*, 2014). Briefly, core biopsies were thawed on ice and core length, diameter, and weight were recorded. Intratumoral concentrations were calculated using core tissue volume (cc; Table 1). Calculations based on core tissue weight (g) gave similar results (Table 2.S5). In this case, the final molar concentration (µM) calculations assume that tissue core density is equivalent to that of water (1 g/cm^3 or 1 g/mL). Patient biopsies were homogenized in EDTA drug-free human plasma + 10% acetonitrile and 10 µg/mL docetaxel (Sigma-Aldrich; 01885-5MG) was added as internal standard prior to pre-extraction to facilitate quantification of sample recovery. Homogenized samples were then applied to C18 Bond Elut solid-phase extraction columns (Agilent) and eluted with acetonitrile by gravity or low vacuum. Solvents were then evaporated to dryness using nitrogen gas and samples were reconstituted in 100 µL acetonitrile and 100 µL of 35 mM acetic acid. Analysis was performed by monitoring the signal of a 50 µL injection at

235 nm during an isocratic elution with 56% 35 mM acetic acid, 44% acetonitrile on an analytical HPLC instrument (Shimadzu LC-20AD with SPD-20A UV Detector and a Waters Nova-Pak C18 4-μm 4.6 × 150 mm column). Calibration curves were obtained using paclitaxel at 10, 25, 50, 100, 250, 500, and 750 ng/mL. Quantification was carried out based on peak area and the linear calibration curve for each compound.

Microscopy

Images were acquired on a Nikon Ti-E inverted microscope driven by Nikon Elements software with focus-drift compensation. Images are maximum projections from 0.2 μm z-stacks collected with a 60×/1.4 or 100×/1.4 numerical aperture (NA) objective after deconvolution using the AQI 3D Deconvolution module in Elements. For MCF10A and Cal51 (transgene) timelapse analysis, cells were placed under 10% CO_2 flow at ~30 mL/min in a heated chamber at 37°C. Images were acquired at 3-min and 4-min intervals, for phase-contrast and fluorescent timelapse, respectively, using a 20×, 0.1 NA objective and focus drift compensation. For MDA-MB-231 and Cal51 (endogenously tagged) 24-hour timelapse analysis, cells were imaged using a Tokai Hit stage top incubator with 5% CO2. Five 2 μm z-planes were acquired every 3 or 7 min, respectively using a 40×/0.75 NA objective and focus drift compensation. Maximum projections of in-focus planes or the maximally focused single z plane were assembled in Elements, exported as jpg files, and converted to .avi files in Fiji/ImageJ. For long term microscopy experiments to determine cell fate, cells were imaged using a Tokai Hit and 5% CO_2. Images were acquired every 4-5 minutes for 64-72 hours with three to five 2 μm z-planes. Cells were treated with drugs approximately 1 hour before observation unless otherwise noted. For Figure 3A-E, cells were treated with paclitaxel 20 hours

before observation. The ratio of time spent multipolar vs bipolar after anaphase onset in Figure 3E was quantified by multiplying the number of frames a cell spent multipolar after anaphase onset by the frame rate (4 minutes) and dividing by the number of frames a cell spent bipolar times the frame rate (4 minutes).

Metastatic cohort immunofluorescence and scoring

For patient immunohistochemistry, 5 μm sections of formalin-fixed, paraffin-embedded tissue sections were subjected to antigen retrieval in citrate buffer, serum-blocked for 30 minutes, and stained with anti-rabbit β-tubulin III (Abcam, ab18207), anti-rabbit P glycoprotein 1 (P-gp1; Abcam, ab129450), Ki67 (Abcam, ab15580), or anti-mouse pan-cytokeratin (Abcam, ab7753). Primary antibodies were diluted 1:1000 for pan-cytokeratin and 1:5000 for the others. They all were incubated for 1 hour at room temperature. Mouse and rabbit HRP-conjugated secondary antibodies (Abcam) were used at 1:500 for 30 minutes at room temperature followed by TSA Plus fluorophore dyes diluted 1:50 (Akoya Biosciences). DNA was stained using DAPI. Ki-67 stain was quantified by dividing the number of Ki-67 positive cells by the total number of cells. The rest of the protein markers were calculated with H-Score using the following formula: 3x(percentage of strongly stained cells) + 2x(percentage of moderately stained cells) + 1x(percentage of weakly stained cells) + 0x(percentage of unstained cells), resulting in a range of 0 to 300.

Fluorescence in situ hybridization (FISH)

Fluorescence in situ hybridization (FISH) was performed using standard techniques, as reported elsewhere (Denu *et al.*, 2016). For each case, a set of 2 tissue

slides were used to stain for probes to centromeres 4, 10, and 17 and 3, 7, and 9, respectively. The number of probed chromosomes were counted in 20 cells per section. The average percent of non-modal chromosomes was calculated as a measurement of chromosomal instability as in (Denu *et al.*, 2016).

Figure 2.S1. Clinically relevant intracellular concentrations of paclitaxel induce multipolar spindles without mitotic arrest in multiple cell types.

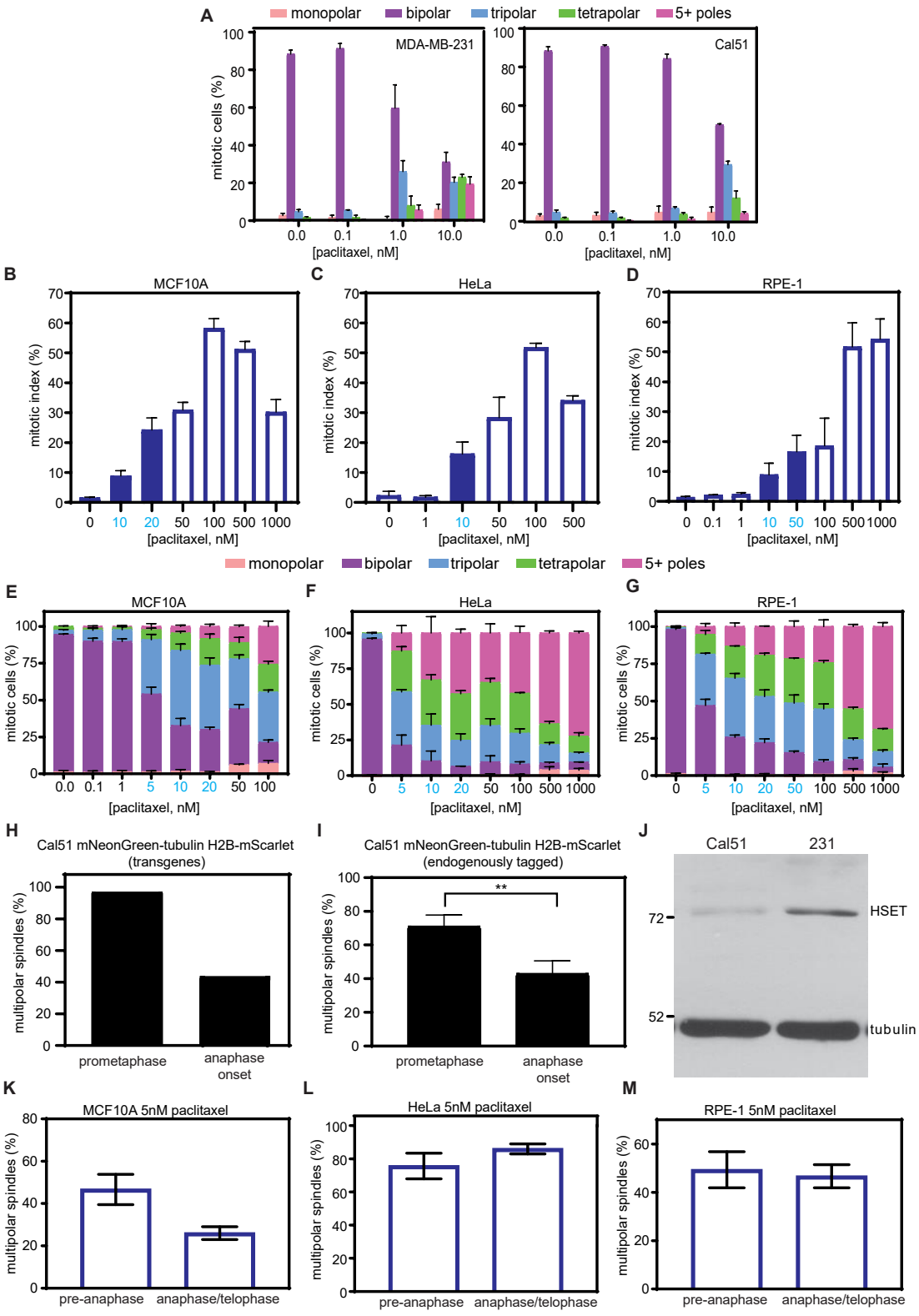

Figure 2.S1. Clinically relevant intracellular concentrations of paclitaxel induce multipolar spindles without mitotic arrest in multiple cell types. A) Mean mitotic spindle pole number +/- SEM in breast cancer cell lines in response to increasing concentrations of paclitaxel. n≥100 cells in each of 3 replicates. **B-D**) Mitotic index quantification in increasing paclitaxel concentrations in MCF10A (**B**), HeLa (**C**), and RPE-1 (**D**) cells. Clinically relevant doses of paclitaxel (as measured in table 2.S2) are indicated by blue font and solid blue bars. n≥2. **E-G**) Spindle polarity in increasing paclitaxel concentrations in MCF10A (**E**), HeLa (**F**), and RPE-1 (**G**) cells. Paclitaxel doses in blue font represent clinically relevant concentrations. n=3. **H-I**) Timelapse analysis of Cal51 cells. Multipolarity before and at anaphase onset in Cal51 cells with fluorescent chromosomes and microtubules due to (**H**) viral-mediated expression of mNeonGreen-tubulin and histone H2B-mScarlet or (**I**) CRISPR/Cas9-mediated labeling of endogenous histone H2B and α-tubulin. Paclitaxel was added either 20 hours before imaging (**H**) or when initiating imaging (I). n ≥25 cells each from one (**H**) or three (**I**) biological replicates. **I**) Data represent mean +/- SEM. **J**) Immunoblot showing HSET expression in Cal51 and MDA-MB-231 cells. **K-M**) MCF10A, HeLa or RPE-1 cells after treatment with 5 nM paclitaxel. Quantification of multipolar spindles +/- SEM in pre-anaphase cells (n≥100 cells from each of 3 replicates) and in anaphase and telophase cells (n≥50 cells from each of 3 independent replicates) in response to paclitaxel in MCF10A (**K**), HeLa (**L**), and RPE-1 (**M**) cells. ***P*<0.001.

Figure 2.S2. Persistent multipolarity, rather than mitotic delay, causes paclitaxel-induced cell death.

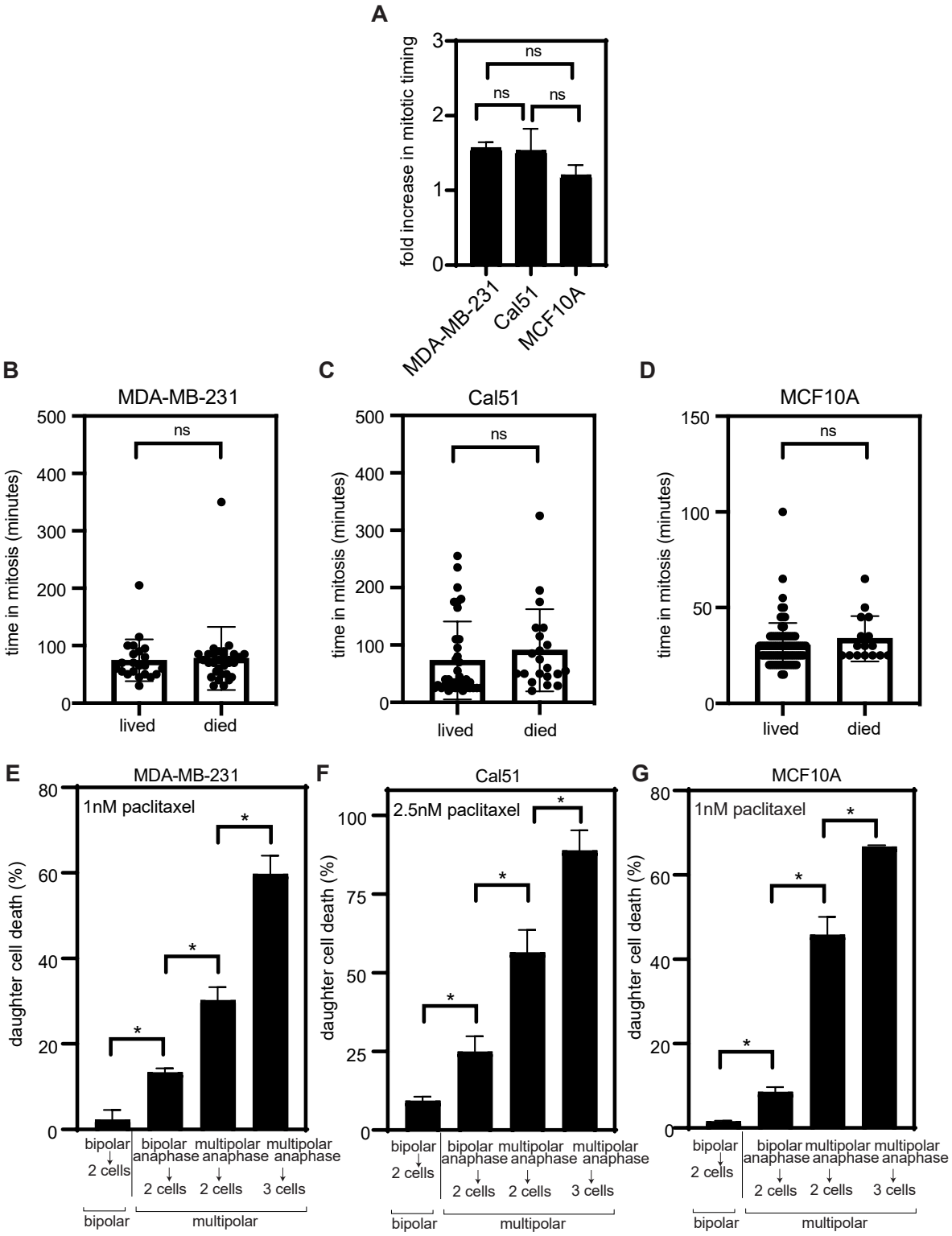

Figure 2.S2. Persistent multipolarity, rather than mitotic delay, causes paclitaxel-induced cell death. A-G) Results of long term timelapse microscopy of control and paclitaxel treated cells expressing fluorescent histone H2B and α-tubulin. **A**) Mean fold increase in mitotic duration +/- SD, relative to DMSO treated control cells, after treatment with 1 nM paclitaxel in MDA-MB-231 and MCF10A cells and 2.5 nM paclitaxel in Cal51 cells. n≥25 cells per replicate from two independent replicates. **B-D**) Mean time in mitosis +/- SD, measured as time from NEB to anaphase onset, for divisions in paclitaxel that resulted in viable daughter cells (left) and divisions in which at least one daughter cell died (right) in MDA-MB-231 (**B**), Cal51 (**C**), and MCF10A (**D**) cells. n≥25 cells per replicate from two independent replicates. **E-G**) Quantitation of daughter cell death (mean +/- SEM) in MDA-MB-231 (**E**), Cal51 (**F)**, and MCF10A (**G**) cells after specified types of divisions in paclitaxel. n≥50 daughter cells per replicate from two independent replicates. *P<0.05. ns=not significant.

Figure 2.S3. HSET inhibition impairs multipolar spindle focusing and increases paclitaxel cytotoxicity.

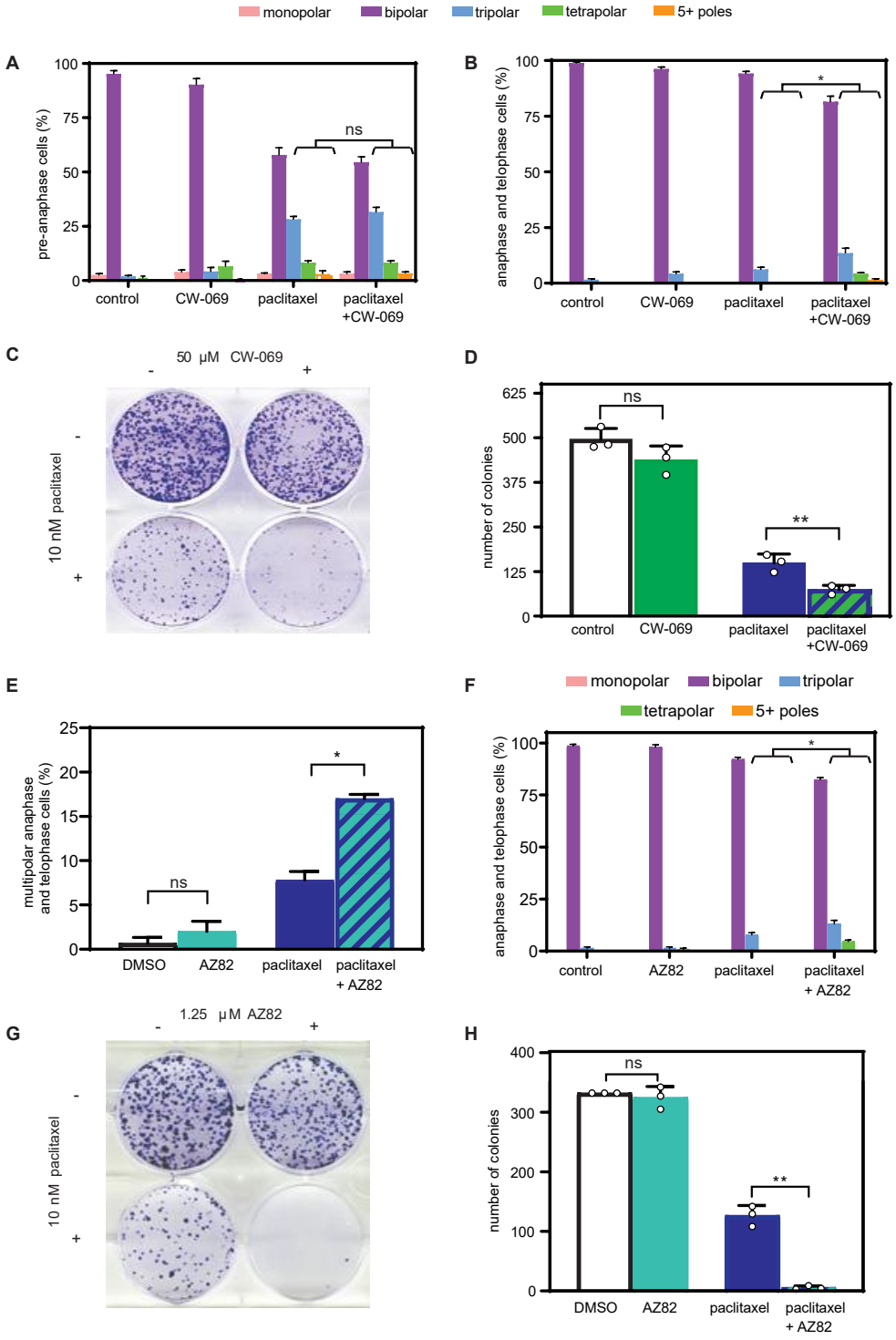

Figure 2.S3. HSET inhibition impairs multipolar spindle focusing and increases paclitaxel cytotoxicity. A-B) CW-069 treatment in Cal51 cells. Quantification of spindle polarity in (**A**) pre-anaphase and (**B**) anaphase and telophase cells from fixed analysis. Data represent the mean +/- SEM from three replicates. n≥100 (**A**) or 50 (**B**) cells per replicate. **C**) Representative colony formation assay in the presence of paclitaxel, CW-069, or paclitaxel and CW-069. **D**) Mean number of colonies formed +/- SD in the presence of DMSO control, paclitaxel, CW-069, or both. n=3. **E-F**) Quantification of spindle polarity in anaphase and telophase cells from fixed analysis. Data represent the mean +/- SEM from three replicates of ≥50 cells per replicate. **G**) Representative colony formation assay in the presence of paclitaxel, 1.25 μM AZ82, or both. **H**) Mean number of colonies formed +/- SD in the presence of DMSO control, paclitaxel, AZ82, or both. n=3. *P<0.05. **P<0.001. ns=not significant.

Figure 2.S4. Plk4 overexpression causes centriole amplification and increases paclitaxel-induced multipolar divisions and cytotoxicity in MCF10A cells.

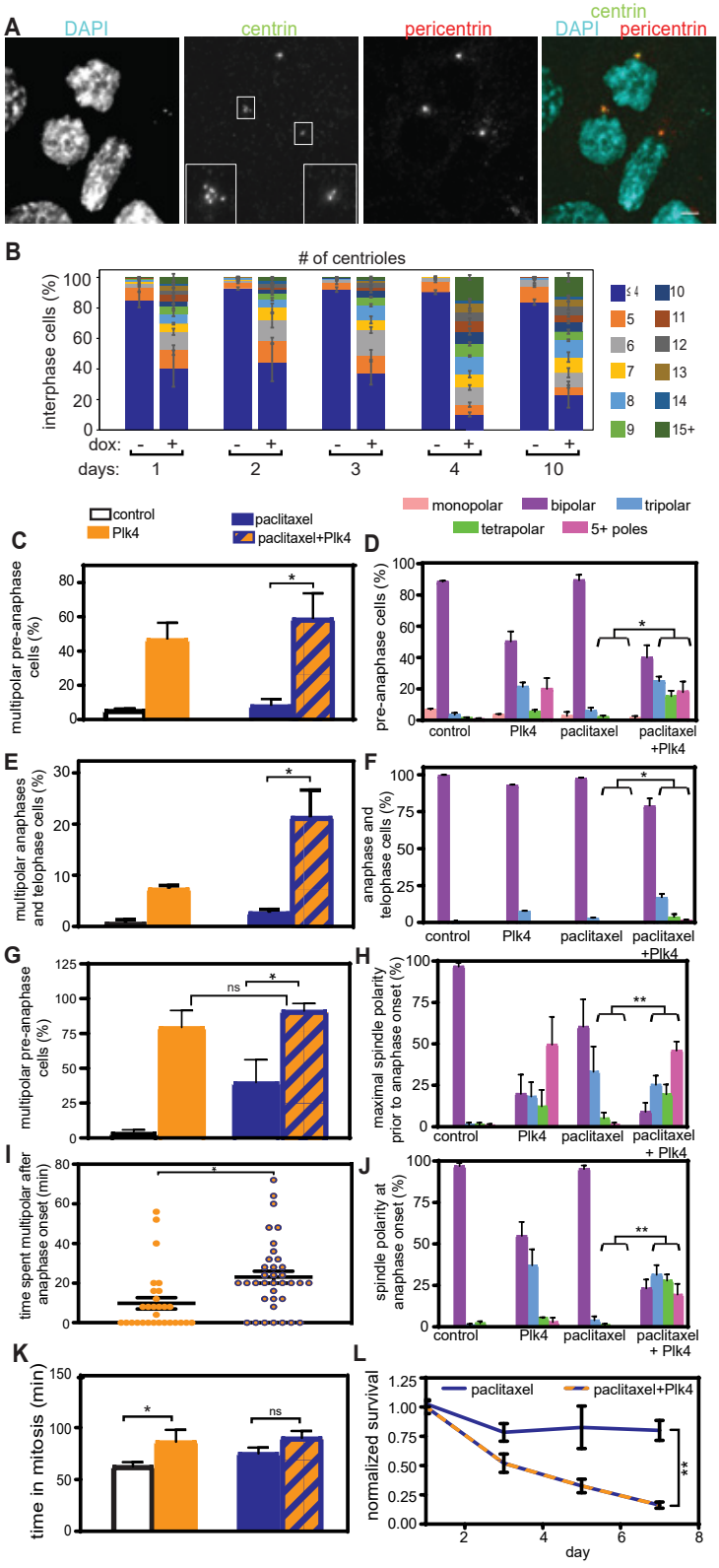

Figure 2.S4. Plk4 overexpression causes centriole amplification and increases paclitaxel-induced multipolar divisions and cytotoxicity in MCF10A cells. A-B) Tet-inducible Plk4 expression in MCF10A cells. **A**) Representative images of centrioles (centrin) and centrosomes (pericentrin) in interphase. Insets show enlargements of normal centrosome with 2 centrioles (right) and centrosome with centriole amplification (left). Scale bar = 5 μm. **B**) Quantification +/- SEM of centriole number after inducible expression of Plk4. n=3 independent experiments of ≥100 cells each. **C-F**) Plk4 overexpression increases the incidence of multipolar spindles and multipolar divisions in a subclinical dose of paclitaxel (1 nM). **C**) Spindle polarity (mean +/- SEM) in pre-anaphase cells assessed by fixed analysis. n≥100 pre-anaphase cells in each of three replicates. **D**) Breakdown of spindle polarity in **C**. **E**) Spindle polarity (mean +/- SEM) in anaphase and telophase cells quantified by fixed analysis. n≥50 anaphase and telophase cells from each of three independent replicates. **F**) Breakdown of spindle polarity in **E**. **G-K**) Quantitation of timelapse analysis of Plk4-inducible MCF10A cells expressing histone H2B-mNeonGreen and mScarlet-tubulin treated with vehicle, doxycycline to induce Plk4, 1 nM paclitaxel, or doxycycline and paclitaxel. Data represent mean +/- SEM. n=2-4 independent movies. Quantification of pre-anaphase cell multipolarity (**G**) and the maximal number of poles in pre-anaphase multipolar spindles (**H**). **I**) Time spent multipolar after anaphase onset. Each dot represents an individual cell. **J**) Breakdown of spindle polarity of cells at anaphase onset. **K**) Time in mitosis (mean +/- SEM), from NEB to daughter cell sitting. **L**) Normalized MTT growth curves (mean +/- SEM) in 1 nM paclitaxel with and without Plk4 overexpression. Each

curve is normalized to the -paclitaxel (DMSO treated) control. n=3. *P<0.05. **P<0.001. ns=not significant.

Figure 2.S5. Mps1 inhibition reduces sensitivity to paclitaxel in MDA-MB-231 cells.

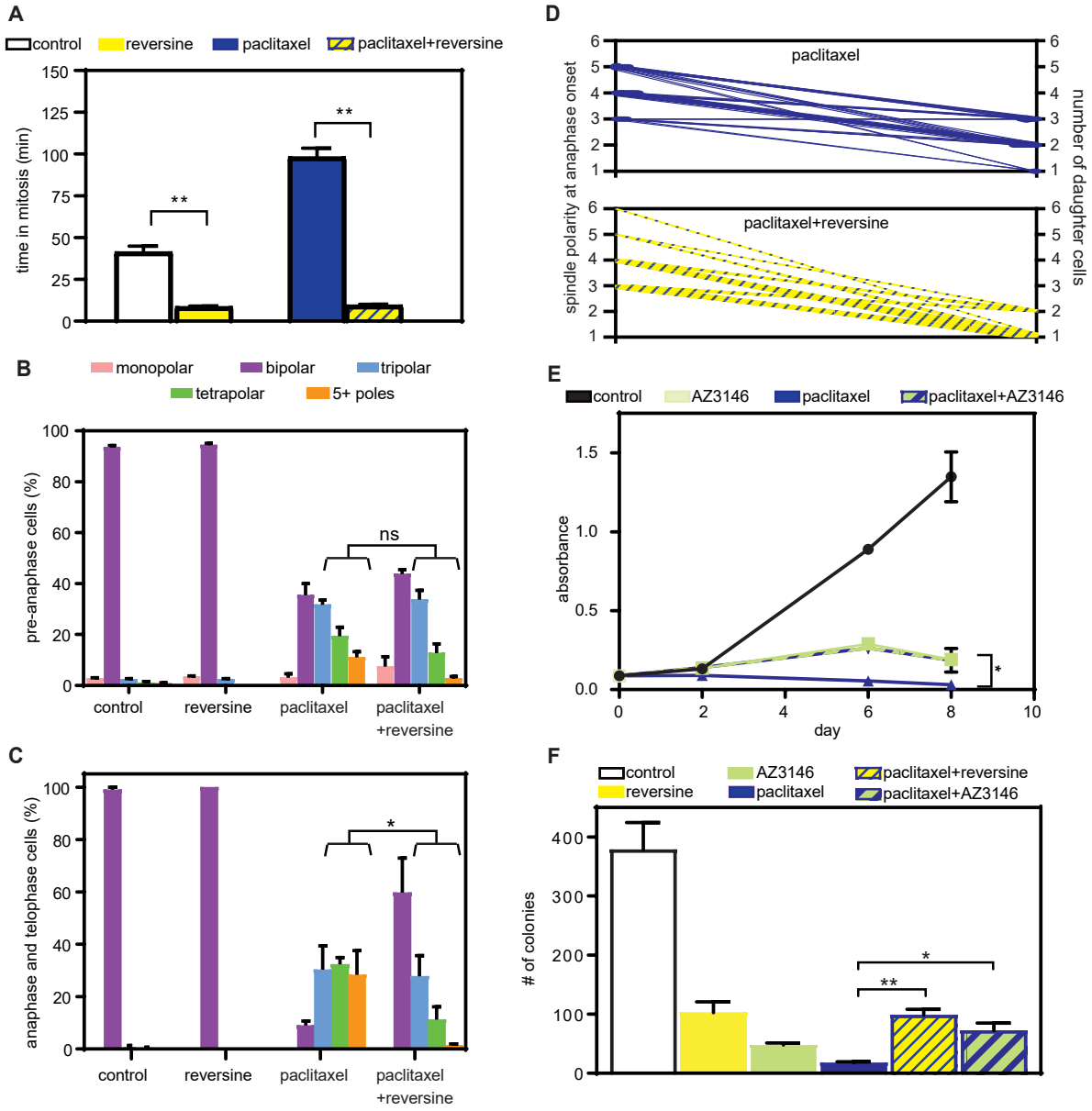

Figure 2.S5. Mps1 inhibition reduces sensitivity to paclitaxel in MDA-MB-231 cells. A) Time in mitosis, quantified by 24-hour fluorescent timelapse microscopy at 3-minute intervals as the time from NEB to anaphase onset. Data represent mean +/- SEM of two movies. n=81, 89, 89, 76 cells, respectively, for each condition. **B-C**) Spindle polarity (mean +/- SEM) in (**B**) pre-anaphase and (**C**) anaphase and telophase cells assessed by fixed analysis. n≥100 cells in each of three (B) or four (C) independent replicates. **D**) Multipolar spindle focusing after anaphase onset in reversine treated cells. Each cell is represented by a line connecting the number of spindle poles at anaphase onset (left) and the number of daughter cells formed (right). **E-F**) The effect of the Mps1 inhibitor, AZ3146, on cell survival in paclitaxel. **E**) MTT metabolic viability assay (mean +/- SEM). n=2. **F**) Colony formation assay following treatment with reversine or AZ3146 in a clinically relevant dose of paclitaxel (10 nM) in MDA-MB-231 cells. n≥2. *P<0.05. **P<0.001. ns=not significant.

Figure 2.S6. Mad1 upregulation in MDA-MB-231 cells decreases multipolar divisions and response to paclitaxel.

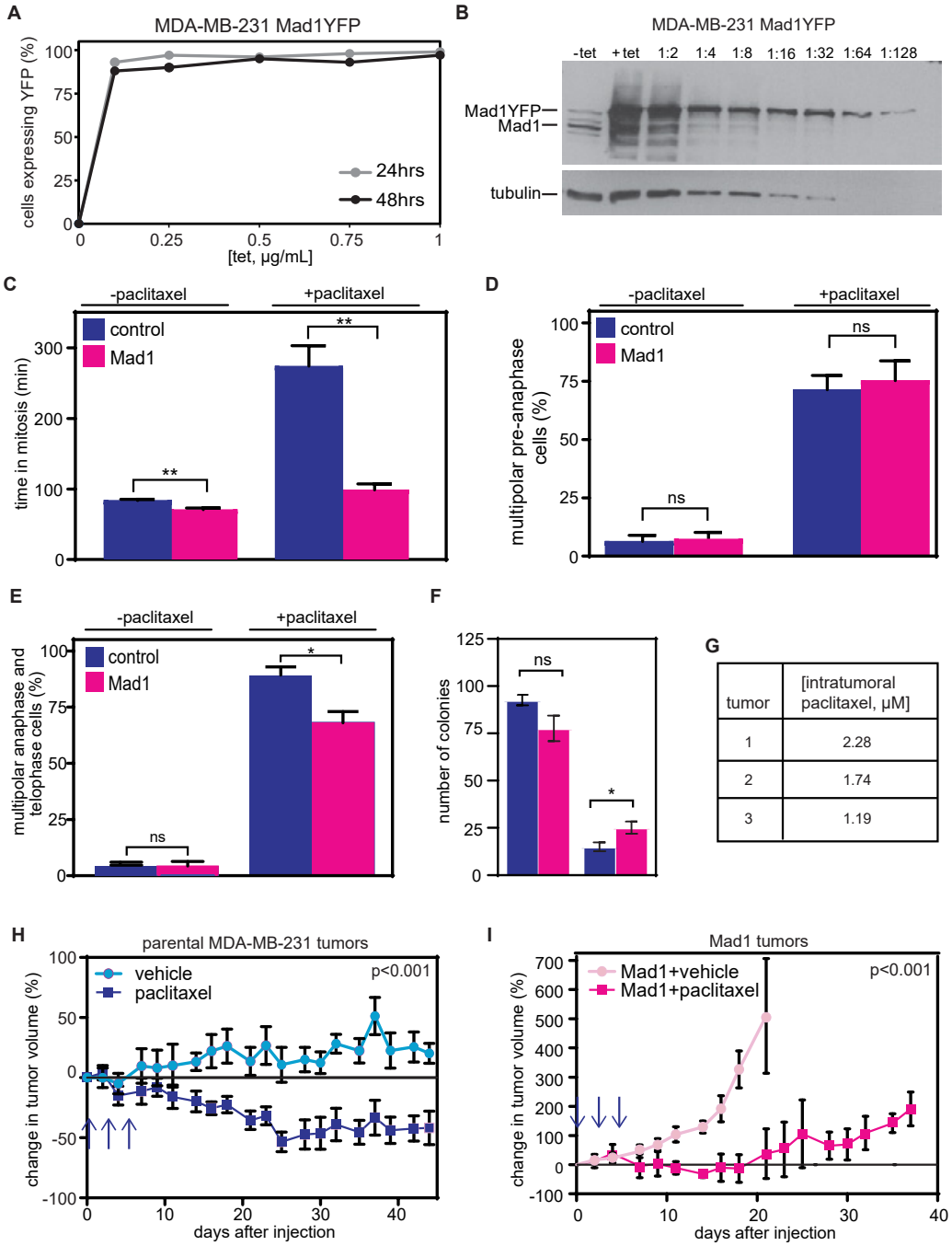

Figure 2.S6. Mad1 upregulation in MDA-MB-231 cells decreases multipolar divisions and response to paclitaxel. A-B) Uniform, tet-inducible expression of Mad1 in MDA-MB-231 cells. **A**) Percent of MDA-MB-231 cells expressing Mad1-YFP 24 and 48 hours after addition of the indicated doses of tet. **B**) Immunoblot showing Mad1 expression 24 hours after addition of 2 μg/mL tet. **C-F**) Effects of Mad1 upregulation in MDA-MB-231 cells treated with 10 nM paclitaxel. **C**) Time in mitosis, assessed as the time from cell rounding to the time the first daughter cell sat down. Data represent the mean +/- SEM of two brightfield movies. n=103, 100, 67 and 87 cells for control, Mad1, paclitaxel, and paclitaxel+Mad1, respectively. **D**) Spindle polarity (mean +/- SEM) in pre-anaphase cells quantified by fixed analysis. n≥100 cells per replicate in each of 3 biological replicates. **E**) Spindle polarity (mean +/- SEM) in anaphase and telophase cells quantified by fixed analysis. n≥50 cells per replicate in each of 3 biological replicates. **F**) Colony formation assay. Data represent mean +/- SEM. n=3. **G**) HPLC measurements of orthotopic intratumoral drug levels 20 hours after iv injection with 30 mg/kg paclitaxel. Each tumor contains a clinically relevant concentration. **H-I**) Percent change in tumor volume after vehicle or paclitaxel treatment in (**H**) parental or (**I**) Mad1 upregulated tumors. Arrows indicate days of paclitaxel treatments. n=6 tumors per treatment condition. *P<0.05. **P<0.001. ns=not significant.

Figure 2.S7. Patient response cannot be predicted by current measures.

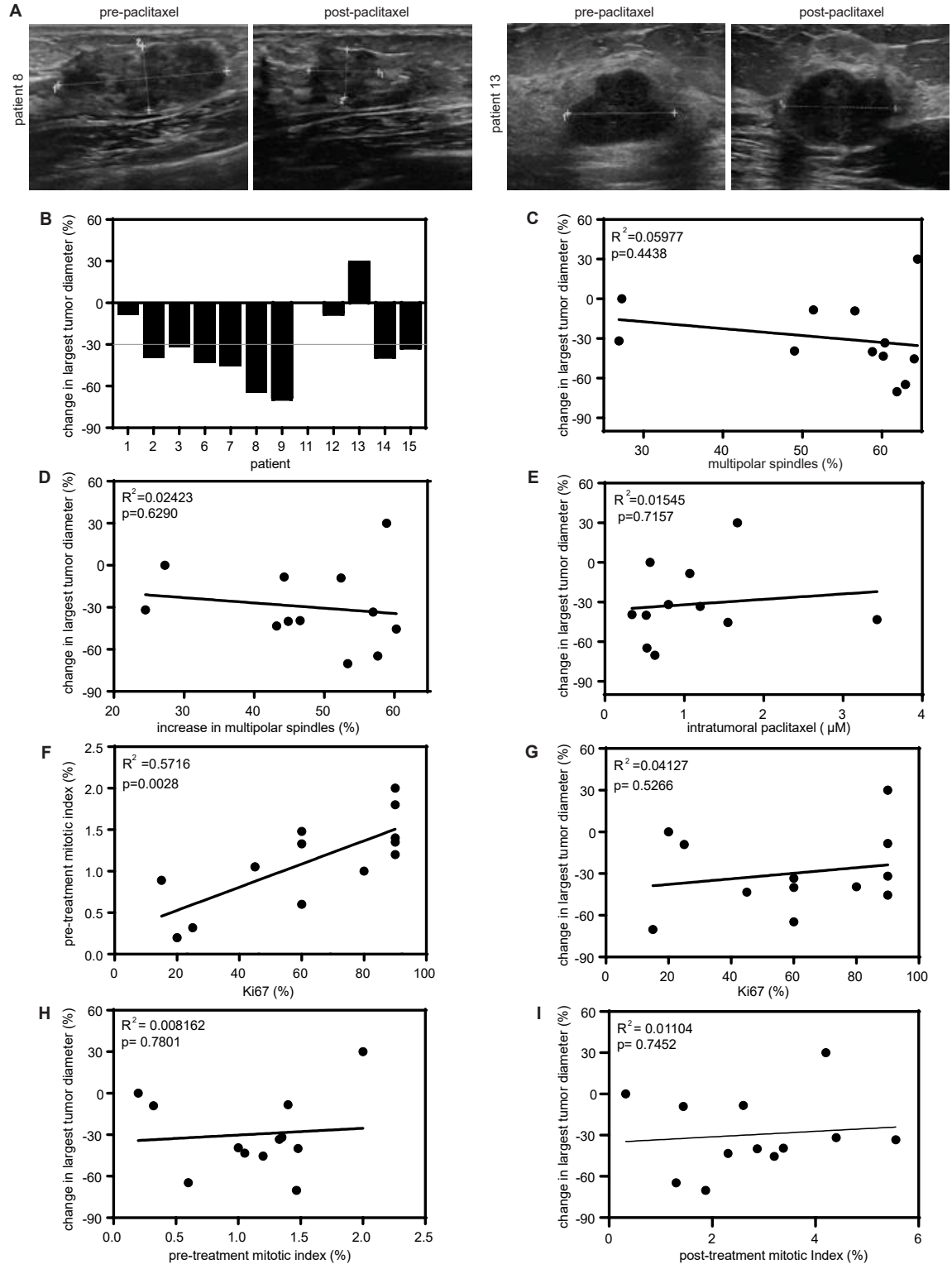

Figure 2.S7. Patient response cannot be predicted by current measures. A) Representative breast ultrasound images of a paclitaxel responder (left) and non-responder (right). **B**) Waterfall plot showing the percent change in largest tumor diameter following paclitaxel treatment. Response to paclitaxel is defined as having a decrease of ≥30% in the largest tumor diameter (grey line), according to RECIST 1.1 criteria (Eisenhauer *et al.*, 2009). Three patients were excluded from response analysis due to the inability to accurately determine tumor measurements (patient 5), deviation from treatment protocol (patient 4), or withdrawal of patient consent (patient 10). **C-E**) Tumor response does not correlate with percent multipolar spindles in patients 20 hours after treatment with paclitaxel (**C**), the increase in multipolar spindles between pre-treatment and 20 hours post-paclitaxel treatment (**D**), or the intratumoral concentration of paclitaxel (**E**). Note that the vast majority of mitotic cells detected in patient tumors have not yet entered anaphase, precluding analysis of the extent to which specific tumors focus multipolar spindles as they proceed through mitosis. **F-G**) Ki-67, a measure of tumor proliferation, correlates with mitotic index (**F**), but not tumor response (**G**). **H-I**) Tumor response does not correlate with mitotic index before (**H**) or after (**I**) 20 hours of paclitaxel.

Figure 2.S8. Inducible expression of Mad1 increases CIN on bipolar spindles and sensitivity to paclitaxel in Cal51 and DLD1 cells.

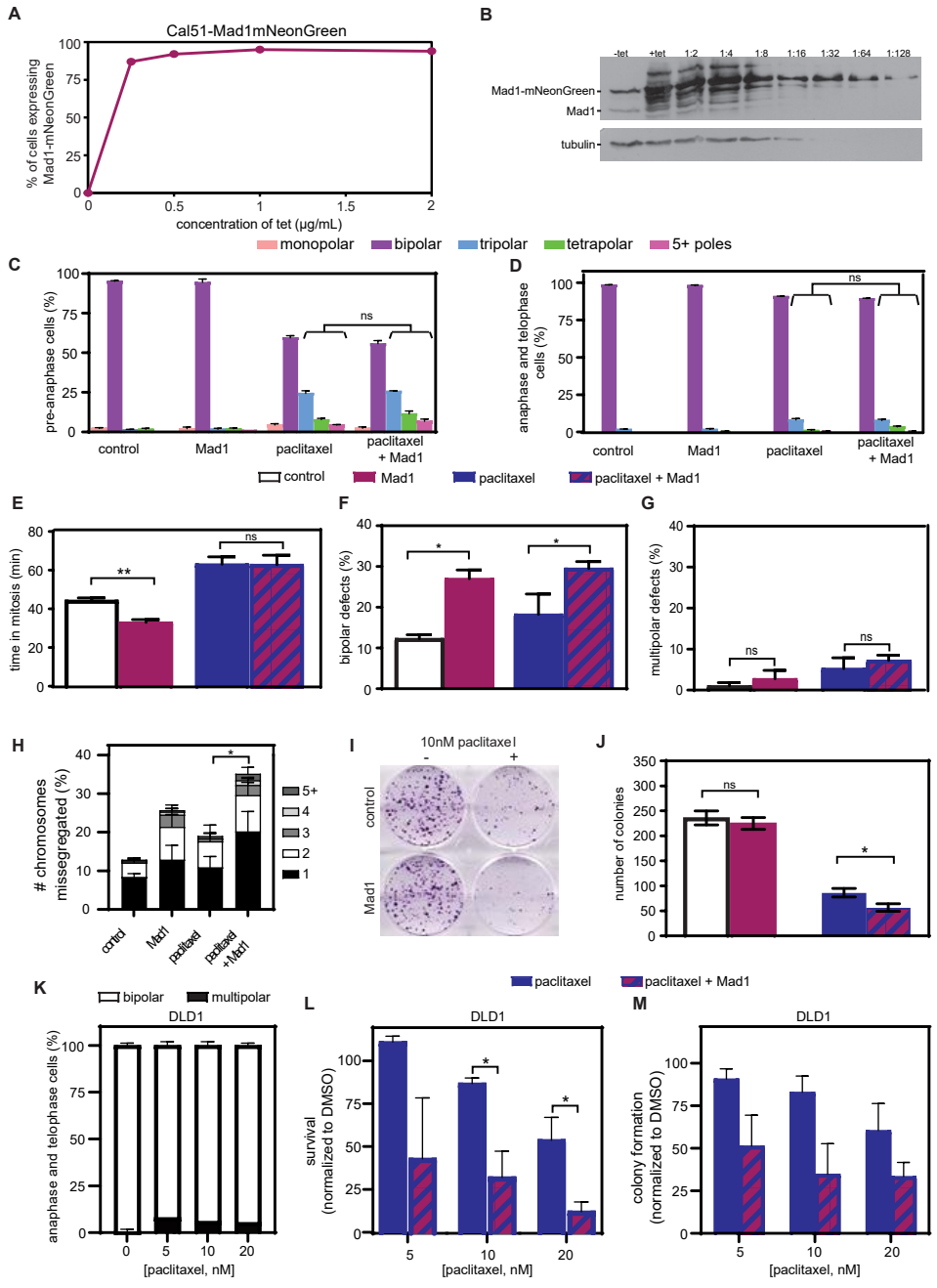

Figure 2.S8. Inducible expression of Mad1 increases CIN on bipolar spindles and sensitivity to paclitaxel in Cal51 and DLD1 cells. A) Quantification of the percent of Cal51 cells expressing Mad1-mNeonGreen 24 hours after addition of the indicated concentrations of tet. **B**) Immunoblot showing level of Mad1 expression in Cal51 cells 24 hours after addition of 2 μg/mL tet. Image is representative of 3 blots. **C-J**) Effects of Mad1 upregulation in Cal51 cells treated with 10 nM paclitaxel. **C**) Spindle polarity (mean +/- SEM) in pre-anaphase cells (n≥100 cells in each of 3 independent replicates) or **D)** anaphase and telophase cells (n≥50 cells in each of 3 independent replicates) assessed by fixed analysis. **E**) Mitotic timing, assessed by brightfield timelapse microscopy, as the time from NEB to anaphase onset. Values indicate mean +/- SEM from ≥40 cells. **F-H**) Quantification of the percent of cells with mitotic errors with **F**) bipolar or **G**) multipolar mitotic spindles. Data represent mean +/- SEM from ≥ 50 anaphase and telophase cells. n≥4. **H**) Quantification of the number of aberrant chromosomes per cell. **I**) Representative image of colony formation assay. **J**) Quantification of I. Data represent mean +/- SEM. n=5 independent experiments. **K-M**) Mad1 upregulation in DLD-1 cells treated with the indicated concentrations of paclitaxel. **K**) Quantification of spindle polarity in anaphase and telophase cells. n=50 cells in each of 3 independent replicates **L**) Cell survival as assessed by cell counts (mean +/- SEM) after 10 days of treatment with low nanomolar doses of paclitaxel. n≥2. **M**) Clonogenic survival (mean +/- SEM) relative to DMSO treated controls. n=2. *P<0.05. **P<0.001. ns=not significant.

Figure 2.S9. Previously suggested biomarkers do not correlate with taxane response in metastatic breast cancer.

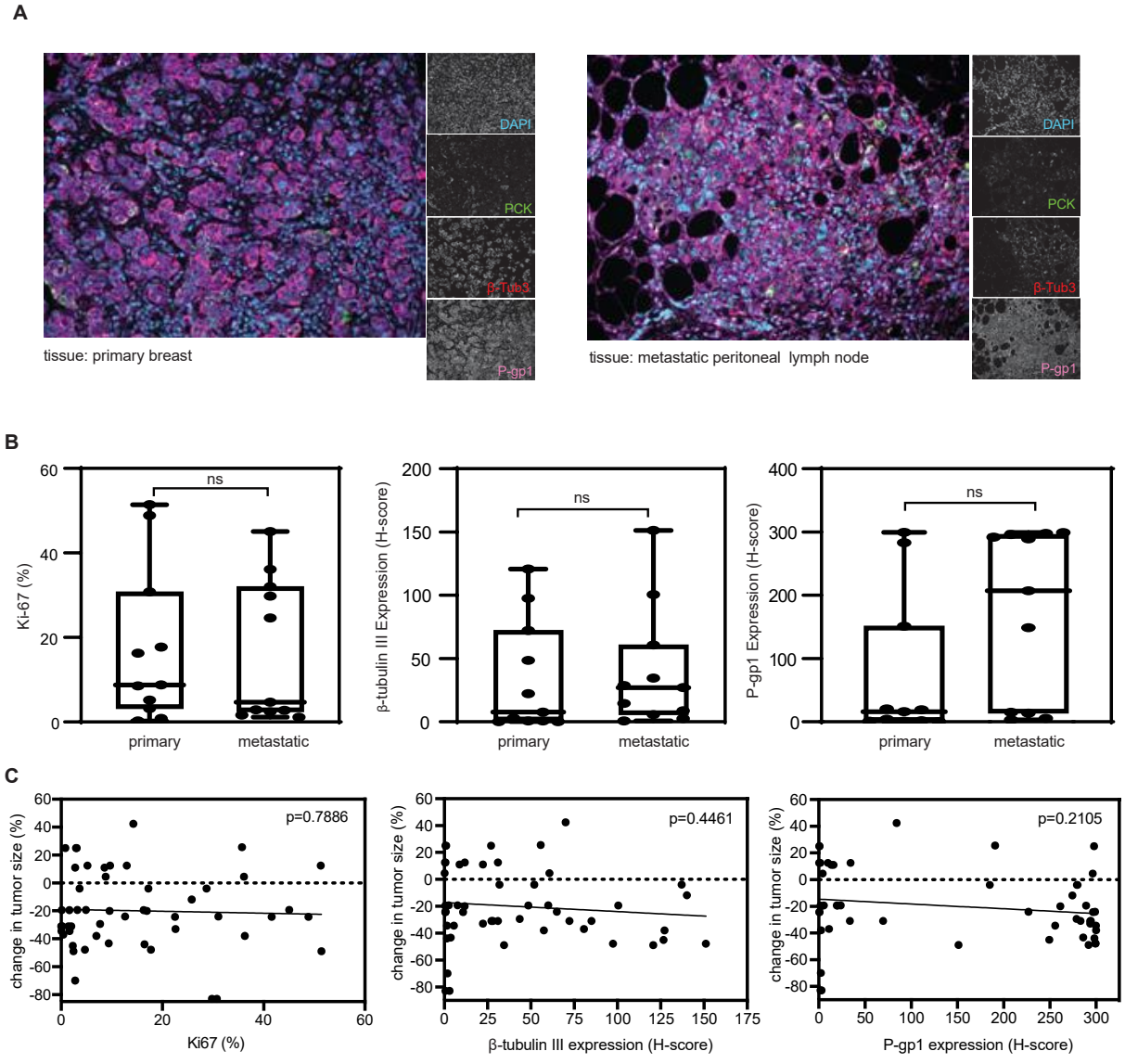

Figure 2.S9. Previously suggested biomarkers do not correlate with taxane response in metastatic breast cancer. A) Potential biomarkers were measured by quantitative immunofluorescence in matched primary (left) and metastatic (right) tumor tissues. PCK=pan-cytokeratin. β-Tub3=β-tubulin III. P-gp1=phospho-glycoprotein 1. **B**) Expression of Ki67, β-Tub3 and P-gp1 does not significantly differ between primary and metastatic breast tumors. **C**) Expression of Ki67, β-Tub3 and P-gp1 does not correlate with response to taxane in metastatic breast cancer.

Table 2.S1. 80 mg/m^2 paclitaxel trial patient characteristics.

Patient	Subtype	Stage	Age	Race	Ethnicity	Ki67
1	TNBC	T1N0M0	38	White	Non-Hispanic or Latino	90%
2	TNBC	T2N2M0	62	White	Non-Hispanic or Latino	80%
3	TNBC	T2N2M0	59	White	Non-Hispanic or Latino	90%
4	TNBC	T2N2M0	58	White	Non-Hispanic or Latino	90%
5	ER+/PR+/HER2-	T3N1M0	57	White	Non-Hispanic or Latino	25%
6	TNBC	T2N2M0	50	White	Non-Hispanic or Latino	45%
7	ER+/PR+/HER2-	T2N1M0	46	White	Non-Hispanic or Latino	90%
8	TNBC	T2N2M0	43	White	Non-Hispanic or Latino	60%
9	ER+/PR+/HER2-	T2N1M0	37	White	Non-Hispanic or Latino	15%
10	consent withdrawn					
11	ER+/PR+/HER2-	T3N1M0	52	White	Non-Hispanic or Latino	20%
12	ER+/PR+/HER2-	T2N0M0	55	Black	Non-Hispanic or Latino	25%
13	TNBC	T2N0M0	49	White	Non-Hispanic or Latino	90%
14	ER-/PR+/HER2-	T1N0M0	44	White	Non-Hispanic or Latino	60%
15	TNBC	T2N0M0	37	White	Non-Hispanic or Latino	60%

Table 2.S1. 80 mg/m^2 paclitaxel trial patient characteristics.

TNBC: Triple negative breast cancer. ER: Estrogen Receptor. PR: Progesterone Receptor. HER2: human epidermal growth factor receptor 2. TNM: primary tumor (T), regional lymph nodes (N), distant metastases (M). T1 indicates a tumor ≤ 2 cm, T2 indicates a tumor >2 cm but no more than 5 cm, and T3 indicates a tumor >5 cm in greatest dimension. Node (N) indicates the regional lymph node status according to the American Joint Committee on Cancer (AJCC). All patients in this study were M0, meaning there was no evidence of metastatic spread. Patient 9 was diagnosed with invasive lobular carcinoma. All other patients were diagnosed with invasive ductal carcinoma.

Table 2.S2. Intracellular paclitaxel measurements.

	[Intracellular paclitaxel, μM] ± SEM			
treatment (nM)	MDA-MB-231	MCF10A	HeLa	RPE
DMSO	ND	ND	ND	ND
0.01	-	ND	-	-
1	-	0.22 ± 0.06	-	-
5	6.8 ± 2.61	1.24 ± 0.11	0.94 ± 0.07	0.84 ± 0.05
10	8.0 ± 2.01	2.56 ± 0.43	1.86 ± 0.14	1.79 ± 0.09
20	17.7 ± 5.49	4.72 ± 0.70	2.79 ± 0.14	2.84 ± 0.43
50	39.9 ± 13.75	11.19 ± 1.90	9.51 ± 0.21	7.17 ± 0.99
100	55.2 ± 12.01	22.48 ± 4.06	18.21 ± 2.70	10.99 ± 1.04
500	78.7 ± 16.14	-	43.01 ± 1.62	25.82 ± 0.85
1000	104.4 ± 12.20	-	47.39 ± 2.41	32.15 ± 5.94

Intracellular paclitaxel levels were measured by LC-MS/MS 20 hours after addition of paclitaxel to cell culture media. Values represent mean ± SEM. n=3. ND indicates not detected. (-) indicates not tested.

Table 2.S3. CENP-E inhibition is synergistic with clinically relevant doses of paclitaxel.

Compound 1	Compound 2	Fraction Affected	parameters			Combination Index (CI)
[paclitaxel, nM]	[GSK923295, nM]		m	Dm	r	
1	0	0.18	0.74103 +/- 0.13876	3.53579	0.95122	NA
5	0	0.54				NA
10	0	0.788				NA
20	0	0.868				NA
500	0	0.961				NA
0	25	0.075	3.12554 +/- 0.32587	59.4719	0.9893	NA
0	50	0.286				NA
0	75	0.663				NA
0	100	0.864				NA
1	50	0.355	NA	NA	NA	1.65082
5	50	0.812				0.72281
10	50	0.832				0.83041
20	50	0.872				0.87968
500	50	0.963				2.03580

Chou-Talalay non-constant ratio synergy testing of paclitaxel and the CENP-E inhibitor GSK923295 in Cal51 cells. Combination Index (CI)=1 indicates an additive response, CI>1 an antagonistic one, and CI<1 is synergistic. m = kinetic order of single drug curves, Dm = IC_{50}, r = linear correlation coefficient for median affect plot, NA=not applicable.

Table 2.S4. Metastatic patient characteristics and taxane response.

Patient Characteristics (n=37)	
Age (Mean +/- SD)	59.7 +/- 12.8
Hormone receptor positive (%)	54 (20/37)
HER2 positive (%)	22 (8/37)
TNBC (%)	24 (9/37)
Stable disease (%)	51 (19/37)
Partial response (%)	41 (15/37)
Progressive disease (%)	8 (3/37)
Mean reduced tumor size (%)	-34
Range of reduced tumor size (%)	-4 to -83
Mean duration of taxane therapy (days)	177.9
Range of taxane therapy (days)	43 to 883

TNBC: Triple negative breast cancer. Hormone receptor positive (ER: Estrogen Receptor or PR: Progesterone Receptor positive). HER2: human epidermal growth factor receptor 2. Stable disease, partial response, and progressive disease were evaluated by RECIST 1.1 guidelines (Eisenhauer *et al.*, 2009).

Table 2.S5: Paclitaxel concentration measurements in patient tumors by tumor weight.

patient	[plasma paclitaxel, μM]	[intratumoral paclitaxel, μM]	degree of concentration
1	0.023	1.17	51x
2	0.040	0.39	10x
3	0.030	0.56	19x
4	0.027	0.72	27x
5	0.031	ND	-
6	0.020	3.61	181x
7	0.013	2.24	172x
8	0.011	0.53	48x
9	0.020	0.60	30x
11	0.038	0.88	23x
12	0.040	ND	-
13	0.094	1.98	21x
14	0.048	0.66	14x
15	0.035	2.16	62x

Intratumoral and plasma paclitaxel levels were measured by HPLC analysis 20 hours after the first dose of paclitaxel. Paclitaxel was quantified per tumor weight assuming a tumor density of 1 g/cm^3 or 1 g/mL. Paclitaxel was not determined (ND) in the tumor biopsies for subjects 5 and 12 due to insufficient tumor tissue collected by biopsy. Patient 10 withdrew consent.

APPENDIX ONE: The mitotic effects and change in paclitaxel concentrations after subsequent doses

Christina M. Scribano, Meng Xu, Kari B. Wisinski, Amye J. Tevaarwerk, Ruth O'Regan,

Lingjun Li, Mark E. Burkard, and Beth A. Weaver

*The work in this appendix is ongoing and unpublished.

We recently showed that paclitaxel did not reach sufficiently high concentrations to induce mitotic arrest in patient biopsies 20 hours after the first dose of either 175 mg/m^2 or 80 mg/m^2 paclitaxel therapy. Instead, multipolar mitotic spindles were observed in all patient tumors following paclitaxel treatment. These data led us to hypothesize that paclitaxel causes cell death in primary breast tumors due to chromosome missegregation that results from cell division on multipolar spindles. Previous work in cell culture models demonstrated that paclitaxel accumulates intracellularly to varying degrees, ranging from 67- to over 1000-fold, depending on the concentration used and cell type studied (Jordan *et al.*, 1993; Jordan *et al.*, 1996). Although previous studies have measured paclitaxel levels in patient serum, clinically relevant intratumoral concentrations of paclitaxel in breast cancer had not been determined prior to our work.

Furthermore, there are limited studies investigating the retention of paclitaxel within patient tumors after multiple doses over time. One such study looked in uterine cervical cancer patients that were treated with weekly 60 mg/m^2 paclitaxel for 2-4 weeks found that approximately 400 nM paclitaxel remained in their tumors six days after their final dose was administered (Mori et al., 2006). These results suggest that paclitaxel is retained in uterine cervical tumors for a prolonged period of time. However, whether paclitaxel is retained in human breast tumors over time remains unknown. Given this, we determined how paclitaxel concentrations changed in patient plasma and tumor samples after multiple doses of paclitaxel. If there is little paclitaxel turnover and concentrations stack with subsequent doses, intratumoral concentrations could reach high enough levels to induce mitotic arrest during treatment. Since the resistance

mechanisms underlying mitotic arrest and CIN-inducing multipolar spindles are distinct, it is important to determine whether mitotic arrest or multipolarity is achieved in human tumors throughout the duration of paclitaxel treatment, which consists of 12 weekly doses of 80 mg/m^2 in the low dose treatment regimen.

It is also important to understand the effects of paclitaxel in peripheral normal tissue. We recently found that approximately 18 chromosomes are missegregated per division in Cal51 cells treated with a clinically relevant dose of paclitaxel (Lynch et al., 2021). This high level of missegregation represents an effective therapeutic strategy for tumor cells but would likely be detrimental to normal cells. Previous studies in brain and gynecological tumors have found decreased or undetectable levels of paclitaxel in peripheral normal tissue compared to tumor tissue (Fine et al., 2006; Koshiba et al., 2009). However, these measurements have not yet been performed in breast cancer patients. Furthermore, determining the effects of paclitaxel on peripheral normal tissue may improve our understanding of the mechanisms underlying paclitaxel associated toxicities. Measurement of the intracellular concentration of paclitaxel in peripheral non-cancerous tissue would help elucidate its effects on these tissues.

Here we set out to address those questions by examining serial biopsies from patients receiving paclitaxel therapy. In addition to a diagnostic biopsy and biopsy 20 hours after the first dose of paclitaxel obtained from all patients enrolled in our 80 mg/m^2 paclitaxel clinical trial, we obtained biopsies after the third and twelfth (final) dose of paclitaxel from a subset of patients. Moreover, to determine the effects of paclitaxel on normal surrounding tissue, we collected skin biopsies from a subset of patients enrolled in our ongoing study. Chapter Two contains data from the first 15 patients enrolled, data

from three additional patients are reported here (ages 26-71, median 49; Table A.1). One patient withdrew from the study and three patients were evaluated for a subset of endpoints due to insufficient biopsy material (2) or deviation from treatment protocol (1). The biopsies from patients 17 and 20 were also evaluated for a subset of endpoints, as they have not yet been analyzed for mitotic index or spindle multipolarity, and intratumoral concentration measurements have not yet been performed for patient 20.

The trial design is depicted in Figure A.1A. After diagnostic core needle biopsy, tumors were measured by ultrasound or MRI before patients received 12 weekly doses of 80 mg/m^2 paclitaxel infused over 1 hour. For all enrolled patients, a second core biopsy and blood draw were obtained 20 hours after the initiation of the first infusion of paclitaxel. The 20 hour timepoint was selected because cultured breast cancer cells mount a robust mitotic arrest to high doses of paclitaxel at this timepoint, showing ≥15 fold increase in mitotic index as compared to vehicle treated cells (Zasadil *et al.*, 2014). Therefore, we expect that mitotic arrest would be evident at 20 hours. A subset of patients (8) received a third biopsy 20 hours after the third dose of paclitaxel, although one was excluded from analysis due to insufficient tumor collected by biopsy after the first dose and two have not yet been analyzed yet for mitotic index or spindle multipolarity. One patient received a fourth biopsy 20 hours after the final dose of paclitaxel. Additional protocol amendments were added to obtain skin biopsies from a subset of patients (2) for the measurement of paclitaxel concentrations in normal tissue and for the use of MALDI-TOF to determine paclitaxel distribution in patient tumors.

Plasma paclitaxel levels are effectively cleared between doses, while paclitaxel turnover in tumors is variable among patients

Quantification of paclitaxel levels in patient samples revealed that intratumoral concentrations ranged from 0.32 to 3.43 μM 20 hours after the first dose, and 0.12 to 2.40 μM 20 hours after the third dose. Paclitaxel was not detected in a single tumor biopsy obtained after the twelfth and final dose of 80 mg/m^2 paclitaxel (Table A.2). It is possible that paclitaxel was not detected after the final dose of paclitaxel due to minimal residual tumor tissue after the duration of paclitaxel treatment (average cellularity of adjacent biopsies after the twelfth dose was 6.5%, compared to 15.22% after the third dose, and 44.55% after the first dose). Plasma concentrations of paclitaxel 20 hours after the first infusion ranged from 0.011 to 0.094 μM in our patient cohort (Table A.2), in agreement with previous measurements (Hertz *et al.*, 2018), and similar to what was observed after 175 mg/m^2 paclitaxel (Zasadil *et al.*, 2014). Plasma paclitaxel levels 20 hours after the third dose ranged from 0.013 to 0.062 μM and was 0.018 μM 20 hours after the twelfth and final dose of paclitaxel.

While plasma paclitaxel measurements 20 hours after the third dose and final dose of paclitaxel were similar to those measured 20 hours after the first dose of paclitaxel, the intratumoral concentrations after the third paclitaxel dose were, in some patients (3 out of 7), approximately three times the concentration measured after the first dose (Table A.2). In 3 of the remaining 4 patients, intratumoral paclitaxel concentrations were similar after the first and third dose, suggesting complete clearance of the first dose within the intervening two weeks. In one patient, the intratumoral concentration of paclitaxel was lower after the third dose than the first dose, though this

could due to reduced cellularity (from 60% to 10% in adjacent biopsies), rather than a true reduction in the intratumoral paclitaxel concentration. In the other 6 patients, normalizing based on tumor cellularity in adjacent biopsies did not account for this observed difference in paclitaxel turnover. These results suggest that while plasma paclitaxel is efficiently cleared between doses, paclitaxel turnover in tumors is quite variable between patients over a two-week period.

We previously showed that patients treated with 175 mg/m^2 paclitaxel exhibited intratumoral concentrations of 1-9 μM and that these levels were insufficient to induce mitotic arrest (Zasadil *et al.*, 2014). In cell culture, we found that peak mitotic indices indicative of mitotic arrest were achieved when cells were treated with high doses of paclitaxel (5 μM), resulting in intracellular concentrations that ranged from 46 to 248 μM in Cal51 and MDA-MB-231 cells, respectively (Zasadil *et al.*, 2014). Based on these measurements, in the unlikely event that no paclitaxel turnover occurred over a 12-week period and intratumoral concentrations were expected to stack with each dose in every patient, the majority of patients (9/16) that received low dose weekly paclitaxel would not accumulate intratumoral paclitaxel levels by the end of treatment that would exceed 9 μM. Furthermore, no patient (0/16) would achieve an intratumoral concentration of paclitaxel that was shown, on an intracellular level, to induce mitotic arrest in cell culture. These data indicate that paclitaxel concentrations stack in some patient tumors upon subsequent doses of paclitaxel, although intratumoral levels are unlikely to reach sufficiently high levels to induce a mitotic arrest.

Multipolarity is increased or maintained after subsequent doses of paclitaxel and is accompanied by relatively subtle changes in the mitotic index

We demonstrated that 80 mg/m^2 paclitaxel induces multipolar spindles, without mitotic arrest, 20 hours after the first dose (see Chapter Two). We next wanted to assess the change in spindle multipolarity and mitotic index 20 hours after the third and final dose of paclitaxel. Similar to the analysis conducted at 20 hours after the first dose of paclitaxel, tumor core biopsies were analyzed by immunofluorescence. Mitotic cells were identified based on DNA morphology and the presence of a mitotic spindle, labeled by Nuclear Mitotic Apparatus protein (NuMA), which localizes to spindle poles. Pan-cytokeratin was used to discriminate between stromal and breast epithelial (tumor) cells present in the biopsies. While the majority of mitotic cells prior to paclitaxel therapy displayed a normal bipolar mitotic spindle (Figure A.1B, top), 20 hours of 80 mg/m^2 paclitaxel frequently induced multipolar mitotic cells (Figure A.1B, bottom). Indeed, all patients exhibited an increase in multipolar spindle incidence following the first dose of paclitaxel treatment, with increases ranging from 25-73% (Figure A.1C). After the third dose of paclitaxel, the level of multipolarity continued to increase in four out of five patients and remained at a similar level in one patient (Figure A.1C, pink arrows). A further increase in multipolar spindles was observed in the patient biopsy after the final dose of paclitaxel, reaching a level of 87.5% multipolar mitotic spindles, and representing an increase of 13.3% when compared to the third dose of paclitaxel. These substantial increases in multipolar spindles were accompanied by only modest effects on the percentage of cells in mitosis (mitotic index; Figure A.1D). Thus, both standardly used doses of paclitaxel induce multipolar spindles without mitotic arrest in patient tumors, demonstrating this is the conserved mechanism of paclitaxel in breast cancer.

Subsequent doses of paclitaxel increase or maintain mitotic spindle multipolarity, but are insufficient to induce mitotic arrest.

Response correlations after subsequent doses of paclitaxel are not more predictive than after the first dose of paclitaxel

Response to paclitaxel therapy was evaluated according to RECIST 1.1 guidelines (Eisenhauer *et al.*, 2009), in which a 30% reduction in the largest tumor diameter was considered a partial response (Figure A.2 A and B). As discussed in Chapter Two, following the first dose of paclitaxel, we found that patient response did not correlate with the overall incidence of multipolar spindles, nor the percent increase in multipolar spindles from baseline in the first 15 patients evaluated. Inclusion of data from three subsequently enrolled patients did not change the results of these correlations (Figure A.2, C and D). This can likely be explained by the fact that our analysis included predominately pre-anaphase cells which could subsequently be focused into bipolar spindles with varying efficiency.

We next tested if these factors were predictive of response when looking at the third dose of paclitaxel. Similar to what we observed after the first dose of paclitaxel (Figure A.2 C and D), response did not correlate with the overall incidence of multipolar spindles after the third dose (Figure A.3C), nor the change in multipolarity between baseline and third paclitaxel dose biopsies (Figure A.3D). The change in multipolarity between the first and third paclitaxel dose was also not predictive of response (Figure A.3E). It is again important to note that our analysis included predominately pre-anaphase cells which could subsequently be focused into bipolar spindles with varying efficiency, providing a possible explanation for the lack of correlation observed here.

Just like intratumoral levels of paclitaxel following the first dose did not correlate with patient response (Figure A.2E), we found that intratumoral paclitaxel concentrations after the third dose of paclitaxel did not correlate with response (Figure A.3F), nor did the change in intratumoral paclitaxel levels between the first and third dose (Figure A.3G). Finally, we found that the mitotic index after the first dose of paclitaxel was not predictive of response in all of patient samples analyzed to date (Figure A.2J), arguing against the predominant dogma that mitotic arrest is necessary for the cytotoxicity of paclitaxel. When looking after the third dose of paclitaxel, we again found that mitotic index did not correlate with response (Figure A.3H), nor did the change in mitotic index between the third and first dose (Figure A.3I). Therefore, these biomarkers evaluated at the first and third dose of paclitaxel are not sufficient to predict the response of individual tumors to paclitaxel and an additional metric(s) is necessary. In Chapter Two, we proposed that pre-existing chromosomal instability can be used as a predicative biomarker of response.

Low variability between and within patient biopsies

Next, we estimated the error in these patient metrics. First, we estimated the error in our assessment of multipolarity between patient biopsies (Figure A.4A). Each dot represents the quantification of the percent of mitotic cells with multipolar spindles in independent biopsies from the same patient at the given timepoint, showing approximately a ten percent variability between biopsies. Subsequently, we quantified the error in our assessment of mitotic index within different regions of a patient biopsy. Mitotic index was quantified in at least three different regions of a patient biopsy at various timepoints (Figure A.4B). Comparing these values, we found that the mitotic

indices showed approximately a five percent variability between different regions within the same biopsy. These data suggest that the error in our measurements between and within patient biopsies is relatively low.

Paclitaxel levels were undetectable in peripheral normal tissue

The concentration and effects of paclitaxel in normal tissue remain unknown. At clinically relevant intratumoral concentrations, paclitaxel induces multipolar spindles that result in high rates of chromosome missegregation and cell death (Lynch *et al.*, 2021; Zasadil *et al.*, 2014). It remains to be determined whether paclitaxel induces these deleterious effects to the same extent in normal tissue. Based on the side effect profile of paclitaxel, it is known that this drug also affects normal, non-cancerous cells within the body. Common side effects include nausea and hair loss, presumably due to the effects of paclitaxel on the rapidly dividing normal cells in the gut and hair follicle, respectively. To begin to determine how paclitaxel affects normal tissue, we added an amendment to our clinical trial protocol to measure paclitaxel levels in patient skin biopsies. Of the two patient skin biopsies measured thus far, we were unable to detect quantifiable amounts of paclitaxel (Table A.2). These results are consistent with a previous study that showed that paclitaxel levels were undetectable in adjacent normal tissues of gynecologic cancer patients receiving weekly 60 mg/m^2 paclitaxel (Koshiba *et al.*, 2009). In a second study of primary and metastatic brain cancer patients receiving 175 mg/m^2 paclitaxel, paclitaxel levels in the normal surrounding brain were also significantly lower in peripheral normal tissue compared to intratumoral concentrations. Specifically, paclitaxel concentrations in the normal surrounding brain were approximately nine times lower than the level measured in the tumor center and four

times lower than the level measured in the tumor periphery (Fine *et al.*, 2006). Taken together, these data suggest that although paclitaxel seems to have an effect on normal tissues in patients treated with this drug, paclitaxel levels found in skin tissue are undetectable by our current methods.

In the future, paclitaxel measurements could be performed in additional peripheral normal tissues to corroborate our paclitaxel measurements in patient skin biopsies. To this end, we added an amendment to our clinical trial protocol to measure paclitaxel concentrations in peripheral blood mononuclear cells (PBMCs). These measurements will need to be performed in future enrolled patients, since the blood processing requirements for PBMC measurements are different than the way in which blood samples were processed for previously enrolled patients. In the future, of the 15 mL of blood collected from patients, 10 mL will be used for PBMC paclitaxel measurements and 5 mL of blood will be used for plasma paclitaxel measurements.

We cannot exclude the possibility that we were unable to detect paclitaxel levels in patient skin biopsies and after the final dose of paclitaxel due to the fact that their levels were too low to be detected by HPLC. In the future, more sensitive methods for drug quantitation, such as LC-MS/MS, may be used to measure paclitaxel levels in our patient samples. LC-MS/MS also has the added advantage of providing more specificity. With HPLC, paclitaxel levels are quantitated using a detector which measures the intensity of ultraviolet (UV) absorbance. Compounds with conjugated systems (including paclitaxel) absorb UV light, moving electrons between the highest occupied electrical orbital (HOMO) to the lowest unoccupied molecular orbital (LUMO). The presence of other molecules with conjugated systems within samples means that

quantitation is not specific for paclitaxel, but rather encompasses all quantities of conjugated molecules at a particular elution time. On the other hand, LC-MS/MS only quantifies molecules with the correct molecular weight and corresponding daughter ions after the parental compound is fragmented. Therefore, it is highly specific to paclitaxel. Even if there are other molecules present in the samples with similar molecular weights, it is unlikely that they would exhibit the same fragmentation pattern and daughter ions as paclitaxel. Therefore, switching to the use of LC-MS/MS as a method of quantitation in the future has multiple benefits and can be particularly useful for quantitation of low abundance drug levels, as in peripheral normal tissue.

Variable paclitaxel distribution observed in Patient 103 after the 3rd dose of paclitaxel

While the changes in mitotic indices between paclitaxel doses remained relatively subtle across all patient tumors examined, an increase of 2.44% was observed between the first and third dose of paclitaxel in patient 103. Observation of the patient biopsy by immunofluorescence revealed a particular region of the tumor with a relatively high mitotic index (Figure A.5A, bottom), while other regions of the tumor had a lower mitotic index comparable to what was seen in most other patient tumors (Figure A.5A, top) . Given this, we added a clinical trial protocol amendment to measure paclitaxel level distribution within patient biopsies. To do this, we started a collaboration with Lingjun Li and her graduate student, Meng Xu, to perform matrix assisted laser desorption ionization-time of flight mass spectrometry (MALDI-TOF MS). In MALDI-TOF MS, samples are embedded in a matrix and ablated from the surface of the sample using a short laser pulse. The matrix helps to dampen some of the laser power and contains

ions that will ionize the analyte. Application of an electric field allows desorbed charged ions to be directed to the detector. Components of differing masses are separated based on their time of flight to the detector; if all ions start at the same time, the lighter ions will arrive first followed by the heavier ions. A MALD-TOF protocol to measure paclitaxel distribution in tissue samples was developed, and a linear calibration curve was generated (Figure A.4B). Future experiments are needed to determine paclitaxel distribution in patient tumors.

Our current data suggest that multipolar spindles uniformly increase over baseline after the first paclitaxel treatment. After subsequent doses of paclitaxel, the level of multipolarity either continued to increase (observed in the vast majority of patients) or is at least maintained at a similar level compared to previous doses of paclitaxel. Changes in the mitotic index after the first, third, and twelfth doses of paclitaxel were relatively subtle. Although the error in these measurements between and within patient biopsies were relatively low, these metrics were insufficient to predict patient response. Furthermore, our data demonstrated that plasma paclitaxel levels are efficiently turned over, as plasma paclitaxel measurements 20 hours after the third dose and twelfth dose of paclitaxel were similar to those measured 20 hours after the first dose of paclitaxel. On the other hand, intratumoral paclitaxel levels appeared to stack in some patients but not others. Importantly, this difference does not predict response (Figure A.3, Table A.2). Paclitaxel levels were undetectable in patient skin biopsies and in one tumor after the twelfth and final dose of paclitaxel. Future studies of a larger cohort of patients would strengthen our analysis. Nonetheless, taken together, data

from this cohort support the conclusion that paclitaxel exerts its anticancer effects due to mitotic spindle multipolarity. Furthermore, concentrations of paclitaxel achieved in primary breast cancer are insufficient to induce mitotic arrest, even after subsequent doses of drug.

Materials and Methods

80 mg/m^2 paclitaxel study design

Patients who volunteered to participate in this study were enrolled in a prospective trial at the UW Carbone Cancer Center specifying the treatment, biopsy, and analysis plan. The protocol was approved by UW Health Sciences Institutional Review Board, ID 2016-1489, assigned UWCCC protocol number UW16106, conducted in accordance with the ethical standards established in the 1964 Declaration of Helsinki and registered on clinicaltrials.gov (NCT03096418). Patients were enrolled if they had previously untreated locally advanced breast cancer for which neoadjuvant chemotherapy was indicated. Subjects received four cycles of standard-dose paclitaxel 80 mg/m^2 with biopsy and treatment as outlined in Figure A.1A. One patient withdrew and 3 patients were excluded from specific endpoints because of insufficient sample collected by biopsy (2) or deviation from treatment protocol (1). There were no major complications from protocol-mandated research biopsy.

This is an ongoing study of the mechanism of paclitaxel in human breast cancer. The patient sample size was selected to provide a sufficient number of biopsies for sampling intratumoral drug concentrations, effects on mitosis, and patient response. All

subjects had newly diagnosed breast cancer for which neoadjuvant chemotherapy was recommended per standard of care. Subjects received initial chemotherapy with paclitaxel 80 mg/m^2 dosed weekly for 12 weeks. A research biopsy was obtained 18–22 hours after start of the first infusion. After four cycles of paclitaxel, follow-up ultrasound or MRI imaging was performed to assess response to therapy and patients continued with surgery and anthracycline-based chemotherapy, per physician discretion. The objectives were to measure intratumoral paclitaxel concentrations, and to determine its effects on mitosis, chromosomal instability, and cell proliferation and to correlate these with response to treatment.

Imaging response criteria

Baseline imaging was performed by ultrasound or MRI as part of a complete diagnostic imaging evaluation including mammography. All imaging was performed as closely as possible to the beginning of treatment. Tumors were again evaluated by ultrasound for all patients, except for patients 18 and 19 whose tumors were evaluated by MRI, within two weeks of completion of paclitaxel chemotherapy and prior to any additional chemotherapy or surgery. A single board-certified breast imaging radiologist with seven years of experience (AMF) retrospectively reviewed the reports and saved images from the prospectively performed ultrasound exams for patients 1-15, response for subsequent patients were evaluated based on imaging reports obtained from the patients' medical records. These measurements should be verified by a board-certified breast imaging radiologist in the future. Imaging response was evaluated using RECIST 1.1 criteria (Eisenhauer *et al.*, 2009) and the single longest dimension measured on the baseline and post-paclitaxel ultrasound or MRI images. Three patients were excluded

from this analysis due to the inability to accurately determine tumor measurements (1), deviation from treatment protocol (1), or withdrawal of patient consent (1).

Immunohistochemistry

For patient immunohistochemistry, 5 μm sections of formalin-fixed, paraffin-embedded tissue sections were subjected to antigen retrieval in citrate buffer, serum-blocked overnight, and stained with rabbit anti-NuMA antibody [a kind gift from Duane Compton; (Compton et al., 1991)], mouse anti- γ-tubulin (Sigma, T6557), and pan-cytokeratin (to mark epithelial cells; Novus Biologicals, NBP2-33200AF647) antibodies diluted 1:100 overnight at 4°C. Alexa Fluor-conjugated secondary antibodies (Invitrogen) were used at 1:200 for one hour at room temperature. DNA was stained using DAPI.

Paclitaxel measurements

Patient tissue core biopsies were analyzed as in (Zasadil *et al.*, 2014). Briefly, core biopsies were thawed on ice and core length, diameter, and weight were recorded. Intratumoral concentrations were calculated using core tissue volume (cc) (Table 2). Calculations based on core tissue weight (g) gave similar results (Table S4). In this case, the final molar concentration (μM) calculations assume that tissue core density is equivalent to that of water (1 g/cm^3 or 1 g/mL). Patient biopsies were homogenized in EDTA drug-free human plasma + 10% acetonitrile and 10 μg/mL docetaxel (Sigma-Aldrich; 01885-5MG) was added as internal standard prior to pre-extraction to facilitate quantification of sample recovery. Homogenized samples were then applied to C18 Bond Elut solid-phase extraction columns (Agilent) and eluted with

acetonitrile by gravity or low vacuum. Solvents were then evaporated to dryness using nitrogen gas and samples were reconstituted in 100 µL acetonitrile and 100 µL of 35 mM acetic acid. Analysis was performed by monitoring the signal of a 50 µL injection at 235 nm during an isocratic elution with 56% 35 mM acetic acid, 44% acetonitrile on an analytical HPLC instrument (Shimadzu LC-20AD with SPD-20A UV Detector and a Waters Nova-Pak C18 4-µm 4.6 × 150 mm column). Calibration curves were obtained using paclitaxel at 10, 25, 50, 100, 250, 500, and 750 ng/mL. Quantification was carried out based on peak area and the linear calibration curve for each compound.

Microscopy

Images were acquired on a Nikon Ti-E inverted microscope driven by Nikon Elements software with focus-drift compensation. Images are maximum projections from 0.2 µm z-stacks collected with a 60×/1.4 or 100×/1.4 numerical aperture (NA) objective after deconvolution using the AQI 3D Deconvolution module in Elements.

Statistical Analysis

Statistical analysis was performed using GraphPad Prism, SAS, R, or Mstat 6.4.2 software (http://www.mcardle.wisc.edu/mstat/index.html). Student's t-tests were used to assess significance, unless otherwise noted, and simple linear regression was used for correlation plots. Other statistical parameters including the number of cells analyzed and the number of replicates are reported in the respective figure legends.

Figure A.1. Clinically relevant concentrations of paclitaxel cause multipolar spindles without mitotic arrest in breast cancer patients and cells.

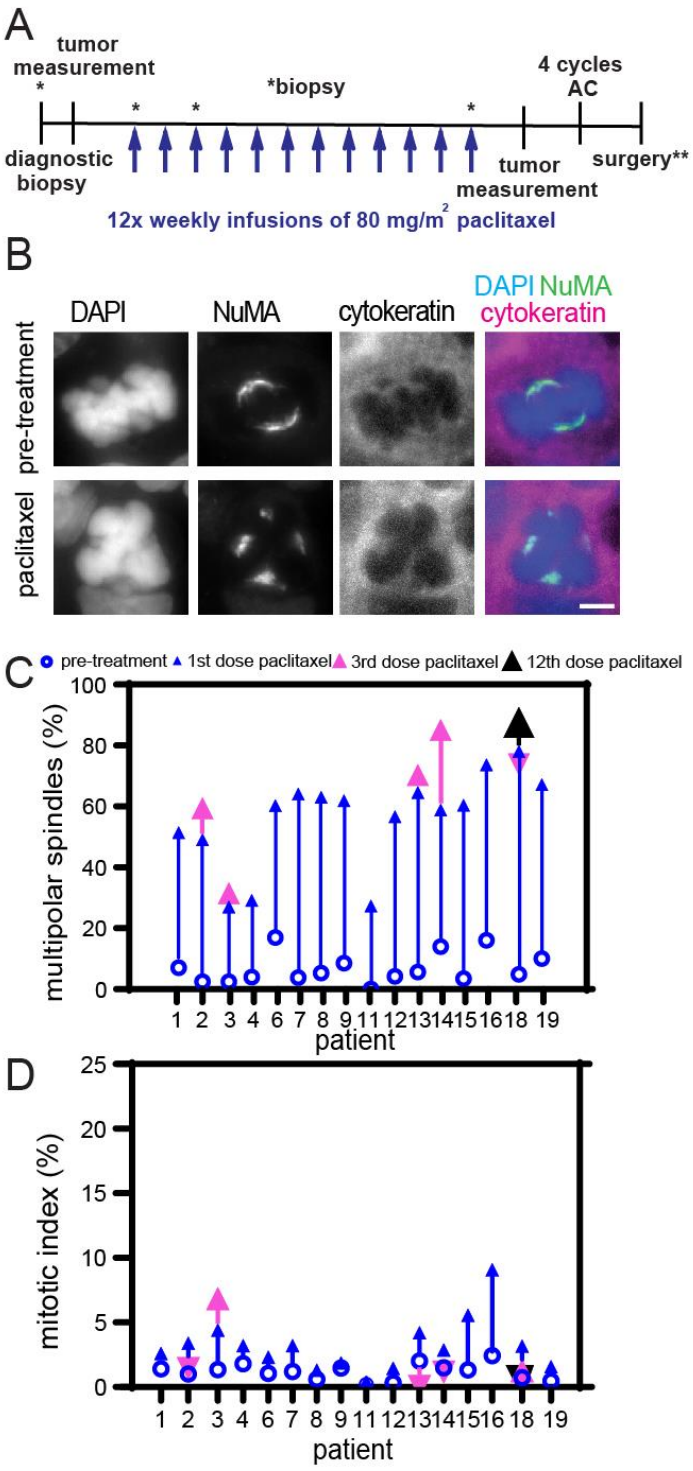

Figure A.1. Clinically relevant concentrations of paclitaxel cause multipolar spindles without mitotic arrest in breast cancer patients and cells. A) Schematic showing trial design. Research biopsies were obtained prior to paclitaxel treatment and 20 hours after the first dose of paclitaxel for all patients, and 20 hours after the third and twelfth doses of paclitaxel for a subset of patients. AC = Adriamycin and cyclophosphamide. **indicates that surgery could occur before or after AC, per physician recommendation. **B**) Representative images of bipolar (top) and multipolar (bottom) mitotic cells in patient tumors before and after paclitaxel treatment. Mitotic cells were identified based on DNA morphology and the presence of a mitotic spindle, labeled by Nuclear Mitotic Apparatus protein (NuMA), which localizes to spindle poles. Pan-cytokeratin was used to discriminate between breast epithelial (tumor) cells and stroma. Scale bar, 5 μm. **C-D**) 80 mg/m^2 paclitaxel induces multipolar spindles without mitotic arrest in primary breast cancer. Quantification of (**C**) multipolar mitotic spindles, defined as containing >2 NuMA foci, and (**D**) mitotic index before (open circle) and after (arrowhead; the direction indicates increase or decrease) paclitaxel treatment. Blue arrowhead indicates 20 hours after the first dose, pink arrowhead indicates 20 hours after the third dose, and black arrowhead indicates 20 hours after the final dose of paclitaxel. D, n≥500 cells. For assessment of multipolar spindles in C, mitotic cell sample sizes for patients are 113, 41, 100, 101, 106, 79, 75, 35, 6, 24, 106, 86, 116, 106, 42, and 30 cells, respectively, pre-treatment and 109, 100, 104, 103, 108, 103, 27, 63, 11, 30, 110, 102, 101, 104, 214, and 70 cells, respectively, 20 hours after the first treatment. After the third dose of paclitaxel, mitotic cell sample sizes are 32, 105, 101, 20, and 23 cells, respectively. 8 mitotic cells were counted in the patient sample after

the final dose of paclitaxel. Samples from patients 5 and 10 could not be analyzed due to insufficient tumor tissue collected by biopsy and withdrawal of consent, respectively.

Figure A.2. Patient response cannot be predicted by current measures.

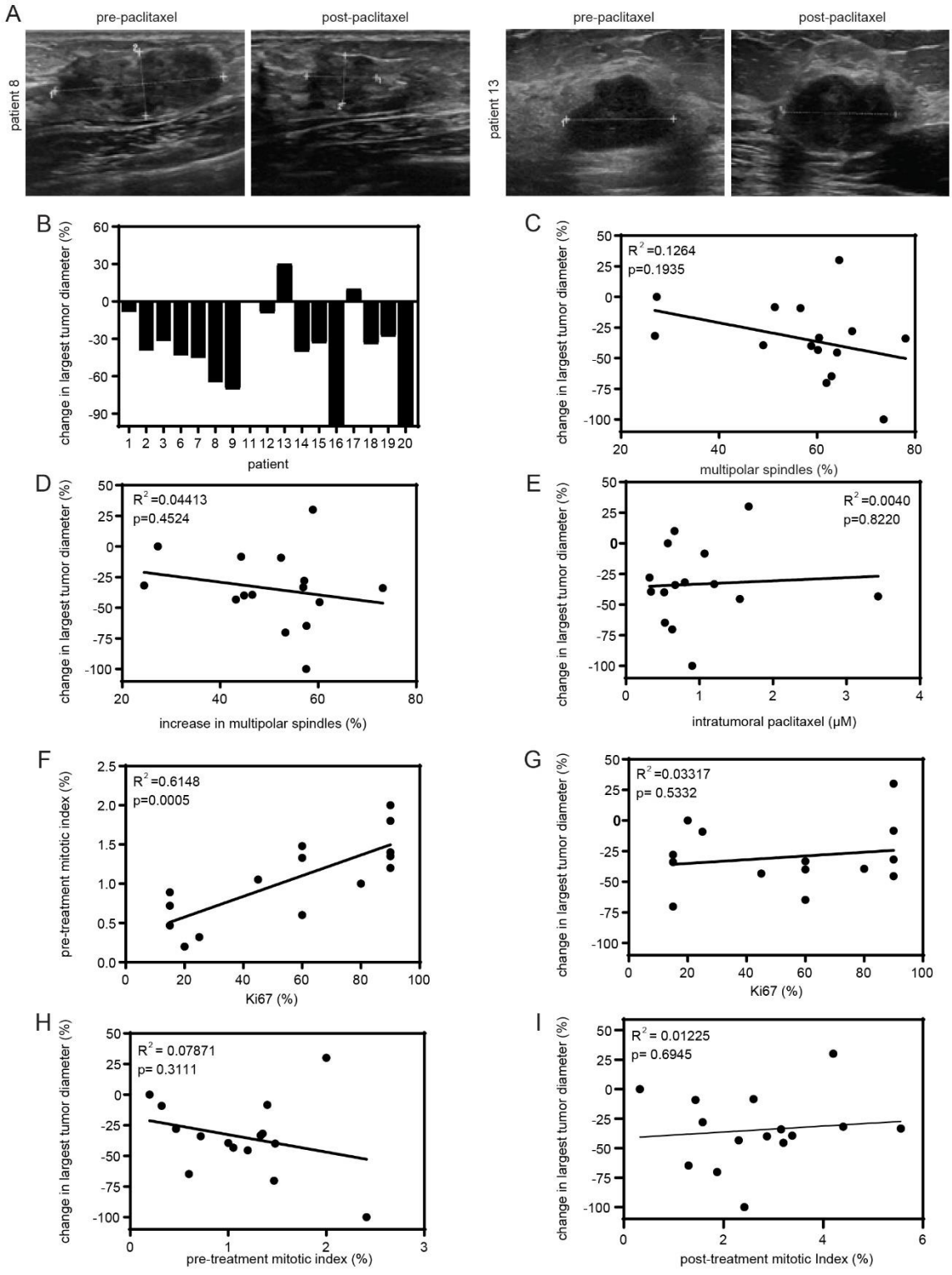

Figure A.2. Patient response cannot be predicted by current measures. A) Representative breast ultrasound images of a paclitaxel responder (left) and non-responder (right). **B**) Waterfall plot showing the percent change in largest tumor diameter following paclitaxel treatment. Response to paclitaxel is defined as having a decrease of ≥30% in the largest tumor diameter (grey line), according to RECIST 1.1 criteria (Eisenhauer *et al.*, 2009). Three patients were excluded from response analysis due to the inability to accurately determine tumor measurements (patient 5), deviation from treatment protocol (patient 4), or withdrawal of patient consent (patient 10). **C-E**) Tumor response does not correlate with percent multipolar spindles in patients 20 hours after treatment with paclitaxel (**C**), the increase in multipolar spindles between pre-treatment and 20 hours post-paclitaxel treatment (**D**), or the intratumoral concentration of paclitaxel (**E**). Note that the vast majority of mitotic cells detected in patient tumors have not yet entered anaphase, precluding analysis of the extent to which specific tumors focus multipolar spindles as they proceed through mitosis. Response correlations for spindle multipolarity includes patients 1-3, 6-9, 11-16, and 18-19. Biopsies from patients 17 and 20 have not been analyzed yet for spindle multipolarity. Response correlations for intratumoral drug levels includes patients 1-4, 6-9, and 11-19. Biopsies from patient 20 have not been analyzed yet for intratumoral dug levels. **F-G**) Ki-67, a measure of tumor proliferation, correlates with mitotic index (**F**), but not tumor response (**G**). Patient 10 was excluded from this analysis due to consent withdrawal, and patient 16 was excluded since their Ki67 evaluation did not include an exact number, but rather was classified as >20% (Table A.2). **H-I**) Tumor response does not correlate with mitotic index before (**H**) or after (**I**) 20 hours of paclitaxel. Response

correlations for mitotic index includes patients 1-3, 6-9, 11-16, and 18-19. Biopsies from patients 17 and 20 have not been analyzed yet for spindle multipolarity.

Figure A.3. Patient response correlations after the third dose of paclitaxel.

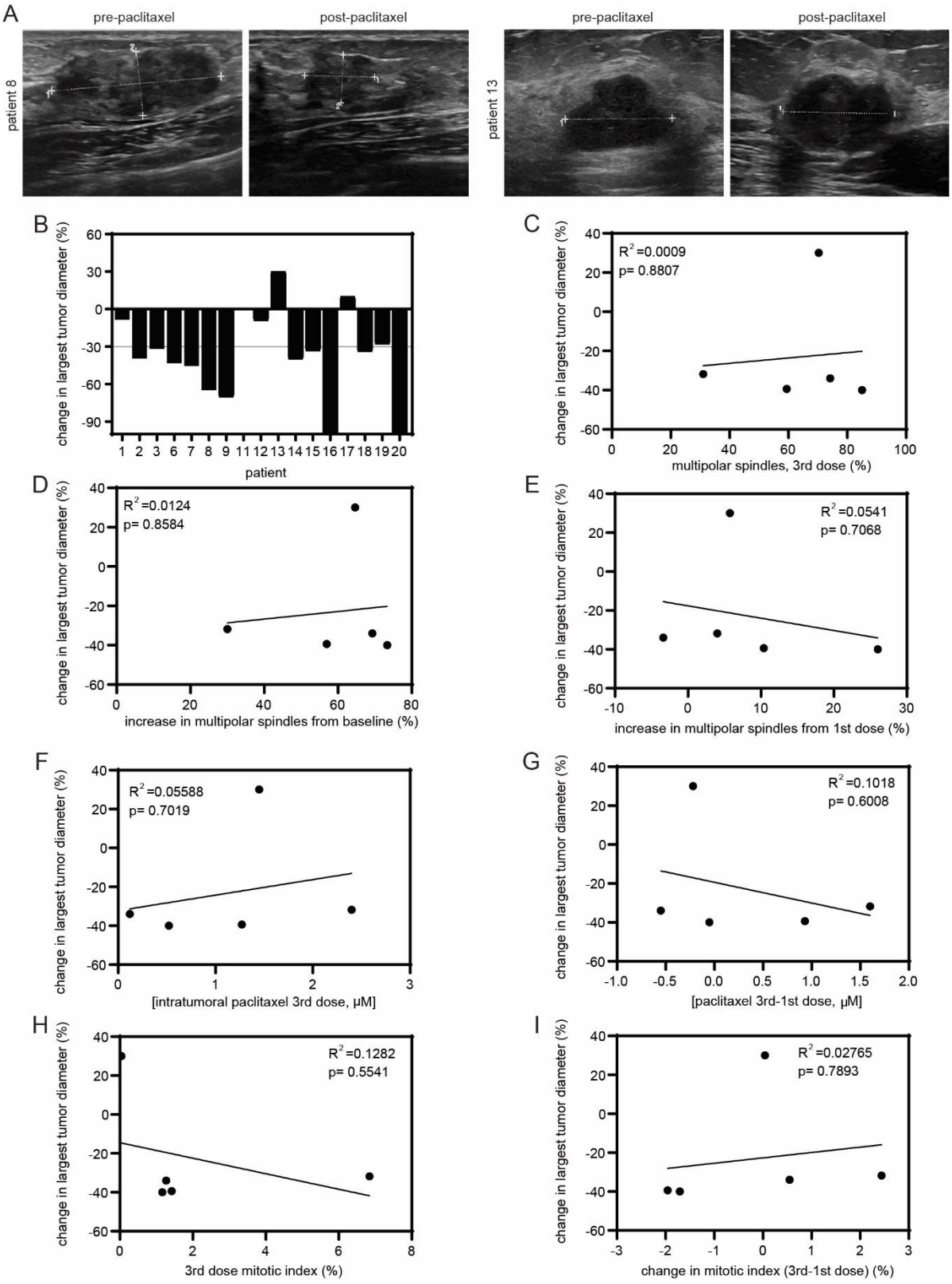

Figure A.3. Patient response correlations after the third dose of paclitaxel. A) Representative images of a paclitaxel responder (left) and non-responder (right). **B**) Waterfall plot showing the percent change in largest tumor diameter following paclitaxel treatment. Response to paclitaxel is defined as having a decrease of ≥30% in the largest tumor diameter (grey line), according to RECIST 1.1 criteria (Eisenhauer *et al.*, 2009). Three patients were excluded from response analysis due to the inability to accurately determine tumor measurements (patient 5), deviation from treatment protocol (patient 4), or withdrawal of patient consent (patient 10). Tumors were again by ultrasound for all patients, except for patients 18 and 19 whose tumors were evaluated by MRI. **C-I**) Response correlations for patients 2, 3, 13, 14, and 18, all of which had an additional biopsy after the 3rd dose of paclitaxel. **C-E**) Tumor response does not correlate with percent multipolar spindles in patients 20 hours after the third dose of paclitaxel (**C**), the increase in multipolarity between 20 hours post- third paclitaxel dose and pre-treatment (**D**) or first dose (**E**) multipolarity. Patient response does not correlate with the intratumoral concentration of paclitaxel after the third dose (**F**) or the change in concentration between the third and first paclitaxel dose (**G**). Tumor response does not correlate with mitotic index at the third dose (**H**) or the change in mitotic index between third and first paclitaxel treatment (**I**).

Figure A.4. Estimations of error between and within patient biopsies.

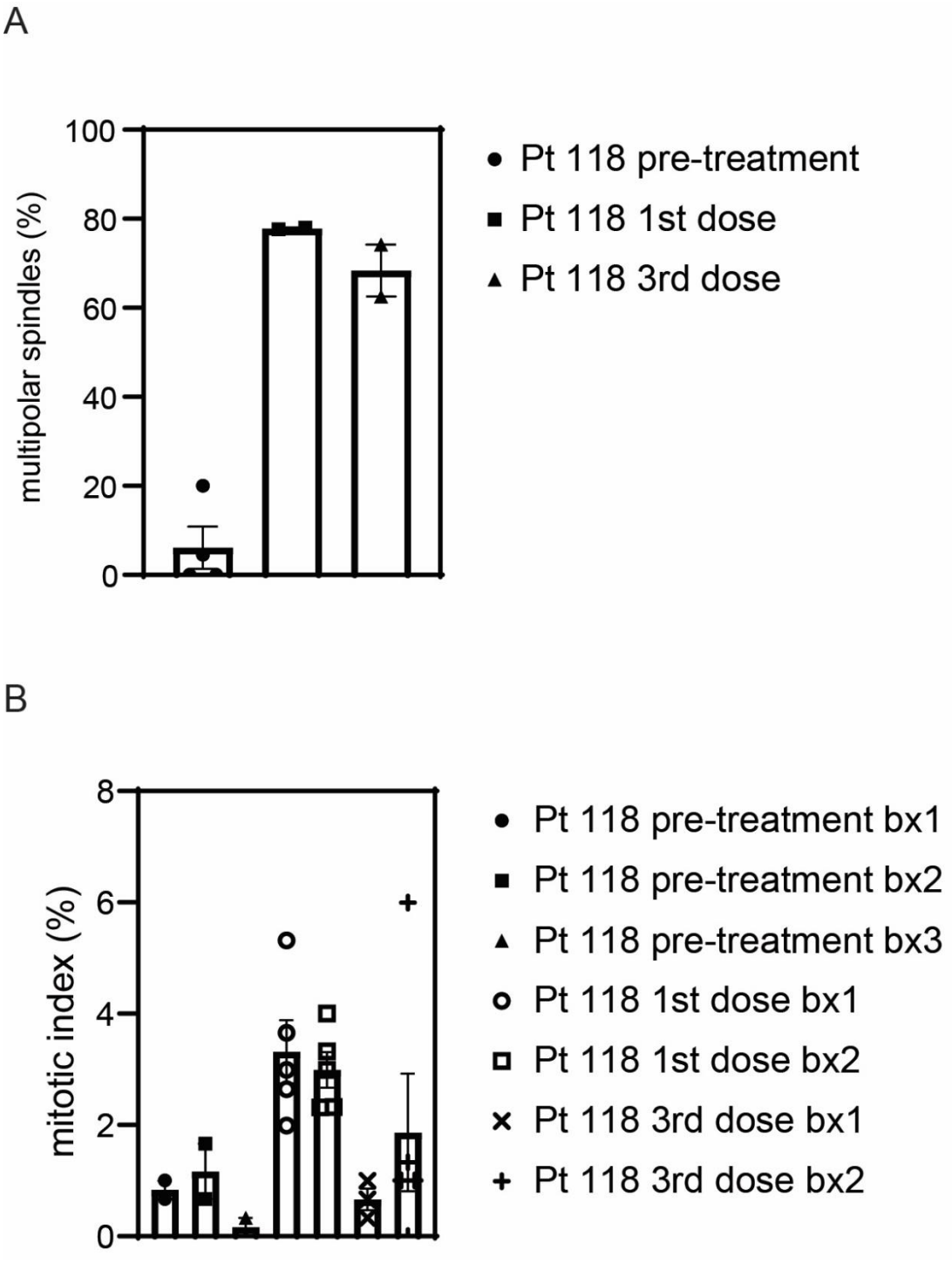

Figure A.4. Estimations of error between and within patient biopsies. A) Estimation of error between patient biopsies. Each dot represents the quantification of multipolar spindles in an independent biopsy from the same patient, showing approximately a ten percent variability between biopsies. Mitotic cell sample sizes for each biopsy are 10, 5, 22, and 5 cells, respectively, pre-treatment and 107 and 107 cells, respectively, 20 hours after the first treatment. After the third dose of paclitaxel, mitotic cell sample sizes are 8 and 23 cells, respectively. **B**) Estimation of error within patient biopsies. Each dot represents the quantification of mitotic index in independent regions of a patient biopsy, showing approximately a five percent variability between different regions within a biopsy. n≥ 300 cells per region.

Figure A.5. Paclitaxel tissue distribution and MALDI-TOF mass spectrometry.

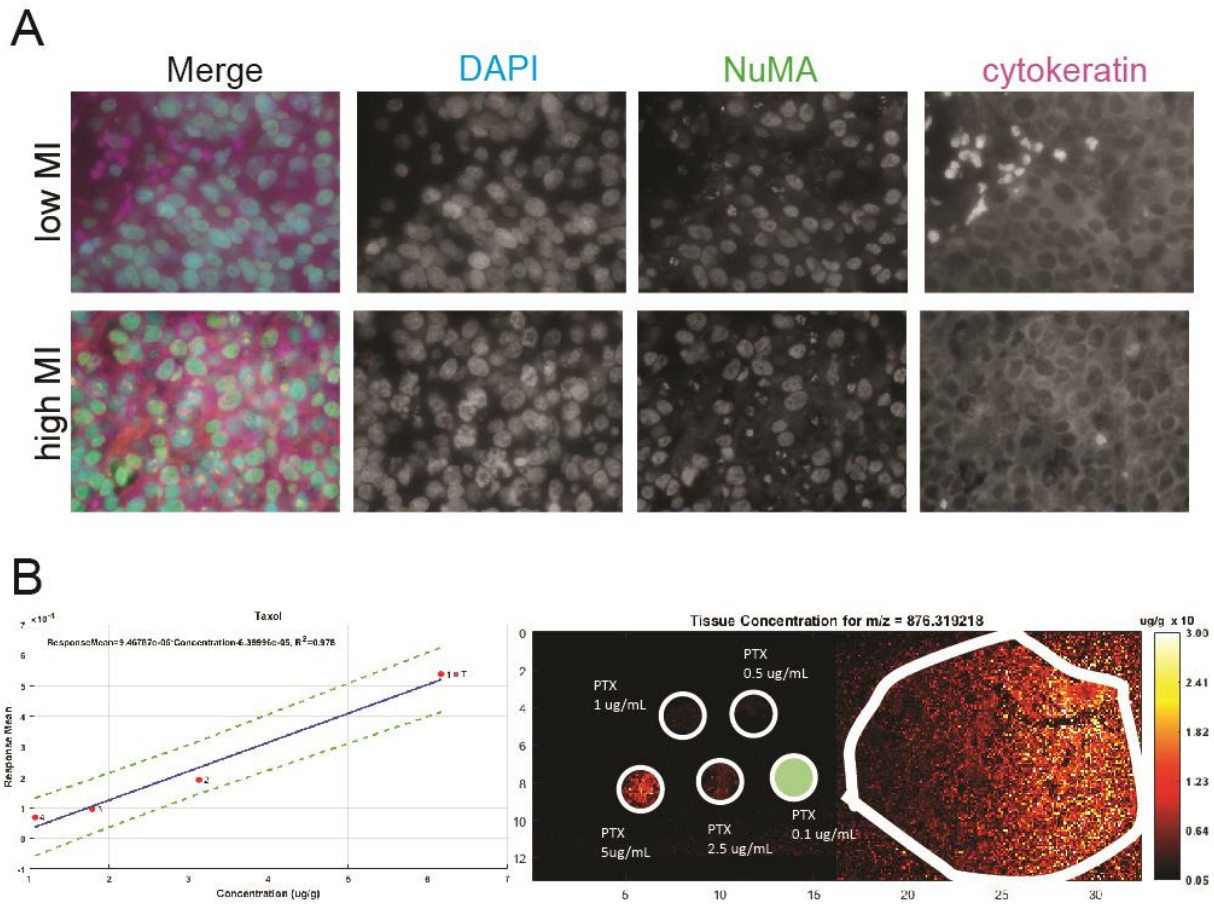

Figure A.5. Paclitaxel tissue distribution and MALDI-TOF mass spectrometry. A) Representative image of region within patient biopsy with a relatively low mitotic index (MI) (top). Note the few mitotic cells within the field of view. Bottom representative image of region within patient biopsy with a relatively high mitotic index. Note the high prevalence of mitotic cells within the field of view. **B**) MALD-TOF standard curve generation by spotting paclitaxel standards on human breast tissue.

Table A.1. 80 mg/m^2 paclitaxel trial patient characteristics.

Patient	Subtype	Stage	Age	Race	Ethnicity	Ki67
1	TNBC	T1N0M0	38	White	Non-Hispanic or Latino	90%
2	TNBC	T2N2M0	62	White	Non-Hispanic or Latino	80%
3	TNBC	T2N2M0	59	White	Non-Hispanic or Latino	90%
4	TNBC	T2N2M0	58	White	Non-Hispanic or Latino	90%
5	ER+/PR+/HER2-	T3N1M0	57	White	Non-Hispanic or Latino	25%
6	TNBC	T2N2M0	50	White	Non-Hispanic or Latino	45%
7	ER+/PR+/HER2-	T2N1M0	46	White	Non-Hispanic or Latino	90%
8	TNBC	T2N2M0	43	White	Non-Hispanic or Latino	60%
9	ER+/PR+/HER2-	T2N1M0	37	White	Non-Hispanic or Latino	15%
10	consent withdrawn					
11	ER+/PR+/HER2-	T3N1M0	52	White	Non-Hispanic or Latino	20%
12	ER+/PR+/HER2-	T2N0M0	55	Black	Non-Hispanic or Latino	25%
13	TNBC	T2N0M0	49	White	Non-Hispanic or Latino	90%
14	ER-/PR+/HER2-	T1N0M0	44	White	Non-Hispanic or Latino	60%
15	TNBC	T2N0M0	37	White	Non-Hispanic or Latino	60%
16	TNBC	T2N0M0	71	White	Non-Hispanic or Latino	>20%

17	ER+/PR+/HER2-	T2N1M0	26	White	Non-Hispanic or Latino	20%
18	ER+/PR-/HER2-	T3N3M0	70	White	Non-Hispanic or Latino	15%
19	ER+/PR+/HER2-	T3N2M0	47	White	Non-Hispanic or Latino	15%
20	TNBC	T1N0M0	40	Black	Non-Hispanic or Latino	80%

TNBC: Triple negative breast cancer. ER: Estrogen Receptor. PR: Progesterone Receptor. HER2: human epidermal growth factor receptor 2. TNM: primary tumor (T), regional lymph nodes (N), distant metastases (M). T1 indicates a tumor ≤ 2 cm, T2 indicates a tumor >2 cm but no more than 5 cm, and T3 indicates a tumor >5 cm in greatest dimension. Node (N) indicates the regional lymph node status according to the American Joint Committee on Cancer (AJCC). All patients in this study were M0, meaning there was no evidence of metastatic spread. Patient 9 and 18 were diagnosed with invasive lobular carcinoma, all other patients were diagnosed with invasive ductal carcinoma.

Table A.2: Paclitaxel concentration measurements in patient tumor and skin biopsies.

Patient	[intratumoral paclitaxel, uM] 1st dose	[plasma paclitaxel, μM] 1st dose	[intratumoral paclitaxel, uM] 3rd dose	[plasma paclitaxel, μM] 3rd dose	[intratumoral paclitaxel, uM] 12th dose	[plasma paclitaxel, μM] 12th dose	[paclitaxel in skin, uM]
1	1.07	0.023	-	-	-	-	-
2	0.34	0.040	1.27	0.028	-	-	-
3	0.80	0.030	2.40	0.022	-	-	-
4	0.57	0.027	-	-	-	-	-
5	ND	0.031	2.23	0.022	-	-	-
6	3.43	0.020	-	-	-	-	-
7	1.55	0.013	-	-	-	-	-
8	0.53	0.011	-	-	-	-	-
9	0.63	0.020	-	-	-	-	-
10	Consent withdrawn	-	-	-	-	-	-
11	0.57	0.038	-	-	-	-	-
12	ND	0.040	-	-	-	-	-
13	1.67	0.094	1.45	0.062	-	-	-
14	0.57	0.048	0.52	0.037	-	-	-
15	1.85	0.035	-	-	-	-	-
16	0.90	0.022	-	-	-	-	-
17	0.66	0.014	0.48	0.013	-	-	-
18	0.67	0.031	0.12	0.019	ND	0.018	ND
19	0.32	0.019	1.28	0.023	-	-	ND

Intratumoral paclitaxel levels were measured by HPLC analysis 20 hours after the patient's first dose of paclitaxel for all patients, and 20 hours after the patient's third and final dose of paclitaxel for a subset of patients. Paclitaxel was not determined (ND) in the tumor biopsies for patients 5 and 12 due to insufficient tumor tissue collected by biopsy. Patient 10 withdrew consent, and paclitaxel levels have not yet been measured for patient 20. Paclitaxel levels were measured but undetectable in patient skin biopsies.

CHAPTER 3: CHROMOSOME MISSEGREGATION ON MULTIPOLAR SPINDLES IS A COMMON MECHANISM OF CYTOTOXICITY FOR CLINICALLY USED MICROTUBULE POISONS.

Christina M. Scribano, Kari B. Wisinski, Amye J. Tevaarwerk, Ruth O'Regan, Mark E. Burkard, and Beth A. Weaver

*The work in this chapter is ongoing and unpublished.

ABSTRACT

Paclitaxel (Taxol™) and other microtubule poisons, including docetaxel, vinorelbine, eribulin, and ixabepilone are chemotherapeutic agents used in the treatment of breast cancer; however, their mechanism of cytotoxicity is incompletely understood. Recently our lab showed that patients receiving 175 mg/m^2 paclitaxel do not exhibit mitotic arrest in their primary tumors, as had been assumed for past three decades. Instead, clinically relevant concentrations of paclitaxel induce multipolar spindle formation in patients and in cell culture with subsequent cell death as a result of chromosome missegregation following multipolar mitotic divisions (Zasadil *et al.*, 2014). We have now extended this to demonstrate that 80 mg/m^2 paclitaxel, a lower but equally clinically effective standard-of-care dose, also induces multipolar spindles without mitotic arrest in primary breast cancer patients. The clinically relevant concentration of other microtubule poisons and their mechanistic consequences remain understudied and it is unclear whether they induce mitotic arrest, as long expected, or chromosome missegregation on multipolar spindles like paclitaxel. Here we demonstrate that docetaxel, vinorelbine, eribulin, and ixabepilone induce spindle multipolarity without mitotic arrest in breast cancer cell lines and metastatic breast cancer patient tumors, suggesting that multipolar mitoses may be a common mechanism of cytotoxicity for this class of drugs.

INTRODUCTION

For approximately three decades it was assumed that paclitaxel caused cell death due to mitotic arrest, as was observed at high concentrations used in cell culture (Jordan *et al.*, 1993; Schiff and Horwitz, 1980); however, recently our lab showed that lower, clinically relevant concentrations of paclitaxel cause cell death in breast cancer due to chromosome missegregation on multipolar spindles (Zasadil *et al.*, 2014). In a small clinical trial of breast cancer patients treated with 175 mg/m^2 paclitaxel, an increase in multipolar spindles was observed in the tumors of all patients following treatment. Importantly, mitotic arrest was not required for patient response to paclitaxel (Zasadil *et al.*, 2014). We have now extended this to show that 80 mg/m^2 paclitaxel also causes multipolar spindles without mitotic arrest. Timelapse analysis of cultured cells shows that multipolar divisions lead to a brief mitotic delay, chromosome missegregation, aneuploid daughter cells, and increased cell death (Ganem *et al.*, 2009; Zasadil *et al.*, 2014). Taken together, these data suggest an alternate mechanism of cytotoxicity in which clinically relevant intratumoral concentrations of paclitaxel cause cell death via chromosome missegregation on multipolar spindles (Zasadil *et al.*, 2014). Whether this mechanism of cytotoxicity is shared amongst other drugs related to paclitaxel remains undetermined.

Paclitaxel is one of many drugs belonging to the microtubule poison drug family. As their name suggests, microtubule poisons target microtubules and inhibit their spontaneous growth and shrinkage, a property called dynamic instability (Mitchison and Kirschner, 1984). Microtubule poisons have been classically divided into two subgroups,

microtubule stabilizers and destabilizers. At high concentrations, microtubule stabilizers promote microtubule polymerization and increase microtubule polymer mass (Perez, 2009). Conversely, high concentrations of microtubule destabilizers inhibit microtubule polymerization and decrease polymer mass (Perez, 2009). Interestingly, both microtubule stabilizers and destabilizers are used clinically and are thought to work by arresting cells in mitosis as a result of mitotic checkpoint activation (Jordan and Wilson, 2004; Waters *et al.*, 1998).

Several microtubule stabilizers have been developed as chemotherapeutic agents and are used in the treatment of breast cancer. Isolated from the bark of the Pacific yew tree, the natural product paclitaxel was the first agent to be identified as a microtubule stabilizer and undergo clinical development (Weaver, 2014). Shortly after paclitaxel was approved for clinical use, docetaxel, a semi-synthetic analog of paclitaxel, was approved (Jordan and Wilson, 2004). Subsequently, two additional naturally occurring microtubule stabilizing agents were identified, epothilones A and B (Lee and Swain, 2008). While not used clinically themselves, the semisynthetic derivative of epothilone B, ixabepilone, was recently approved for clinical use (Cobham and Donovan, 2009). Since paclitaxel, the founding member of the microtubule stabilizing drugs, was thought to function by arresting cells in mitosis, this mechanism of cytotoxicity has been ascribed to other clinically used microtubule stabilizing drugs.

Natural and semisynthetic compounds with microtubule destabilizing activity are also used clinically. The first generation vinca alkaloids, vinblastine and vincristine, were isolated from the periwinkle plant and demonstrated clinical utility in the treatment of cancer. Vinblastine is used to treat Hodgkin’s lymphoma and testicular cancers,

whereas vincristine is used to treat leukemia and other lymphomas (Jordan and Wilson, 2004). Second generation semisynthetic vinca alkaloids were then developed, including vinorelbine, which is used in the treatment of breast cancer (Ibrahim et al., 2000). Another semisynthetic drug belonging to the family of microtubule destabilizers is eribulin. Also used in the treatment of breast cancer, eribulin is a synthetic analog of halochondrin B, a compound isolated from a marine sponge (Shetty and Gupta, 2014). Microtubule depolymerization induced by these drugs results in activation of the mitotic checkpoint, and mitotic arrest is thought to underly the cytotoxicity of these drugs (Ngan *et al.*, 2001).

Microtubule poison therapy has proven to be effective for some patients, however a significant subset of patients do not experience any positive therapeutic effects from these drugs. While the response rate for each of the microtubule poisons varies, it is estimated that 27 (Rugo et al., 2015) to 58% (Fountzilas *et al.*, 2009) of patients exhibit tumor regression following treatment. The substantial fraction of patients who are non-responders are not only delayed in receiving an effective therapy, but they are also exposed to the significant negative side effects associated with microtubule poison therapy. These can include potentially life-threatening leukopenia and peripheral neuropathy (Deeken et al., 2014; Goel et al., 2009; Ibrahim *et al.*, 2000; Legha et al., 1986; Rugo *et al.*, 2015; Vahdat et al., 2013; Wiernik et al., 1987). The partial success rate of these drugs is, at least in part, due to an incomplete understanding of their clinically relevant mechanism of cytotoxicity in patients.

It is difficult to reconcile how both microtubule stabilizers and destabilizers demonstrate clinical utility, given their seemingly antagonistic actions on microtubule

polymer mass. It is pertinent that microtubule poisons display concentration dependent effects, and their classification as either microtubule stabilizer or destabilizers is oversimplified and misleading. In fact, excessive concentrations of microtubule destabilizers (high μM doses) can increase the affinity of tubulin for itself and increase microtubule polymer mass through the formation of tubulin paracrystals (Bensch and Malawista, 1968; Bensch *et al.*, 1969; Na and Timasheff, 1982). On the other hand, low (nM) concentrations of both microtubule stabilizers and destabilizers kinetically stabilize microtubules, resulting in reduced dynamicity, without affecting overall microtubule polymer mass (Castle *et al.*, 2017; Jordan and Wilson, 2004). Determining the clinically relevant concentration of microtubule poisons will be crucial to understand their cellular effects and cytotoxic consequences in tumors. Given our recent finding that paclitaxel induces mitotic spindle multipolarity without mitotic arrest, it is necessary to elucidate whether other microtubule poisons cause mitotic arrest or multipolar spindles in patients. This is of critical importance because mechanisms of resistance to mitotic arrest and multipolar spindles are distinct.

RESULTS

Microtubule poisons have concentration dependent effects

As an initial approach to test whether clinically used microtubule poisons other than paclitaxel induced mitotic arrest or multipolar spindles in patient tumors, we first tested whether they were capable of inducing multipolar spindles in vitro. Therefore, we determined the effects of low nanomolar doses of paclitaxel and the other clinically used

microtubule stabilizers, including docetaxel, ixabepilone, and epothilone B on breast cancer cell lines in cell culture. MDA-MB-231 and Cal51 triple negative breast cancer cells were treated with low nanomolar concentrations of these drugs, with doses spanning two to three orders of magnitude.

Consistent with what we have shown previously, low nanomolar, clinically relevant (10 nM) doses of paclitaxel induced multipolar spindles in MDA-MB-231 and Cal51 cells (Figure 3.1 A and B). Similarly, we found that low nanomolar doses of docetaxel, ixabepilone, and epothilone B also induced mitotic spindle multipolarity. At clinically relevant concentrations of paclitaxel, we observed relatively subtle changes in the mitotic index compared to higher doses that induce a peak mitotic index in MDA-MB-231 and Cal51 cells (Figure 3.3A). A similar trend was observed with other clinically used microtubule stabilizers in these cell lines. Whereas higher doses of drug induced significant increases in the mitotic index, at low nanomolar doses in which multipolarity was induced, changes in the mitotic index are comparatively subtle (Figure 3.3B and C). Taken together, these results suggest that other clinically used microtubule stabilizers also induce multipolar spindles without evidence of mitotic arrest in breast cancer cell lines in vitro. It is therefore possible that these other clinically used microtubule stabilizers have the same mechanism of cytotoxicity as paclitaxel in patients.

Given that low nanomolar doses of other clinically used microtubule stabilizers also cause mitotic spindle multipolarity, and not mitotic arrest, we next tested if other drugs belonging to the microtubule poison family displayed a similar mechanism. Microtubule destabilizers have been well characterized for their effects on reducing microtubule polymer mass at high concentrations, but their effects at lower doses remain

understudied. We assessed if clinically used microtubule destabilizers had a similar mechanism of cytotoxicity at lower doses, given that microtubule stabilizers and destabilizers both exhibit clinical efficacy. Notably, a recent study suggested that low nanomolar doses of vinblastine and paclitaxel that do not alter total microtubule polymer mass both kinetically stabilize microtubules and suppress their dynamic instability (Castle *et al.*, 2017), thereby suggesting a common mechanism between microtubule stabilizers and destabilizers at low concentrations. To test this, we treated MDA-MB-231 and Cal51 triple negative breast cancer cell lines with doses of vinorelbine, eribulin, and vinblastine spanning two to three orders of magnitude. In both cell lines, these drugs showed a concentration dependent increase in mitotic spindle multipolarity, with low nanomolar doses sufficient to induce multipolarity (Figure 3.2A-D). When looking at the mitotic index, we again observed that low nanomolar concentrations which induced multipolar spindles did not induce the substantial increase in mitotic index caused by higher doses of these drugs (Figure 3.31). Thus, at low nanomolar doses, microtubule destabilizers induce spindle multipolarity without evidence of mitotic arrest, similar to microtubule stabilizer drugs.

Microtubule poisons induce multipolar spindles without mitotic arrest in metastatic breast cancer

To determine whether multipolar mitotic spindles without mitotic arrest is the conserved mechanism of microtubule poisons in patients, we enrolled metastatic breast cancer patients in an ongoing clinical trial in which subjects consented to timed research biopsies and blood tests, as microtubule poisons other than paclitaxel are only used in the metastatic setting. Enrolled patients were diagnosed with metastatic or incurable

breast cancer wherein treatment with a standard of care antimitotic agent was deemed medically appropriate per the treating physician. Standard anti-mitotic medications approved for this use include taxanes (paclitaxel, nab-paclitaxel, docetaxel), vinca alkaloid (vinorelbine), epothilone (ixabepilone), and the halicondrins (eribulin). Importantly, these drugs are infused as single agents for breast cancer therapy. Patients that were pregnant or breastfeeding were excluded from this study due to the potentially deleterious effects of systemic chemotherapy on the fetus or nursing infants. In addition, patients who had planned treatment with hormonal therapy or oral targeted therapy during the trial duration were unable to participate in this trial. Accordingly, patients with HER2-positive tumors were excluded from this study to remove the confounding variable of concurrent therapy with a HER2-targeted antibody. Data from the first three enrolled patients are reported here.

The trial design is depicted in Figure 3.4A. There are five arms in this study, one arm for each of the four types of microtubule poison therapy indicated for metastatic breast cancer, and a fifth control arm for patients receiving non-microtubule targeted chemotherapy. Such treatments can include liposomal doxorubicin or gemcitabine/carboplatin. Biopsies are obtained at the time of diagnosis (prior to the initiation of treatment), and 20 hours after the patient's first infusion of chemotherapy. This timepoint was selected because cultured breast cancer cells mount a robust mitotic arrest to high doses of paclitaxel at 20 hours, showing ≥15-fold increase in mitotic index as compared to vehicle treated cells (Zasadil *et al.*, 2014). Therefore, we expect that mitotic arrest would also be evident in patient tumors at 20 hours. Initial tumor size was determined by diagnostic imaging, which can include X-ray, CT scan, MRI, and/or PET

scan. Follow up scans were taken every three cycles, as per standard of care. Follow up was discontinued either two months after completion of study treatment or upon systemic imaging following therapy completion (whichever was later). Tumor response was evaluated according to Response Evaluation Criteria in Solid Tumors (RECIST) 1.1 guidelines (Eisenhauer *et al.*, 2009).

In order to determine if microtubule poisons cause mitotic arrest or, like paclitaxel, multipolar spindles without mitotic arrest in patients, tumor biopsies prior and subsequent to microtubule poison therapy were analyzed by immunofluorescence (Figure 3.4B). The majority of mitotic cells before microtubule poison treatment exhibited a normal bipolar spindle (Fig 3.4B top, Fig 3.4C). However, at 20 hours post eribulin, vinorelbine, or nab-paclitaxel treatment, an accumulation of multipolar mitotic spindles was observed (Figure 3.4C), with increases of 12.2%, 12.3%, and 27.8, respectively. This substantial increase in multipolarity was accompanied by only subtle changes in the mitotic index (Fig 3.4D). Increases in the mitotic index ranged from 1.0-2.6%. Therefore, similar to paclitaxel treatment, other standard of care anti-mitotic microtubule poisons induced multipolar spindles and not mitotic arrest in patient tumors, demonstrating a conserved mechanism for this class of drugs in breast cancer.

Determining the clinically relevant concentration of vinorelbine

Given that low nanomolar doses of other clinically used microtubule stabilizers and destabilizers caused multipolar spindles without mitotic arrest, the next step was to determine if these concentrations were in the clinically relevant range. Determination of the clinically relevant concentration requires measurement of drug levels in patient

tumors and identification of the corresponding concentration with which to treat cells or mice to mimic this clinical dose. We started our analysis by developing a liquid chromatography followed by tandem mass spectrometry (LC-MS/MS) method to quantify concentrations of vinorelbine in biological tissue. Cellular samples were used to develop this method and verify its performance prior to quantification of our patient sample.

We first measured intracellular vinorelbine concentrations in MDA-MB-231 and Cal51 triple negative breast cancer cells after treatment of their culture media with a range of doses (0-1000 nM; Table 3.2). We next extended this analysis to include MCF10A nontransformed breast epithelial cells, as well as LM2 cells, a derivate of MDA-MB-231 cells with an increased propensity to metastasize (Table 3.2). We found that the degree of intracellular vinorelbine concentration ranged from 8-fold to 419-fold between cell lines measured, but it remained relatively constant across various concentrations within a given cell line (Table 3.2).

This was surprising given that the degree of in intracellular paclitaxel accumulation varies widely depending on the concentration used (Jordan *et al.*, 1993; Jordan *et al.*, 1996; Yvon *et al.*, 1999; Zasadil *et al.*, 2014). The observed differences in intracellular drug accumulation between paclitaxel and vinorelbine may be due to the fact that as paclitaxel stabilizes microtubules, it results in increased drug binding sites along the interior surface of the microtubule at the β-subunit, whereas vinorelbine would not be expected to do this as a destabilizer that only binds to the plus ends of microtubules (Jordan and Wilson, 2004). Future drug occupancy studies are needed to test this hypothesis. The relatively constant intracellular degrees of vinorelbine

accumulation within a given cell line regardless of the treatment concentration are in agreement with a previous studies showing relatively constant degrees of intracellular accumulation of the microtubule destabilizing drug vinblastine (Dhamodharan et al., 1995). In conclusion, while the degree of intracellular concentration of paclitaxel is highly variable with differing treatment concentrations within a given cell line, it remains relatively stable with differing concentrations of vinorelbine.

Next, we performed a mouse xenograft study to identify the concentration of vinorelbine with which to treat mice in order to achieve a clinically relevant dose. In order to do this, 5-week-old athymic nude mice were injected with $1x10^6$, $2.5x10^6$, or $5x10^6$ Cal51 breast cancer cells. Cells were resuspended in 50:50 Matrigel:media and injected orthotopically into the inguinal mammary fat pads of female mice (2 tumors per mouse). We let tumors grow until they reached their maximum allowed size, 16 mm x 16 mm, and then treated the mice with 0, 3, 6, or 12 mg/kg vinorelbine. These doses were chosen based on previous studies with vinorelbine in mice (Cortes *et al.*, 2018; Orecchioni et al., 2018; Qin et al., 2018; Tsuruo et al., 1994), and did not result in immediate noticeable toxicity or sudden death, as had been observed in some of our previous experiments with high doses of paclitaxel related to its notorious insolubility in aqueous solutions. After a 20-hour treatment, plasma and tumors were harvested from the mice and flash frozen in liquid nitrogen for measurement of drug levels. Using the LC-MS/MS protocol we developed for intracellular drug quantification, vinorelbine doses will next be measured in our mice tissues, and finally in our patient biopsy. Determining the clinically relevant dose of vinorelbine and other microtubule poisons will be critical to understanding their cellular effects and cytotoxic consequence in human tumors.

Discussion

Interestingly, our preliminary data suggest that, like paclitaxel, other clinically useful microtubule poisons are also capable of inducing multipolar spindles at low nanomolar concentrations in vitro, suggesting a possible common mechanism of cytotoxicity and therefore warranting further mechanistic study of these drugs. This effect is concentration dependent. As the concentration of drug increases, so does the incidence of multipolar spindles. Additionally, the number of spindle poles per cell also increases with increasing drug concentration. These low nanomolar concentrations of drug are not capable of inducing a mitotic arrest, as indicated by the relatively low percentages noted for the mitotic index compared to mitotic indices at higher concentrations. Importantly, our evidence from three metastatic breast cancer patients treated with vinorelbine, nab-paclitaxel, and eribulin suggests that multipolar spindles without mitotic arrest is also observed in response to these drugs in patient tumors. Taken together, these results suggest that other clinically used microtubule poisons may cause cell death in human tumors due to chromosome missegregation on multipolar spindles, similar to what we observed with paclitaxel treatment. If these drugs share a common mechanism of cytotoxicity, it is possible that they will also share similar mechanisms of sensitization (pre-existing CIN) and resistance (multipolar spindle focusing), as discussed for paclitaxel in Chapter Two. Thus, these mechanisms may be broadly applicable to other clinically used microtubule poisons in breast cancer including docetaxel, ixabepilone, vinorelbine, and eribulin.

It was unexpected and initially surprising that both microtubule stabilizing and destabilizing drugs had the same effect in MDA-MB-231 and Cal51 cells since these drugs have been historically described as having antagonizing actions on microtubule polymer mass. However, it is important to note that previous data has demonstrated that low nanomolar concentrations of the microtubule poisons, both classically defined stabilizers (paclitaxel) and destabilizers (vinblastine), kinetically stabilize microtubules in vivo by suppressing their dynamic instability (Castle *et al.*, 2017). Therefore, we believe that at the tested concentrations, these microtubule poisons are all functioning similarly by increasing the amount of time microtubules spend in a non-dynamic state, and this results in their ability to form multipolar spindles. The overlapping effects of these drugs at low doses provides mechanistic rationale for the similar phenotypes observed upon classically defined microtubule stabilizer and destabilizer treatment and suggests a possible common mechanism for their cytotoxicity in patients.

It remains to be determined if these low nanomolar doses reflect a clinically relevant concentration for docetaxel, ixabepilone, vinorelbine, and eribulin in metastatic breast cancer. Determination of the clinically relevant concentration for these drugs will provide guidance for which concentrations should be used in future in vitro and in vivo studies in mice. If it is discovered that low nanomolar treatment is not reflective of a clinically relevant dose, these studies will be repeated with the correct concentration in order to properly examine their clinically relevant means of causing cell death.

It should be noted that Matrigel was included in our cellular resuspensions (at a 50:50 ratio with growth media) for our vinorelbine xenograft experiment. Our previous breast cancer xenograft experiments were riddled with low take rates and limited tumor

growth, which significantly hindered our ability to perform in vivo studies in mice. Fortunately, Matrigel has been shown to enhance the take rate and breast tumor xenograft growth rate in athymic nude mice (Mehta et al., 1993), providing rationale for its inclusion in these experiments. While the inclusion of Matrigel significantly improved our take rate and the rate of tumor growth, it remains unknown whether Matrigel will impact the extent to which vinorelbine (or other drugs) accumulate in tumors. Future experiments should be conducted to determine the effect of this additional variable.

Although ixabepilone is included as one of the drugs in our metastatic breast cancer trial, it is unlikely that any patients will be enrolled in this arm. A recent study compared the progression free survival of 783 patients with chemotherapy naïve advanced breast cancer treated with paclitaxel, nab-paclitaxel, or ixabepilone (Rugo *et al.*, 2015). While no significant difference was observed in the progression free survival of patients being treated with paclitaxel or nab-paclitaxel, patients who were treated with ixabepilone had significantly worse progression free survival than patients who were treated with paclitaxel. Ixabepilone treated patients had a progression free survival time of 7.4 months, compared to 11 months for paclitaxel treated patients (Rugo *et al.*, 2015). Therefore, enrollment into the ixabepilone arm of our trial is improbable because of its recently demonstrated inferiority to other microtubule poisons. If this is the case, the number of patients to be enrolled in the ixabepilone arm will be redistributed to other arms in our trial.

Another limitation of this study is the overall low enrollment to date. Only three patients have been recruited thus far, one in each of the vinorelbine, eribulin, and taxane arms. While these patient biopsies demonstrated evidence of multipolar spindle

formation without mitotic arrest, an increased number of patients will be needed to verify this mechanism of cytotoxicity. In addition, no patients have been enrolled in the control non-microtubule targeted chemotherapy (e.g. liposomal doxorubicin or gemcitabine/carboplatin) arm of the trial to date. For the purposes of these experiments, the pre-treatment diagnostic biopsies served as our control samples. Future studies are required to determine if multipolar spindles are also induced by non-microtubule targeted chemotherapy, although this seems mechanistically improbable and previous studies have not reported this phenotype. For example, a previous study investigating the mitotic defects associated with doxorubicin treatment showed a significant increase in lagging chromosomes, but not multipolar spindle formation (Bakhoum et al., 2014a). Furthermore, since these are metastatic samples, we were unable to control for site of biopsy in this study. Sampling was heterogeneous and involved biopsies of convenience of accessible metastatic sites. We were also unable to control for prior treatments, or other sources of biologic variation such as breast cancer subtype or hormone receptor status.

Overall, our results demonstrate that low nanomolar doses of clinically used microtubule stabilizers and destabilizers induce multipolar mitotic spindle formation without evidence of mitotic arrest in breast cancer cell lines. Preliminary results from our metastatic breast cancer clinical trial demonstrated that vinorelbine, eribulin, and nab-paclitaxel treatment induced multipolar spindles, and not mitotic arrest, in patient tumors. Vinorelbine measurements were performed in breast cell lines, but future work is needed to determine the clinically relevant concentration of vinorelbine and other microtubule poisons in patients. Taken together, our data support the premise that

multipolar mitoses may be a common mechanism of cytotoxicity for clinically used microtubule poisons. Thus, the mechanisms of sensitization (pre-existing CIN) and resistance (multipolar spindle clustering) described for paclitaxel may be broadly applicable to other clinically used microtubule poisons in breast cancer.

Materials and Methods

Microtubule poison study design

Patients who volunteered to participate in this study were enrolled in a prospective trial at the UW Carbone Cancer Center specifying the treatment, biopsy, and analysis plan. The protocol was approved by UW Health Sciences Institutional Review Board, assigned UWCCC protocol number UW16151, conducted in accordance with the ethical standards established in the 1964 Declaration of Helsinki and registered on clinicaltrials.gov (NCT03393741). Patients were enrolled if they had metastatic or incurable breast cancer for which anti-mitotic chemotherapy was indicated. Subjects received either control non-microtubule targeted chemotherapy (e.g. liposomal doxorubicin or gemcitabine/carboplatin) or standard of care microtubule poison treatment (either taxane, eribulin, vinorelbine, or ixabepilone) with biopsy and treatment as outlined in Figure 3.4A. There were no major complications from protocol-mandated research biopsy.

This is an ongoing study of the mechanism of microtubule poisons in human breast cancer. The patient sample size was selected to provide a sufficient number of biopsies for sampling intratumoral drug concentrations, effects on mitosis, and patient response. All subjects had metastatic or incurable breast cancer for which microtubule poison anti-

mitotic chemotherapy was recommended per standard of care. A research biopsy was obtained approximately 20 hours after start of the first infusion. Follow up scans were taken every three cycles, as per standard of care. Follow up was discontinued either two months after completion of study treatment or upon systemic imaging following therapy completion (whichever was later). The objectives were to measure intratumoral drug levels, to determine their effects on mitosis, chromosomal instability, and cell proliferation, and to correlate these with response to treatment.

Imaging response criteria

Baseline imaging was performed by X-Ray, CT, MRI and/or PET scan as part of a complete diagnostic imaging evaluation. All imaging was performed as closely as possible to the beginning of treatment. Follow up scans will be recommended every ~3 cycles, per standard-of-care. Subjects will be followed for the duration of treatment while taking part in this study. Follow up will discontinue either 2 months following completion of study treatment or upon the systemic imaging following therapy completion (whichever is later). Imaging response was evaluated using RECIST 1.1 criteria (Eisenhauer *et al.*, 2009). In the metastatic setting, RECIST 1.1 guidelines recommend that up to 5 target lesions (representing all affected organ systems, but no more than 2 target lesions per organ) be measured throughout treatment (Costelloe et al., 2010). To be considered target lesions, at baseline tumors must measure ≥ 10 mm, the short axes of lymph nodes must measure ≥ 15 mm, palpable masses must be ≥ 10 mm as measured with calipers, lung lesions must be ≥ 20 mm, and bone metastases with soft tissue masses must measure ≥ 10 mm (Costelloe *et al.*, 2010). Response is determined by the sum of the measurements of the greatest longitudinal dimension of each target

lesion. A partial response is defined as a decrease in the sum of the diameters of all target lesions by ≥ 30% (Costelloe *et al.*, 2010). Patient response was determined by review of imaging reports.

Cell culture

MDA-MB-231, LM2, and Cal51 cell lines were grown in DMEM supplemented with 10% (vol/vol) FBS, 2 mM L-glutamine, and 50 µg/mL penicillin/streptomycin at 37°C and 5% CO_2. MCF10A cells were grown in DMEM/F12 supplemented with 5% (vol/vol) horse serum, 20 ng/mL hEGF, 0.5 mg/mL hydrocortisone, 100 ng/mL cholera toxin, 10 µg/mL insulin, and 50 µg/mL penicillin/streptomycin at 37°C and 5% CO_2. Paclitaxel (LC Laboratories, P-9600), docetaxel (Enzo Life Sciences, BML-T129-0005), ixabepilone (LC Laboratories, 103547-394), eribulin (UW Madison Pharmacy), vinorelbine (Medkoo, 100930), and vinblastine (Fisher Scientific; V1377) were diluted in DMSO and used at the indicated final concentrations.

Immunofluorescence in cells and patient cohort

Cellular immunofluorescence was performed as in (Ryan *et al.*, 2012). Staining was performed with antibodies to α-tubulin (YL 1/2; Bio-Rad, MCA77G) diluted 1:1000 for one hour at room temperature. For patient immunohistochemistry, 5 µm sections of formalin-fixed, paraffin-embedded tissue sections were subjected to antigen retrieval in citrate buffer, serum-blocked overnight, and stained with rabbit anti-NuMA antibody [a kind gift from Duane Compton; (Compton *et al.*, 1991)], mouse anti-γ-tubulin (Sigma, T6557), and pan-cytokeratin (to mark epithelial cells; Novus Biologicals, NBP2-

33200AF647) antibodies diluted 1:100 overnight at 4°C. Alexa Fluor-conjugated secondary antibodies (Invitrogen) were used at 1:200 for one hour at room temperature. DNA was stained using DAPI.

Vinorelbine measurements

Cells in 6 cm dishes were treated with the indicated concentrations of vinorelbine in 3 mL total volume once they reached 90-100% confluence. After 20 hours, media was collected, and cells were pelleted and resuspended in 1 mL ddH_2O. Both cell and media samples were stored at -20°C until the day of analysis. Cell resuspensions were thawed and sonicated immediately before sample preparation for LC-MS/MS. For solid phase extraction, cell and media samples were applied to an Ostro plate (Waters,186005518). Prior to extraction, vinblastine was added as an internal standard (Fisher Scientific; V1377) was added via diluent to facilitate quantification of sample recovery. Samples were eluted using acetonitrile +1% formic acid with positive pressure (30-50 psi) of nitrogen into a collection plate. LC-MS/MS analysis was performed using a LC-UV-MS/MS system (QTrap 5500; ABSciex) equipped with a Waters Acquity UPLC System binary pump). A Phenomenex Kinetex C18 column (30 mm × 2.1 mm × 2.6 µm) was used with a gradient of acetonitrile/water/formic acid of 65:35:0.1 (v/v/v) to 100:0:0.1 at 0.35 mL/min flow rate. To monitor and quantify the levels of vinorelbine (MedKoo, 100930) and vinblastine (Fisher Scientific; V1377), a multiple-reaction monitoring (MRM) method was developed with signature ion fragments for each molecule. Calibration curves were obtained using vinorelbine at 0.2, 1, 5, 10, 50, 100, 250, 500, and 1000 ng/mL. Quantification was carried out based on peak area of the MRM transition and the linear calibration curve for each compound.

Xenograft experiments

All animal studies were performed in compliance with all relevant ethical regulations for animal testing and research. The study was approved by the Institutional Animal Care and Use Committee of the University of Wisconsin-Madison. $1x10^6$, $2.5x10^6$, or $5x10^6$ Cal51 cells resuspended in 50:50 Matrigel:media were injected orthotopically into the inguinal mammary fat pads of five 5-week-old female athymic nude mice (2 tumors per mouse). Tumor size was measured every 2-3 days using calipers. Tumor volumes were calculated using the formula $V = width^2 \times length/2$. Mice were treated (ip) with sterile saline, 3, 6, or 12 mg/kg vinorelbine diluted in sterile saline and tumors were harvested 20 hours later.

Microscopy

Images were acquired on a Nikon Ti-E inverted microscope driven by Nikon Elements software with focus-drift compensation. Images are maximum projections from 0.2 μm z-stacks collected with a 60×/1.4 or 100×/1.4 numerical aperture (NA) objective after deconvolution using the AQI 3D Deconvolution module in Elements.

Statistical Analysis

Statistical analysis was performed using GraphPad Prism. Student's t-tests were used to assess significance, unless otherwise noted. Other statistical parameters including the number of cells analyzed and the number of replicates are reported in the respective figure legends.

Figure 3.1. Low nanomolar doses of microtubule stabilizers cause multipolar spindles in breast cancer cells.

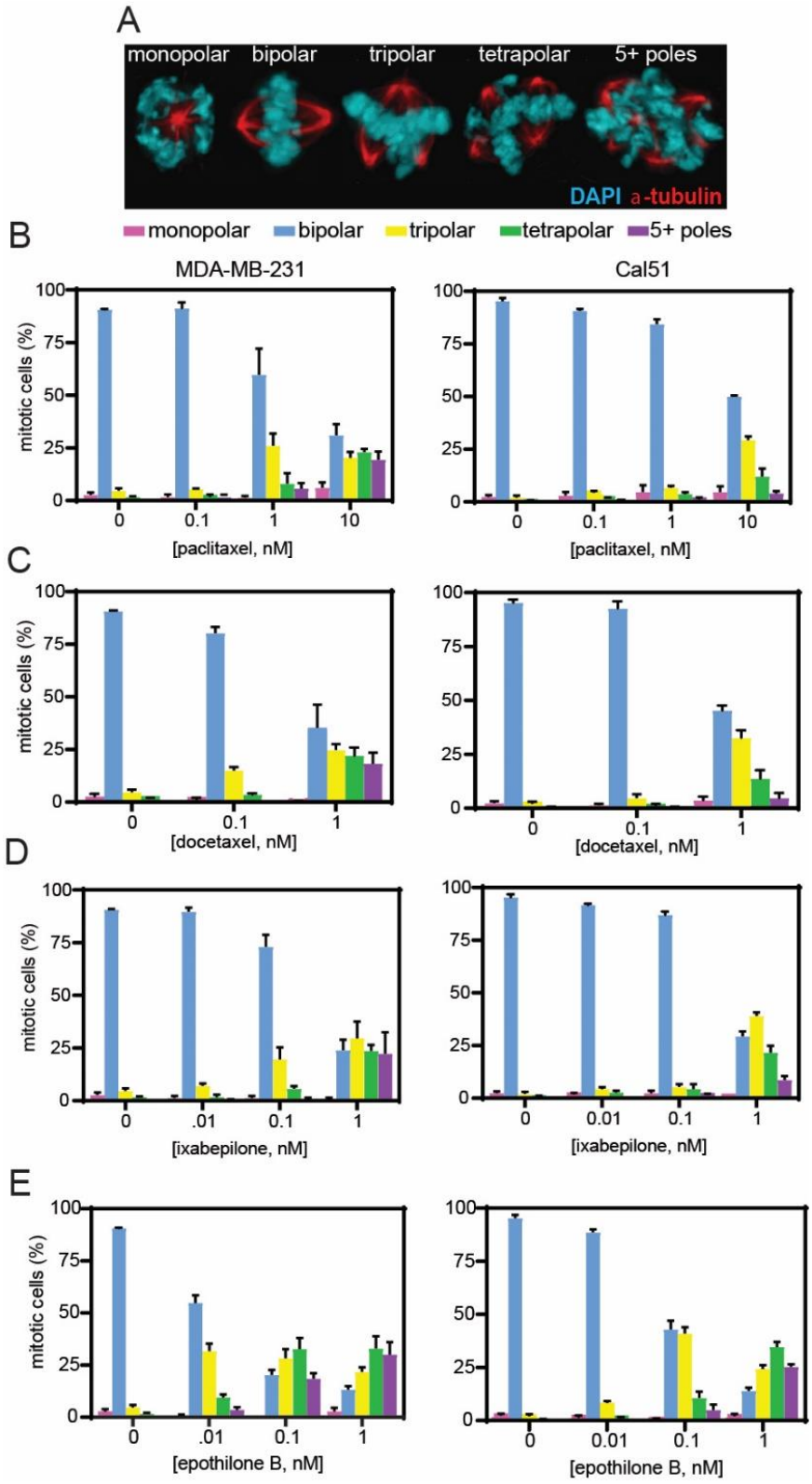

Figure 3.1. Low nanomolar doses of microtubule stabilizers cause multipolar spindles in breast cancer cells. A) Images of MDA-MB-231 mitotic cells with the indicated number of spindle poles after low nanomolar treatment with paclitaxel. Quantification of multipolar spindles (mean +/- SEM) in MDA-MB-231 (left) and Cal51 cells (right) after treatment with low nanomolar doses of paclitaxel (**B**), docetaxel (**C**), ixabepilone (**D**), and epothilone B (**E**). n≥50 cells in each of 3 replicates.

Figure 3.2. Low nanomolar doses of microtubule destabilizers also cause multipolar spindles in breast cancer cells.

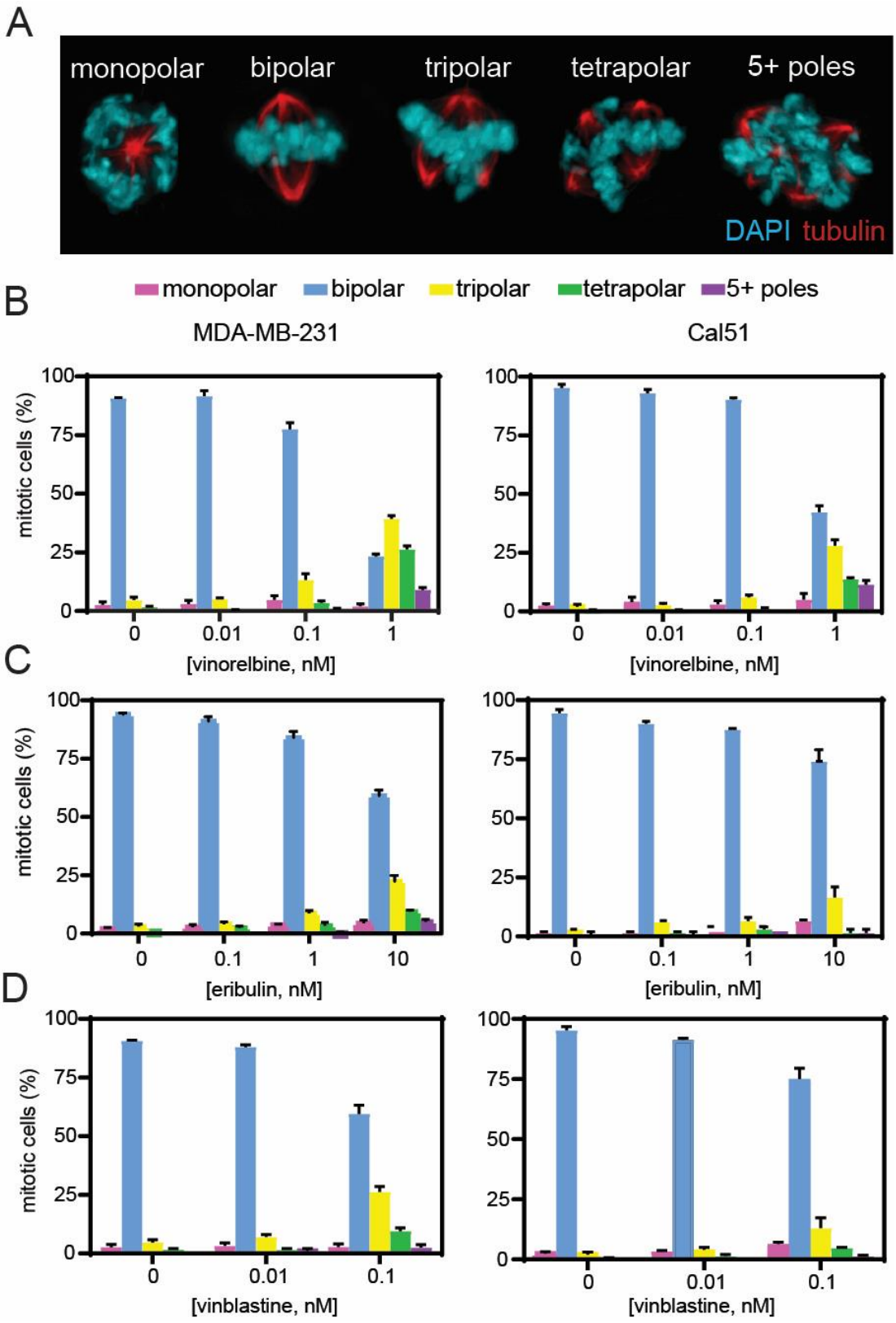

Figure 3.2. Low nanomolar doses of microtubule destabilizers also cause multipolar spindles in breast cancer cells. A) Images of MDA-MB-231 mitotic cells with the indicated number of spindle poles after low nanomolar treatment with paclitaxel. Quantification of multipolar spindles (mean +/- SEM) in MDA-MB-231 (left) and Cal51 cells (right) after treatment with low nanomolar doses of vinorelbine (**B**), eribulin (**C**), and vinblastine (**D**). n≥50 cells in each of 3 replicates.

Figure 3.3. Low nanomolar doses of microtubule stabilizer and destabilizers do not cause mitotic arrest in breast cancer cells.

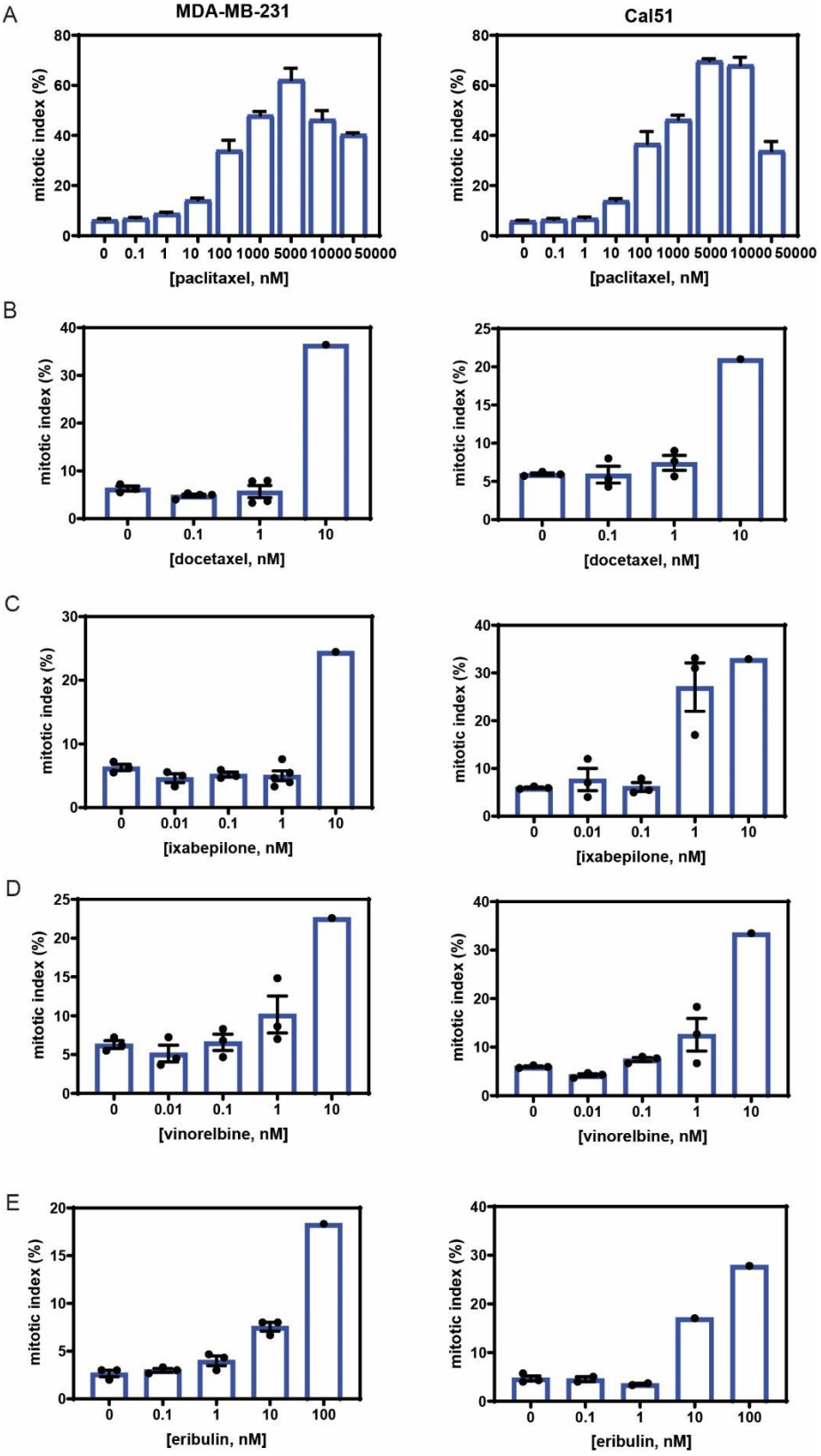

Figure 3.3. Low nanomolar doses of microtubule stabilizer and destabilizers do not cause mitotic arrest in breast cancer cells. Quantification of mean mitotic index, or percent or cells in mitosis, after treatment with the indicated concentrations of paclitaxel (**A**), docetaxel (**B**), ixabepilone (**C**), vinorelbine (**D**), or eribulin (**E**). Error bars represent SEM. n≥300 cells from each of 3 independent experiments.

Figure 3.4. Clinically used microtubule poisons cause multipolar spindles without mitotic arrest in metastatic breast cancer patients.

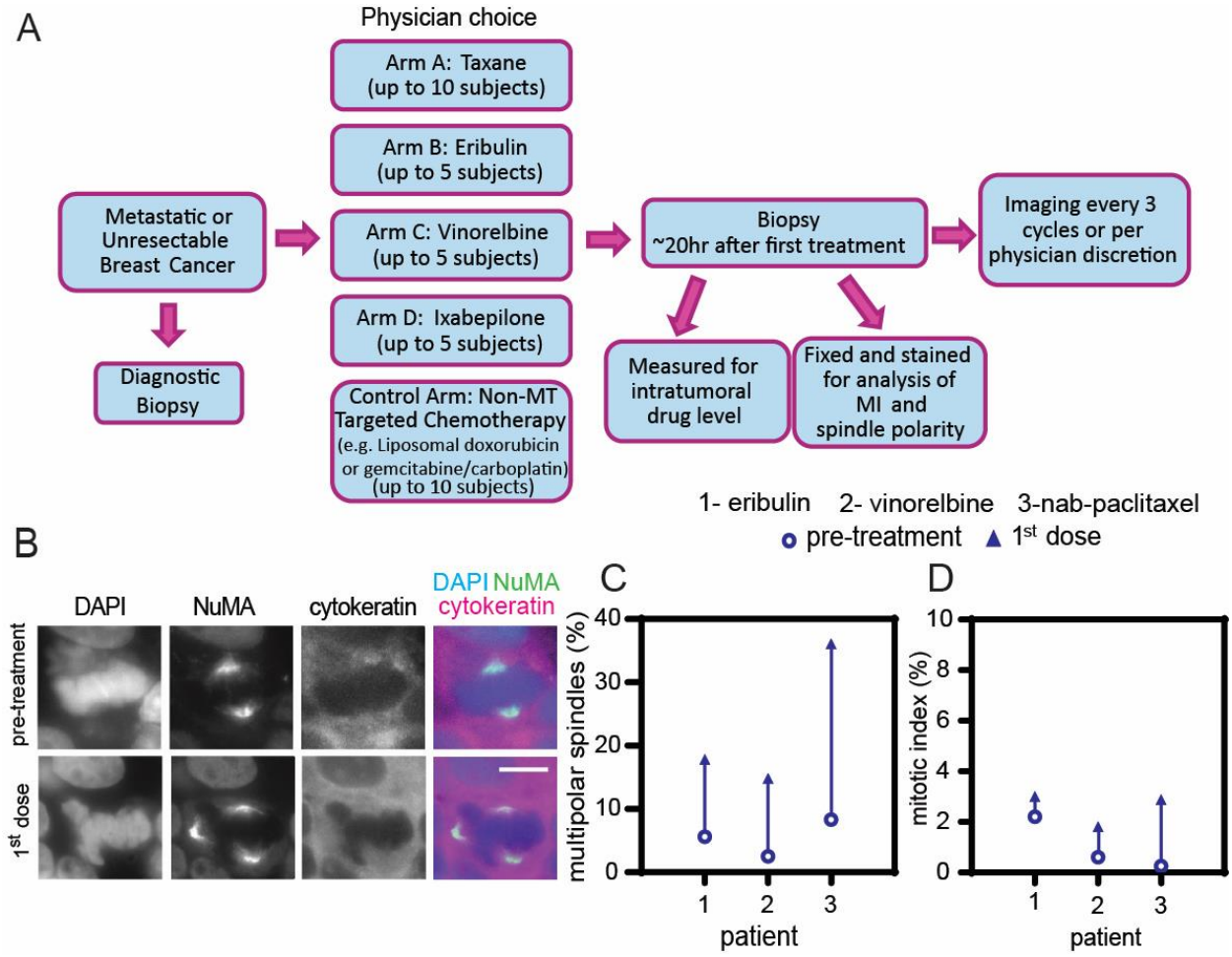

Figure 4. Clinically used microtubule poisons cause multipolar spindles without mitotic arrest in metastatic breast cancer patients. A) Schematic showing trial design. Research biopsies were obtained prior to microtubule poison treatment and 20 hours after the first dose of microtubule poison therapy. **B**) Representative images of bipolar (top) and multipolar (bottom) mitotic cells in patient tumors before and after microtubule poison treatment. Mitotic cells were identified based on DNA morphology

and the presence of a mitotic spindle, labeled by Nuclear Mitotic Apparatus protein (NuMA), which localizes to spindle poles. Pan-cytokeratin was used to discriminate between breast epithelial (tumor) cells and stroma. Scale bar, 5 μm. **C-D**) Microtubule poison therapy induces multipolar spindles without mitotic arrest in primary breast cancer. Quantification of (**C**) multipolar mitotic spindles, defined as containing >2 NuMA foci, and (**D**) mitotic index before (open circle) and 20 hours after (arrowhead; the direction indicates increase or decrease) microtubule poison treatment. D, n≥300 cells. For assessment of multipolar spindles in C, mitotic cell sample sizes for patients are 107, 40, and 12 cells, respectively, pre-treatment and, 73, 54, and 122 cells, respectively, after treatment.

Table 3.1. Metastatic microtubule poison trial patient characteristics.

Patient	Drug	Site of biopsy	Subtype	Age	Race	Ethnicity	Response
1	Eribulin	Liver	ER+/PR+/HER2-	59	White	Non-Hispanic or Latino	N/A
2	Vinorelbine	Peritoneum	ER+/PR-/HER2-	62	White	Non-Hispanic or Latino	Progression
3	Nab-paclitaxel	Liver	ER+/PR+/HER2-	69	White	Non-Hispanic or Latino	Stable Disease

Table 3.1. Metastatic microtubule poison trial patient characteristics.

ER: Estrogen Receptor. PR: Progesterone Receptor. HER2: human epidermal growth factor receptor 2. All patients in this study had metastatic spread. Patient response was determined by review of imaging reports and RECIST 1.1 criteria (Eisenhauer *et al.*, 2009). Response information was not available for Patient 1 because they only received one dose of eribulin.

Table 3.2. Intracellular vinorelbine measurements.

	MDA-MB-231		Cal51		LM2		MCF10A	
Treatment (nM)	[Intracellular vinorelbine, μM] ± SEM	Fold uptake	[Intracellular vinorelbine, μM] ± SEM	Fold uptake	[Intracellular vinorelbine, μM] ± SEM	Fold uptake	[Intracellular vinorelbine, μM] ± SEM	Fold uptake
DMSO	ND	-	ND	-	ND	-	ND	-
5	1.77 ± 0.39	354x	0.25 ± 0.09	37x	1.01 ± 0.23	229x	0.06 ± 0.02	11x
10	2.76 ± 0.51	276x	0.46 ± 0.18	34x	1.99 ± 0.31	219x	0.07 ± 0.02	7x
20	8.43 ± 1.46	421x	1.39 ± 0.57	52x	4.63 ± 0.88	252x	0.24 ± 0.07	12x
50	19.6 ± 3.74	392x	2.34 ± 0.86	35x	11.76 ± 2.63	254x	0.51 ± 0.18	10x
100	33.16 ± 5.36	331x	5.70 ± 1.72	43x	17.97 ± 2.05	192x	1.08 ± 0.10	11x
500	169.66 ± 26.73	311x	26.73 ± 8.25	40x	-	-	6.67 ± 1.79	13x
1000	315.93 ± 66.13	304x	49.31 ± 19.99	42x	143.6 ± 24.3	144x	14.15 ± 4.40	14x
5000	-	-	-	-	526.5 ± 39.8	105x	-	-
Average Fold Uptake		341x		40x		199x		11x

Intracellular vinorelbine levels were measured by LC-MS/MS 20 hours after addition of vinorelbine to cell culture media. Values represent mean ± SEM. n≥3. ND indicates not detected. (-) indicates not tested.

CHAPTER 4: THE MOLECULAR AND TEMPORAL REQUIREMENTS FOR MICROTUBULE POISON INDUCED MULTIPOLAR SPINDLE ESTABLISHMENT AND MAINTENANCE.

Christina M. Scribano, Kari B. Wisinski, Amye J. Tevaarwerk, Ruth O'Regan, Mark E. Burkard, and Beth A. Weaver

*The work in this chapter is ongoing and unpublished.

ABSTRACT

We recently measured the intratumoral paclitaxel concentration in breast cancer patients and found that clinically relevant (low nanomolar) concentrations of paclitaxel cause multipolar divisions rather than mitotic arrest. Importantly, supernumerary centrosomes are not required for microtubule poison-induced multipolar spindles. To gain mechanistic insight into the formation of paclitaxel-induced multipolar spindles, a variety of mitotic regulators were tested for their ability to affect spindle multipolarity in breast cancer cells treated with clinically relevant concentrations of paclitaxel. Our results demonstrate that the mitotic kinesin Eg5 and the kinase Plk1 promote both the formation and the maintenance of paclitaxel-induced spindle multipolarity, while the mitotic kinesin CENP-E and the kinase Mps1 do not. Interestingly, we found that decreasing the time to anaphase onset decreases the number of multipolar divisions in paclitaxel, resulting in reduced cytotoxicity. Additionally, our results suggest that prolonging mitotic duration increases paclitaxel-induced multipolar spindles. Identification of the cellular and temporal requirements for multipolarity induced by paclitaxel, and of agents that increase multipolarity more generally, may improve the clinical utility of paclitaxel and other microtubule poisons.

Introduction

The formation of a bipolar spindle during mitosis is critical for accurate chromosome segregation. The presence of two spindle poles promotes chromosome bi-orientation and equal segregation of DNA content into two daughter cells (Prosser and Pelletier, 2017). The presence of additional spindle poles in multipolar mitotic cells can have detrimental effects on chromosome segregation. Multipolar spindles that persist throughout mitosis result in multipolar cell division, which causes the simultaneous missegregation of multiple chromosomes, often resulting in more chromosome missegregation events than bipolar divisions with lagging or misaligned chromosomes. Indeed, timelapse analysis of cultured cells shows that multipolar divisions often lead to chromosome missegregation, aneuploid daughter cells, and increased cell death (Ganem *et al.*, 2009; Zasadil *et al.*, 2014). Multipolar spindles can also be transient in nature. However, transient multipolarity and bipolar divisions can still generate low levels of chromosomal instability through the formation of merotelic attachments and lagging chromosomes in anaphase (Ganem *et al.*, 2009). Although multiple mechanisms of multipolar mitotic spindle formation have been described, it is currently unknown how and why paclitaxel and other microtubule poisons generate multipolar spindles in cells. Given that we identified multipolar spindle clustering as a mechanism of paclitaxel resistance (Chapter Two), the mechanisms underlying multipolar spindle maintenance and clustering also merit further investigation.

Mitotic spindle multipolarity can arise through several mechanisms including centrosome amplification, centriole disengagement, PCM fragmentation, or the formation of additional acentriolar microtubule nucleating foci (Maiato and Logarinho,

2014). Centrosome amplification can result from cytokinesis failure or dysregulation of centriole duplication, which normally occurs only once per cell cycle (Maiato and Logarinho, 2014; Wang et al., 2014). For example, over-expression of Polo-like kinase 4 (Plk4), the master regulator of centriole duplication (Habedanck *et al.*, 2005), generates centrosome amplification. The presence of supernumerary centrosomes can create additional microtubule organizing centers in cells and thus lead to multipolar spindles. Centriole disengagement occurs when the paired mother and daughter centrioles become separated before chromosome segregation at anaphase onset. This defect is thought to arise due to defects in centriole cohesion (Maiato and Logarinho, 2014). As a result, the separated centrioles can then each nucleate microtubules, thereby generating additional spindle poles. Finally, PCM fragmentation occurs when PCM structural integrity is compromised. Pieces of the PCM can then break away and generate acentriolar PCM fragments capable of nucleating microtubules (Maiato and Logarinho, 2014). The formation of de novo acentriolar microtubule nucleating foci is another mechanism by which multipolar spindles can arise in cells, though the minimal molecular requirements for microtubule nucleation and spindle pole formation are not well described. The mechanisms required for multipolarity induced paclitaxel and other microtubule poisons remain unknown.

The mitotic regulators Eg5 (Kif11) and Plk1 play important roles in preserving spindle bipolarity. Eg5 is a tetrameric kinesin protein comprised of two antiparallel homodimers (Kapitein *et al.*, 2005). Each homodimer exerts plus end directed forces on the microtubule, and its antiparallel orientation allows it to effectively push spindle poles apart. Plk1 is a mitotic kinase that plays diverse roles in mitosis, including a role in

bipolar spindle formation (Barr *et al.*, 2004; Lera and Burkard, 2012). Plk1 participates in signaling required for Eg5 loading, although it likely participates in bipolar spindle formation in other undefined ways (van Ree *et al.*, 2016). Eg5 can be chemically inhibited with an allosteric inhibitor called monastrol (Maliga *et al.*, 2002). Similarly, Plk1 can be chemically inhibited with BI2536, an ATP-competitive inhibitor (Steegmaier *et al.*, 2007). Inhibition of both of these proteins abolishes bipolar spindle integrity and results in the collapse of the mitotic spindle into a monopolar spindle. While their role in bipolar spindle formation has been well described, it remains undetermined if Eg5 and Plk1 play a role in multipolar spindle formation. Identification of the molecular requirements for multipolar spindle establishment and maintenance by microtubule poisons may allow for the selection of biomarkers whose expression is necessary for the efficacy of these anti-cancer drugs.

Spindle polarity can also be compromised independent of cellular centrosome number by disturbing spindle forces (Maiato and Logarinho, 2014). One source of force generation within the mitotic spindle comes from its associated molecular motors (Dumont and Mitchison, 2009). In addition to Eg5, the plus end directed kinesin CENtromere associated Protein E (CENP-E) may also play a role in multipolar spindle formation. A low incidence of multipolar spindles has also been reported following CENP-E inhibition (McEwen *et al.*, 2001; Yao *et al.*, 2000), which is thought to arise from altered forces within the spindle. However, whether CENP-E influences multipolarity induced by paclitaxel and other microtubule poisons has not yet been studied.

Since multipolar spindle clustering represents a mechanism of paclitaxel resistance (Chapter Two), a mechanistic understanding of multipolar spindle maintenance is also imperative. Our evidence demonstrated that inhibition of Mps1 and upregulation of Mad1, which reduced mitotic duration, impaired multipolar spindle maintenance (Chapter Two). Whether Mps1 plays a role in multipolar spindle establishment, and the temporal and spatial requirements for multipolarity induced by microtubule poisons, are topics that are further investigated here.

RESULTS

Multipolar spindles induced by paclitaxel do not require centrosome amplification

To test whether centrosome amplification was required for paclitaxel-induced multipolar spindles we stained our patient samples with gamma tubulin to label the PCM, NuMA to label spindle poles, DAPI to label the DNA, and pan-cytokeratin to distinguish tumor cells from the surrounding stroma. When looking in patient samples, we observed mitotic cells with diverse gamma tubulin phenotypes following paclitaxel treatment. In addition to normal bipolar spindles with two gamma tubulin foci (Figure 4.1 A, top), we found that cells within the same patient biopsy that exhibited diverse multipolar spindle gamma tubulin phenotypes. Some multipolar cells had supernumerary gamma tubulin foci (≥3), with gamma tubulin present at each pole (Figure 4.1A, bottom), while other multipolar spindles cells had just two gamma tubulin foci, and one or more poles that were lacking gamma tubulin (Figure 4.1 A, middle). In every patient tumor examined, a majority of multipolar cells had poles lacking gamma tubulin (Figure 4.1B), suggesting that supernumerary centrosomes are not required for

paclitaxel-induced multipolar spindles. Consistent with this, centrosome amplification relative to pre-treatment samples was not observed in most patients (Figure 4.1C). Following paclitaxel treatment, most patients had a lower or similar percentage of cells with ≥3 gamma tubulin foci when compared to their pre-treatment controls (Figure 4.1C), although it should be noted that the pre-treatment samples had relatively low numbers of multipolar spindles at baseline for comparison. This data is consistent with work by others (Bian et al., 2010), and demonstrates that paclitaxel-induced multipolarity does not require centrosome amplification.

We repeated this experiment in Cal51 triple negative breast cancer cells, which have a low baseline level of centrosome amplification (Figure 4.2A). Consistent with what was observed in patients, we again observed diverse gamma tubulin phenotypes in cells treated with a clinically relevant concentration of paclitaxel. In addition to bipolar spindles with two gamma tubulin foci (Figure 4.2B, top), some multipolar cells had supernumerary gamma tubulin foci (≥3), with gamma tubulin at each pole (Figure 4.2B, middle), while other multipolar spindles cells had just two gamma tubulin foci and poles that were lacking gamma tubulin (Figure 4.2B, bottom). Quantification of these phenotypes revealed that approximately 70% of multipolar cells had poles that were missing gamma tubulin, demonstrating that gamma tubulin is not required for multipolar spindle formation in paclitaxel in Cal51 cells, and centrosome amplification is not observed in most multipolar spindles (Figure 4.2C, acentrosomal poles). Approximately 30% of cells had ≥3 gamma tubulin foci after a 20-hour treatment with a clinically relevant dose of paclitaxel (Figure 4.2C), consistent with the low frequency of multipolar

spindles with gamma tubulin at each pole in patient tumors. Thus, multipolar spindles induced by paclitaxel do not require centrosome amplification.

Given that centrosome amplification was not strictly required for multipolarity induced by paclitaxel, we next wanted to test if multipolar spindles in paclitaxel were caused by centriole disengagement or PCM fragmentation. To test this, we again used Cal51 cells that were treated with a clinically relevant concentration of paclitaxel for 20 hours. These cells were then fixed and stained with centrin to label centrioles and pericentrin to label the PCM, and the number of pericentrin and centrin foci were counted in each cell (Figure 4.2D). While these antibodies do not work well in patient tissue, they can be readily visualized in cultured cells (Figure 4.2E). We again observed multipolar spindles with centrin and pericentrin at all poles, and multipolar cells with poles that were lacking centrin and percentrin (acentriolar/apericentriolar). If centriole disengagement were induced by paclitaxel, we would expect to see spindle poles with singular unpaired centrioles. On the other hand, if paclitaxel caused PCM fragmentation, we would expect to see spindle poles that stained positive for pericentrin but did not contain centrin. Centriole amplification could also be quantified by identifying cells with ≥4 centrin foci. These phenotypes are quantified in Figure 4.2F. While there was a low incidence of centriole amplification, the predominant multipolar phenotype consisted of multipolar cells lacking centrioles and pericentrin (Figure 4.2F). Thus, this data demonstrates that extra spindle poles induced by paclitaxel do not require centriole amplification or, on a molecular level, centrin, pericentrin or gamma tubulin.

Eg5 and Plk1 (to a lesser extent) are required for paclitaxel-induced multipolar spindle establishment and maintenance, while Mps1 and CENP-E are not

To test whether Eg5 is required for paclitaxel induced multipolar spindles, a pharmacological inhibitor of Eg5, monastrol, was used. MDA-MB-231 and Cal51 triple negative breast cancer cells were treated with vehicle control, a clinically relevant concentration of paclitaxel (10 nM), monastrol (10 μM), or a combination of paclitaxel and monastrol. Vehicle control treated MDA-MB-231 and Cal51 cells exhibited predominately normal bipolar spindles, as expected. Treatment of these cells with clinically relevant concentrations of paclitaxel results in approximately 60% and 40% multipolarity in MDA-MB-231 and Cal51 cells, respectively (Figure 4.3 A and B). Inhibition of Eg5 with monastrol prevented spindle pole separation and resulted in the formation of a monopolar spindle in >90% of cells, as expected (Figure 4.3A and B). Simultaneous treatment with paclitaxel and monastrol prevented the formation of multipolar spindles and again resulted in the formation of predominately monopolar spindles in both cell lines (Figure 4.3A and B). Taken together these results demonstrate that Eg5 is required for paclitaxel-induced multipolar spindle formation.

We also wanted to test if Plk1 played a role in multipolar spindle formation in response to paclitaxel treatment. Plk1 is a kinase with multiple mitotic functions, including a role in bipolar spindle assembly (Barr *et al.*, 2004). Accordingly, treatment of cells with high concentrations of BI2536, an ATP-competitive Plk1 inhibitor, results in monopolar spindles (Steegmaier et al., 2007). While the downstream effector substrates of Plk1 linking it to its various mitotic roles are not completely characterized, it is known that Plk1 participates in a signaling cascade that localized Eg5 to the centrosome (van

Ree *et al.*, 2016). To test whether Plk1 is required for paclitaxel-induced multipolar spindle establishment, MDA-MB-231 and Cal51 cells were treated with vehicle control, a clinically relevant concentration of paclitaxel, BI2536, or a combination of paclitaxel and BI2536. As expected, control-treated cells had predominantly bipolar spindles, whereas BI2536 treated cells had predominately monopolar spindles (Figure 4.3 C and D). Multipolar spindles were formed in the presence of clinically relevant concentrations of paclitaxel; however, they were not formed in the combined treatment of paclitaxel and BI2536. Instead, monopolar spindles were observed (Figure 4.3 C and D). Therefore, like Eg5, Plk1 is required for establishing multipolar spindles in response to paclitaxel.

Given that Eg5 is required for establishing paclitaxel-induced multipolar spindles, we next wanted to determine if Eg5 is also necessary for maintaining paclitaxel-induced multipolar spindles. To test this, we treated fluorescent MDA-MB-231 cells with a clinically relevant concentration of paclitaxel to induce multipolar spindle formation. After 20 hours, we began imaging mitotic cells, added monastrol, and observed the spindle at one-minute time intervals. Addition of monastrol resulted in the collapse of the multipolar spindle in the vast majority of cells (27/29, 93%), regardless of the initial polarity of the spindle (2-5+ poles). To quantify the extent of spindle pole collapse, we measured the distance between the center of each of the spindle poles before and after addition of the inhibitor and calculated the percent change in spindle pole distance (Figure 4.3 E and F). Cells in which all spindle poles came together to form a monopolar spindle had a greater than 25% decrease in spindle pole distance and were classified as having a complete collapse. This phenotype was observed in 19 of 29 cells (65.5%) after Eg5 inhibition (Figure 4.3F). Cells that had a partial collapse, in which the poles

moved closer but did not completely collapse into a monopolar spindle, had a change in spindle pole distance between -5% and -25%, which occurred in 27.5% of monastrol treated cells (Figure 4.3F). Overall, 27 of 29 cells, or 93% of multipolar spindles, exhibited at least partial collapse after monatrol treatment. These data demonstrate that Eg5 plays a role in both establishing and maintaining multipolar spindle poles in paclitaxel.

To determine whether Plk1 was also involved in maintaining multipolar spindles paclitaxel, fluorescent MDA-MB-231 cells were treated with a clinically relevant concentration of paclitaxel for 20 hours to allow for multipolar spindle formation. After initiating imaging, BI2536 was added and images were taken at one-minute intervals to observe the mitotic spindle over time. Spindle pole distance measurements were taken at the initial time frame and at the final time frame after one hour to calculate the percent change in spindle pole distance (Figure 3F). Inhibition of Plk1 resulted in a milder spindle collapse phenotype. 89% (17 of 19) multipolar spindles exhibited at least partial collapse, similar to 94% of monastrol treated spindles. However, the fraction of complete collapses was decreased: 42% underwent a complete collapse after addition of BI2536 as compared to 66% of multipolar spindles treated with monastrol. Nearly half (9 of 19, or 47%) of cells displayed a partial spindle pole collapse, as compared to 28% of Eg5-inhibited cells. The overall extent of spindle pole collapse was also reduced after Plk1 inhibition compared to Eg5 inhibition (compare Figure 4.3 F and G). These results are in agreement with previous evidence suggesting that Eg5 can localize independently of Plk1 (Smith et al., 2011). All together, these results suggest that Eg5

and (to a lesser extent) Plk1 are required for paclitaxel-induced multipolar spindle establishment and maintenance.

Since low nanomolar doses of other clinically used microtubule poisons induced mitotic spindle multipolarity, like paclitaxel, we wondered if there would be shared molecular requirements for multipolar spindle establishment and maintenance. To test this hypothesis, we treated MDA-MB-231 and Cal51 cells with DMSO, BI2536, low nanomolar doses of vinorelbine shown to induce spindle multipolarity, or a combination of vinorelbine and BI2536. Normal bipolar mitotic spindles were observed in DMSO-treated control cells, as expected. BI2536 was sufficient to induce monopolar spindles with nearly complete penetrance when used individually, suggesting substantial inhibition of its protein target, Plk1 (Figure 4.S1A and B). Importantly, while multipolar spindles were observed after 20 hours of low dose (5 nM) vinorelbine treatment, predominately monopolar spindles were observed in the combined treatment of vinorelbine and BI2536 (Figure 4.S1A and B). These results demonstrate that Plk1 is required for both paclitaxel and vinorelbine to establish multipolar spindles and suggest there are shared molecular requirements for multipolar spindle formation induced by diverse microtubule poisons.

CENP-E and Mps1 were also evaluated for their role in multipolar spindle establishment in paclitaxel. CENtromere associated Protein E (CENP-E) is a plus end directed kinesin which attaches to spindle microtubules at its N-terminus and to kinetochores of chromosomes at its C-terminus to power chromosome alignment (Kim et al., 2008). Inhibition of CENP-E has been shown to substantially increase the incidence of misaligned chromosomes (Wood et al., 2010). A low incidence of

multipolar spindles has also been reported following CENP-E inhibition (McEwen et al., 2001; Yao et al., 2000), which is thought to arise from altered forces within the spindle. To test whether CENP-E was required for multipolar spindle establishment in paclitaxel, we treated MDA-MB-231 and Cal51 cells with paclitaxel and the CENP-E inhibitor GSK923295 (Figure 4.S2A and B). However, addition of GSK923295 to paclitaxel did not affect the level of multipolarity as compared to paclitaxel treatment alone (Figure 4.2S2A and B). Therefore, CENP-E is not required for multipolar spindle formation induced by paclitaxel.

Mps1, or monopolar spindle 1, was first identified in budding yeast with mutant *mps1*, which displayed monopolar spindles (Fisk et al., 2004). However, its role in centrosome duplication in humans remains controversial (Fisk et al., 2004). Inhibition of Mps1 with reversine in MDA-MB-21 and Cal51 cells did not prevent bipolar spindle establishment in control-treated cells or multipolar spindle establishment in paclitaxel-treated cells (Figure 4.S2C and D). Note that spindle polarity was quantified looking at all stages of mitosis in this experiment, which differs from the experiments discussed in Chapter Two in which multipolarity was assessed separately in pre-anaphase and anaphase/telophase cells after treatment with paclitaxel and reversine. Thus, while Mps1 plays a role in multipolar spindle maintenance (Chapter Two), it does not affect multipolar spindle establishment in paclitaxel.

Temporal and spatial requirements for paclitaxel-induced multipolar spindle maintenance

We recently discovered that accelerating transit through mitosis through two mechanisms (inhibition of Mps1 or upregulation of Mad1) caused reduced multipolar

spindle maintenance and increased spindle pole clustering in MDA-MB-231 cells treated with a clinically relevant concentration of paclitaxel (Chapter Two). These data suggested that there may be a temporal requirement for multipolar spindle maintenance in paclitaxel. If this were true, we hypothesized that increasing mitotic duration would increase multipolar spindles in paclitaxel. To prolong mitotic duration, we pre-treated cells with a clinically relevant concentration of paclitaxel for 20 hours, then added low dose nocodazole or the proteosome inhibitor MG-132 for one hour prior to timelapse microscopy. While cells in the presence of MG-132 never entered anaphase and remained rounded throughout the 24 hour duration of timelapse imaging (resulting in a significantly increased mitotic duration), combining low doses of nocodazole with paclitaxel prolonged the time to anaphase onset over paclitaxel treatment alone (Figure 4.4A).

We next wanted to assess the effects of a prolonged mitosis on spindle multipolarity. To test this, we pre-treated MDA-MB-231 and Cal51 cells for 20 hours with a clinically relevant concentration of paclitaxel (10nM) and then added vehicle, MG-132 (10 μM), or nocodazole (5 ng/mL) for 1 hour prior to fixation. Control cells that were treated with DMSO for 20 hours and nocodazole or MG-132 for one hour all displayed predominately bipolar spindles, suggesting that the these concentrations and treatment duration were insufficient to induce multipolar spindles by themselves (Figure 4.4 B and C). Treatment with clinically relevant concentrations of paclitaxel resulted in approximately 60% and 32% multipolarity in MDA-MB-231 and Cal51 cells, respectively. However, multipolar spindles were further increased an additional 10-15% following a one-hour treatment with nocodazole or MG-132 in Cal51 cells and an additional 20% in

MDA-MB-231 cells (Figure 4.4 B and C). Therefore, paclitaxel-induced multipolar spindles exhibit time dependency. Decreasing mitotic duration reduces multipolar spindles, whereas increasing mitotic duration increases multipolarity.

Consistently, a recent study found that multipolar spindles induced by depletion of CSAG1 in HeLa cells showed time dependent effects. Similar to our results, they found that reversine treatment significantly reduced time in mitosis and the incidence of multipolar spindle formation following CSAG1 depletion (Sapkota *et al.*, 2020). Conversely, treatment with low dose nocodazole (5ng/mL), low dose paclitaxel (0.75 nM), or the APC/C inhibitor PROTAME (5 μM) prolonged mitotic duration. In control cells, nocodazole, paclitaxel, and ProTAME increased the time from nuclear envelope breakdown to anaphase onset, but did not cause a significant increase in multipolar spindles (Sapkota *et al.*, 2020). However, in their CSAG1 depleted cells, prolonging mitotic duration exacerbated their multipolar spindle phenotype (Sapkota *et al.*, 2020). These data suggest that multipolar spindles induced by mechanisms other than paclitaxel directly correlated with mitotic duration.

It is not yet fully understood why reducing time in mitosis leads to reduced multipolar spindle maintenance. We first hypothesized that accelerated transit through mitosis led to a decrease in multipolar divisions in MDA-MB-231 cells because the cells treated with paclitaxel entered mitosis with a bipolar spindle that then become multipolar over time. We considered that reducing mitotic duration could prevent cells that start with a bipolar spindle from becoming multipolar before anaphase onset. To test this hypothesis, we performed live cell imaging using MDA-MB-231 cells expressing GFP-tubulin and RFP-histone H2B to visualize the mitotic spindle and chromosomes, respectively. The first

half of that hypothesis turned out to be true, 121/121 cells examined had a bipolar spindle or two microtubule nucleation sites at G2 initially. However, all cells had acquired multipolar spindles before anaphase onset. This data suggested that accelerated transit through mitosis did not cause a reduction in multipolar spindles in anaphase and telophase because multipolar spindles had insufficient time to form, as 121/121 MDA-MB-231 cells entered anaphase with a multipolar spindle in clinically relevant concentrations of paclitaxel. Therefore, the temporal requirement is for multipolar spindle maintenance rather than establishment, but the exact mechanisms underlying this effect are still unclear.

Discussion

In summary, centrosome amplification is not required for paclitaxel-induced multipolar spindles. Eg5 and (to a lesser extent) Plk1 are required for both establishing and maintaining paclitaxel-induced multipolar spindles. In contrast, Mps1 and CENP-E are not required for multipolar spindle establishment in paclitaxel, but data discussed in Chapter 2 suggests that Mps1 functions in maintaining paclitaxel-induced multipolar spindles. Identification of the molecular requirements for multipolarity induced by paclitaxel may lead to the identification of new biomarkers of paclitaxel response. Moreover, identification of the mechanisms that contribute to multipolar spindle maintenance may elucidate strategies to prevent multipolar spindle clustering and paclitaxel resistance.

We identified Eg5 and Plk1 as proteins with important roles in paclitaxel-induced multipolar spindle establishment and maintenance. Although this increased our

understanding of how multipolar spindles are formed and maintained in response to paclitaxel in cells, they are unlikely to translate to predictive biomarkers of paclitaxel response in patients, as alterations in these genes are quite rare in breast cancer. According to the Cancer Genome Atlas (TCGA), alterations in Eg5 occurred in only 1.01% of 1,084 cases of breast invasive carcinoma (with mutations occurring in 0.74% of patients (8 cases), amplification occurring in 0.09% of patients (1 case), and deep deletions occurring in 0.18% of patients (2 cases)). On the mRNA level, 16.63% of patients exhibit high mRNA expression of Eg5, whereas 15.12% of patients display low mRNA expression of Eg5. Alterations in Plk1 are slightly more common, but still quite rare. According to the Cancer Genome Atlas (TCGA), alterations in Plk1 occurred in only 3.6% of 1,084 cases of breast invasive carcinoma (with mutations occurring in 0.28% of patients (3 cases), amplification occurring in 3.23% of patients (35 cases), and multiple alterations occurring in 0.09% of patients (1 case)). On the mRNA level, 14.9% of patients exhibit high mRNA expression of Plk1, whereas 15.55% of patients display low mRNA expression of Plk1. This is not entirely surprising, as mutations in mitotic genes are infrequently observed in cancer because their functionality is required for the cancer cells to continue to proliferate.

Spindle pole distance measurements revealed a role for Eg5 and Plk1 in multipolar spindle maintenance. However, it should be noted that these measurements were performed on two-dimensional (2D) maximum projections. In the future, these experiments should be repeated using a three-dimensional (3D) analysis. Manual measurements from the approximate center of each spindle pole could be improved upon by automated distance measurements between the centroid of each spindle pole

(for instance using Imaris software). This would also permit a higher throughput analysis and larger sample size.

Further work is necessary to determine whether the molecular requirements for paclitaxel-induced multipolarity are also required for multipolar spindles caused by other clinically used microtubule poisons. Preliminary data suggests that Plk1 is required for multipolar spindles induced by paclitaxel and vinorelbine. It remains to be determined whether Eg5, Mps1, and CENP-E contribute to multipolarity induced by vinorelbine and other clinically used microtubule poisons.

Microtubules can nucleate from other pre-existing microtubules, in a phenomenon called branching microtubule nucleation (Petry et al., 2013). Recently, microtubule nucleation was biochemically reconstituted using purified *Xenopus laevis* proteins including the microtubule nucleator gamma-tubulin ring complex (γ-TuRC), and the branching effectors augmin and TPX2 (Alfaro-Aco et al., 2020). Interestingly, like paclitaxel-induced multipolar spindle formation, this pathway of microtubule nucleation also appears to have time dependent effects. Augmin was found to preferentially accumulate on longer lived microtubules (David et al., 2019). Whether this time dependent mechanism of microtubule nucleation is linked to the time dependent mechanism of multipolarity induced by paclitaxel remains to be determined.

There is also evidence for spatial requirements for multipolar spindle maintenance and spindle pole clustering. A recent study found that HSET initiates a motorized phase of clustering when spindle poles are 7-8 μm apart (Rhys et al., 2018). On the other hand, poles that did not cluster showed a mean distance of 11-12 μm (Rhys *et al.*, 2018). Two additional experiments were performed to demonstrate the

distance requirement for HSET mediated spindle pole clustering. First, the distance between spindle poles was manipulated by increasing or decreasing cortical contractility. Forcing spindle poles closer together by increasing cortical contractility with calyculin A, which increases myosin II activity, increased spindle pole clustering. Conversely, inhibition of cortical contractility with blebbistatin, a myosin II inhibitor, did not restrain spindle pole distance and resulted in reduced spindle pole clustering (Rhys *et al.*, 2018). In addition, overexpression of Plk4 increased the number of centrosomes per cell, thereby increasing the proximity of microtubule organizing centers, and resulting in increased spindle pole clustering (Rhys *et al.*, 2018). Taken together, these data suggest that there is a spatial component to spindle pole clustering.

Combined with the current evidence in the literature and results from our own experiments, I propose that there are spatiotemporal requirements for paclitaxel-induced multipolar spindle clustering. It is possible that paclitaxel-induced multipolar spindles start off in close proximity to one another and then move apart over time. In the context of accelerated transit through mitosis, I hypothesize that spindle poles do not have sufficient time to separate from one another, making it more likely that they will cluster together. Future live cell imaging experiments with high temporal and spatial resolution, coupled with automated spindle pole tracking and distance measurements will permit a more robust test of this hypothesis.

Materials and Methods

Cell culture

MDA-MB-231 and Cal51 cell lines were grown in DMEM supplemented with 10% (vol/vol) FBS, 2 mM L-glutamine, and 50 µg/mL penicillin/streptomycin at 37°C and 5% CO_2. Paclitaxel (10nM, LC Laboratories), vinorelbine (5nM, Medkoo), monsatrol (10µM, Tocris), BI2536 (200nM, Sellek Chemicals), reversine (1µM, Sigma Aldrich), and GSK923295 (200nM, AdooQ Biosciences), used in cell culture experiments were dissolved in DMSO.

Immunofluorescence

Immunofluorescence was performed as in (Ryan *et al.*, 2012). Cellular staining was performed with antibodies to α-tubulin (YL 1/2; Bio-Rad, MCA77G) and γ-tubulin (Sigma, T6557), diluted 1:1000 for one hour at room temperature. For patient immunohistochemistry, 5 µm sections of formalin-fixed, paraffin-embedded tissue sections were subjected to antigen retrieval in citrate buffer, serum-blocked overnight, and stained with rabbit anti-NuMA antibody [a kind gift from Duane Compton; (Compton *et al.*, 1991)], γ-tubulin (Sigma, T6557), and pan-cytokeratin (to mark epithelial cells; Novus Biologicals, NBP2-33200AF647) antibodies diluted 1:100 overnight at 4°C. Alexa Fluor-conjugated secondary antibodies (Invitrogen) were used at 1:200 for one hour at room temperature. DNA was stained using DAPI.

Microscopy

Images were acquired on a Nikon Ti-E inverted microscope driven by Nikon Elements software with focus-drift compensation. Images are maximum projections from 0.2 µm z-stacks collected with a 60×/1.4 or 100×/1.4 numerical aperture (NA)

objective after deconvolution using the AQI 3D Deconvolution module in Elements. For multipolar spindle maintenance timelapse analysis, cells were placed under 10% CO_2 flow at ~30 mL/min in a heated chamber at 37°C. Images were acquired at 1-minute intervals using a 60×, 1.4 NA objective and focus drift compensation. Cells were pre-treated with paclitaxel 20 hours before observation to allow multipolar spindle formation. Cells were then treated with monastrol or BI2536 after imaging was initiated. Maximum projections of in-focus planes or the maximally focused single z plane were assembled in Elements, exported as jpg files, and converted to .avi files in Fiji/ImageJ.

Spindle pole distance measurements

Spindle pole distance measurements were performed manually using the length measurement feature in Nikon Elements. Distances were measured between spindle poles by drawing a straight line between the approximate center of each spindle pole. The total distance between each spindle pole was then summed to obtain one distance per cell. Distances were measured at the initial time point prior to addition of inhibitor and again at the final time frame of the timelapse movie. The percent change in spindle pole distance was calculated using the following formula: (Final distance – initial distance) / (initial distance).

Statistical Analysis

Statistical analysis was performed using GraphPad Prism. Student's t-tests were used to assess significance, unless otherwise noted. Other statistical parameters

including the number of cells analyzed and the number of replicates are reported in the respective figure legends.

Figure 4.1. Centrosome amplification is not required for multipolarity induced by paclitaxel in primary breast cancer patients.

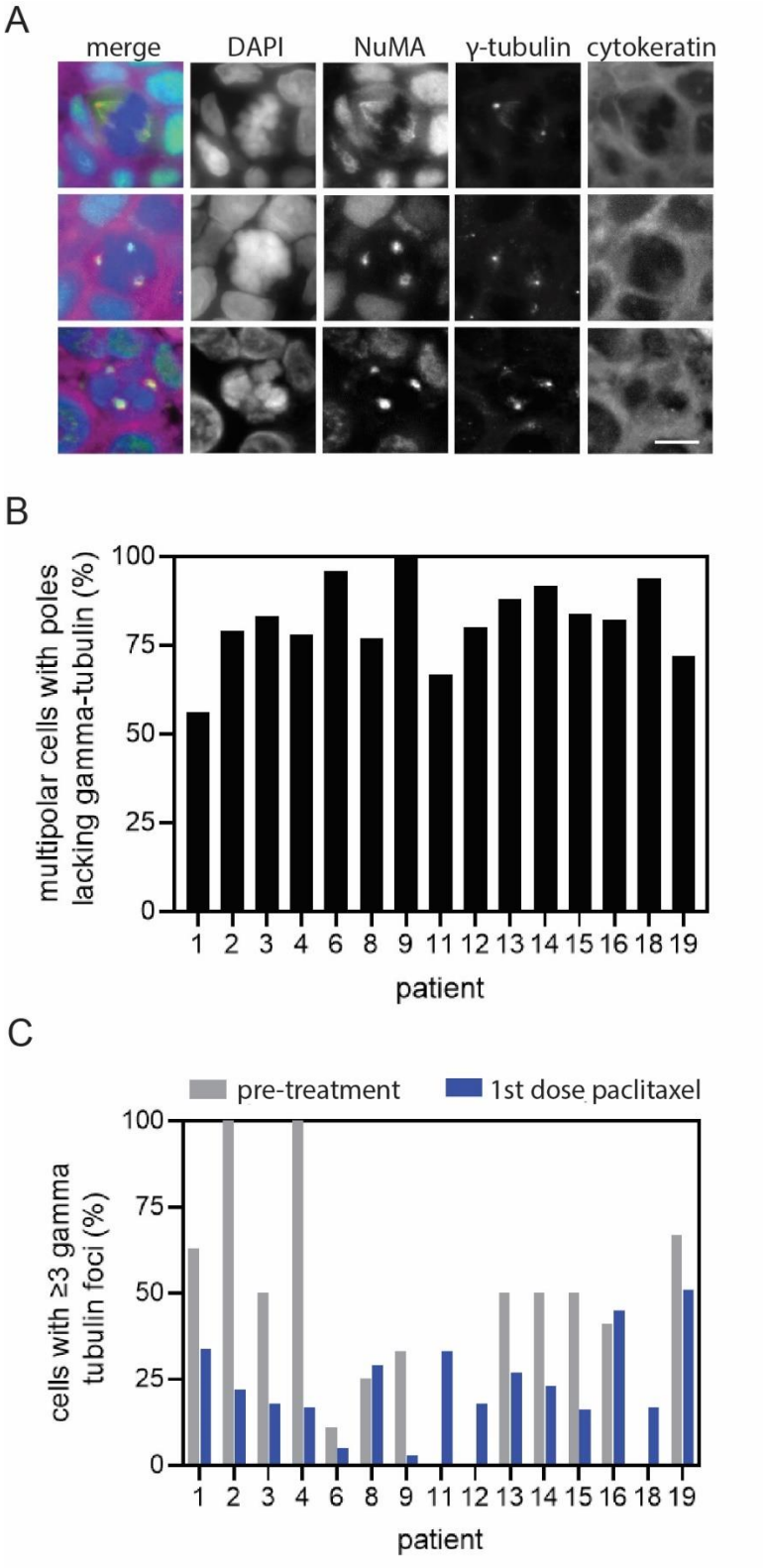

Figure 4.1. Centrosome amplification is not required for multipolarity induced by paclitaxel in primary breast cancer patients. A) Representative images of gamma-tubulin staining in breast cancer patient biopsies. Normal bipolar spindle with two gamma-tubulin foci (top), multipolar spindle with all poles containing gamma-tubulin foci (middle), and multipolar spindle with at least one pole missing gamma-tubulin foci (bottom). **B**) Quantification of the percent of multipolar cells with poles lacking gamma-tubulin foci in primary paclitaxel patient cohort. **C**) Quantification of multipolar cells with ≥3 gamma-tubulin foci in primary paclitaxel patient cohort. **B-C**) Multipolar mitotic cell sample sizes for patients are 8, 2, 2, 2, 18, 4, 3, 0, 1, 6, 12, 4, 17, 2, and 3 cells, respectively, pre-treatment and 56, 49, 28, 30, 65, 17, 39, 3, 17, 71, 60, 61, 78, 83, and 47 cells, respectively, 20 hours after the first treatment.

Figure 4.2. Gamma tubulin, pericentrin, and centrin are not required for multipolarity induced by paclitaxel.

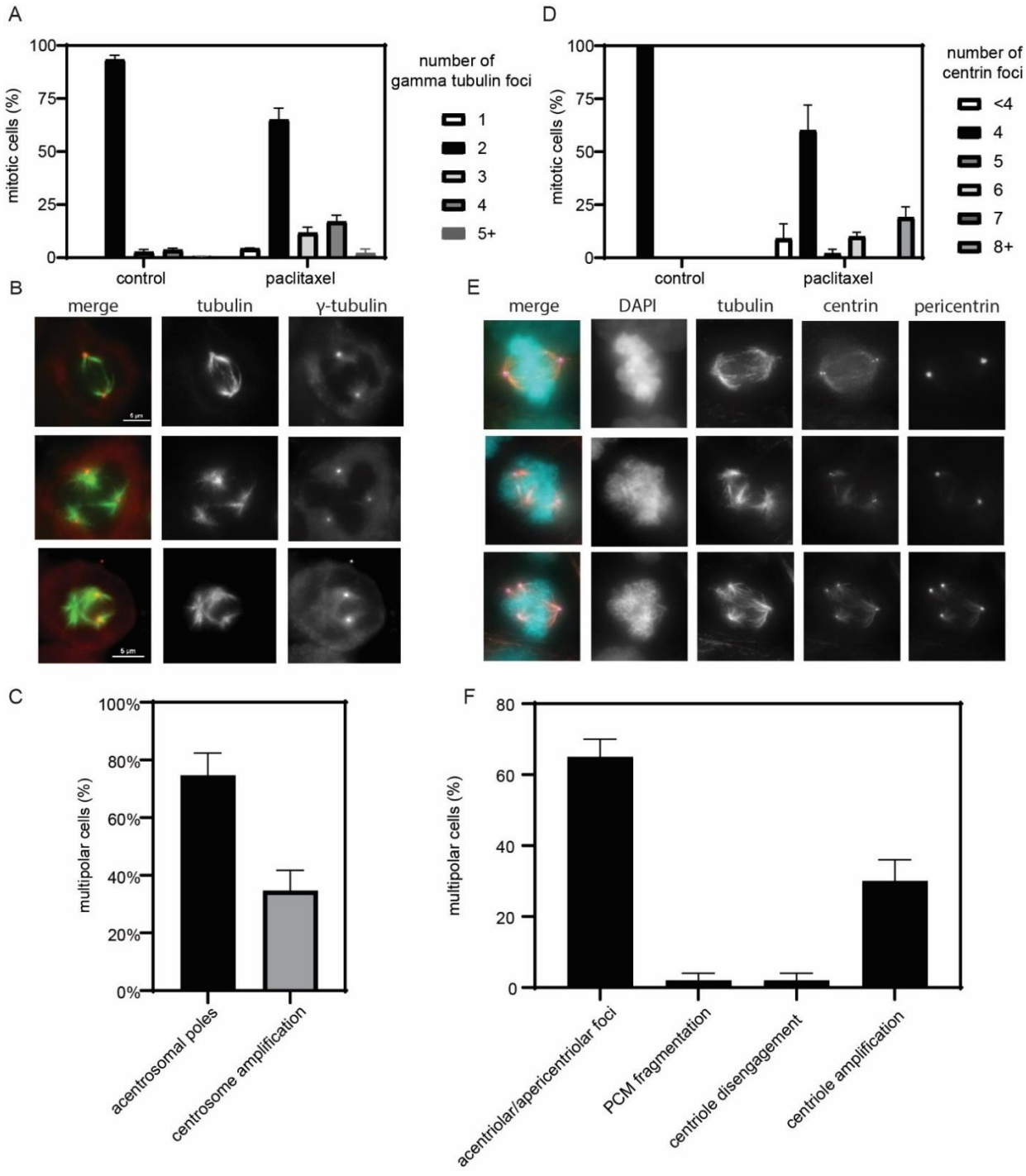

Figure 4.2. Gamma tubulin, pericentrin, and centrin are not required for multipolarity induced by paclitaxel. A) Quantification of the number of gamma tubulin foci per cell in control and paclitaxel treated (10 nM) Cal51 cells. n≥50 cells from each of 3 independent experiments. **B**) Representative images of gamma-tubulin staining Cal51 cells. Normal bipolar spindle with two gamma-tubulin foci (top), multipolar spindle with all poles containing gamma-tubulin foci (middle), and multipolar spindle with at least one pole missing gamma-tubulin foci (bottom). **C**) Quantification of gamma tubulin phenotypes observed in Cal51 cells, representing the percent of cells containing acentrosomal poles (as in B, bottom) or the percent of cells with centrosome amplification (>2 gamma tubulin foci). n≥50 cells from each of 3 independent experiments. **D**) Quantification of the number of centrin foci per cell in control and paclitaxel treated (10 nM) Cal51 cells. n≥25 cells from each of 2 independent experiments (paclitaxel) or one independent experiment (control). **E**) Representative images of centrin and pericentrin staining Cal51 cells. Normal bipolar spindle with two gamma-tubulin foci (top), multipolar spindle with at least one pole missing centrin and pericentrin foci (middle), and multipolar spindle with all poles containing centrin and pericentrin (bottom). **F**) Quantification of gamma tubulin phenotypes observed in Cal51 cells, representing the percent of cells containing acentriolar and apericentriolar poles (as in D, middle) centriole amplification (>4 gamma tubulin foci), centriole disengagement (as in D, bottom), or PCM fragmentation. n≥25 cells from each of 2 independent experiments.

Figure 4.3. Eg5 and Plk1 are required for microtubule poison-induced multipolar spindle establishment and maintenance.

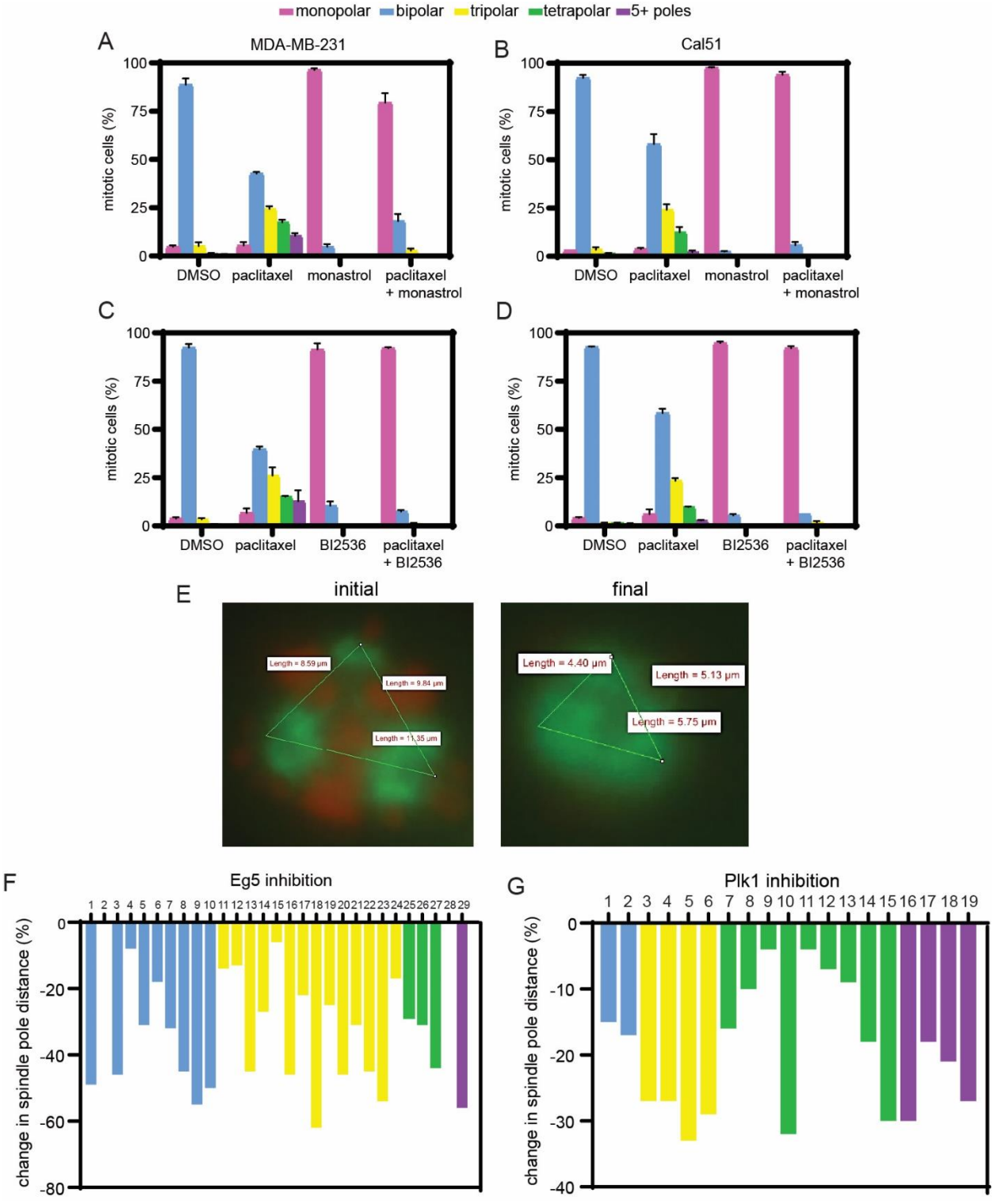

Figure 3. Eg5 and Plk1 (to a lesser extent) are required for microtubule poison-induced multipolar spindle establishment and maintenance. A-B) Eg5 is required for multipolar spindle establishment in paclitaxel. Quantification of mitotic cell spindle polarity in response to paclitaxel, monastrol, or both in MDA-MB-231 (**A**) or Cal51 cells (**B**). Data represent mean +/- SEM, n≥100 cells in each of three independent replicates. **C**-**D**) Plk1 is required for multipolar spindle establishment in paclitaxel. Quantification of mitotic cell spindle polarity in response to paclitaxel, BI2536, or both in MDA-MB-231 (**C**) or Cal51 cells (**D**). Data represent mean +/- SEM, n≥100 cells in each of three independent replicates. **E**-**G**) Eg5 and Plk1 are required for multipolar spindle maintenance in paclitaxel. **E**) Representative image of spindle pole distance measurement at the first and final frame of timelapse microscopy demonstrating a collapse of the multipolar mitotic spindle. Quantification from time-lapse microscopy of spindle pole distance change after addition of inhibitors of Eg5 (**F**) and Plk1 (**G**) following a 20hr pretreatment with paclitaxel. Dotted lines indicate cut offs for defining partial and complete collapses. Cells with partial collapses had a -5% to -25 percent change in spindle pole distance, whereas cells with a complete collapse shrank by more than 25%.

Figure 4.4. Increased mitotic duration increased multipolarity in response to paclitaxel.

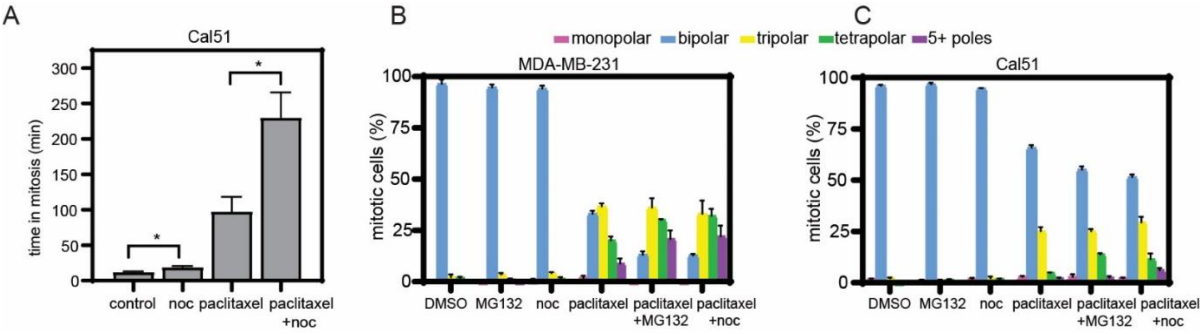

Figure 4. Increased mitotic duration increased multipolarity in response to paclitaxel. A) Quantification of time in mitosis, assessed as the time from cell rounding to the time of elongation determined by brightfield microscopy Cal51 cells. Note that cells treated with MG132 remained rounded for the duration of timelapse microscopy, so their time to elongation could not be determined. Data represent the mean +/- SEM, n≥10 cells. **B-C**) Increasing mitotic duration with a 1 hr treatment of MG-132 or low dose nocodazole after 20 hours in paclitaxel increases spindle multipolarity. Quantification of mitotic cell spindle polarity in response to DMSO, 10 nM paclitaxel, 10 μM MG-132 or 5 ng/mL nocodazole, or a combination in MDA-MB-231 (**B**) or Cal51 cells (**C**).

Figure 4.S1. Plk1 is required for vinorelbine-induced multipolar spindle establishment.

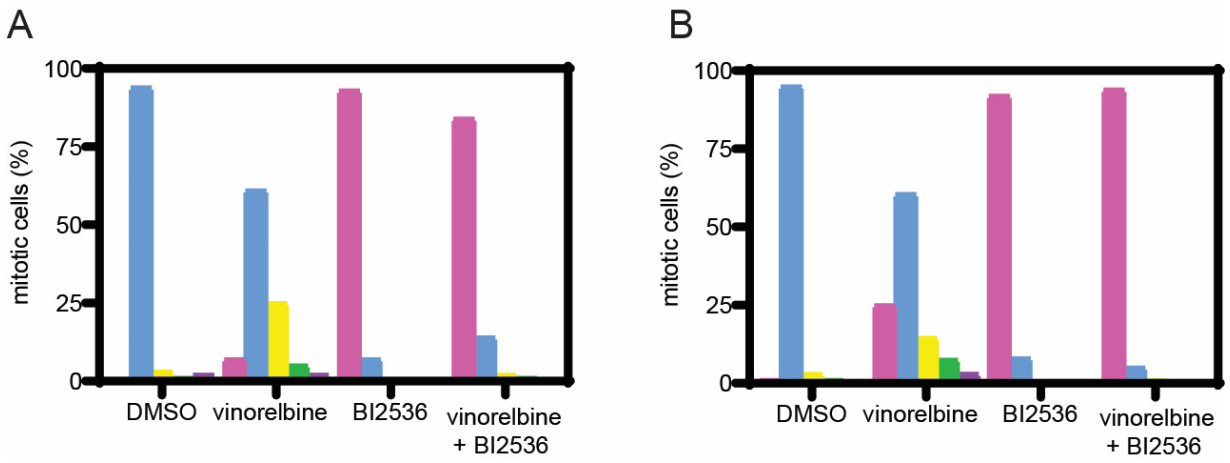

Figure 4.S1. Plk1 is required for vinorelbine-induced multipolar spindle establishment. A-B) Plk1 is required for the establishment of multipolar spindles induced by vinorelbine. Quantification of mitotic cell spindle polarity in response to DMSO, vinorelbine (5 nM), BI2536 (200 nM), or both vinorelbine and BI2536 in MDA-MB-231 (**A**) or Cal51 cells (**B**). n≥100 cells from one replicate.

Figure 4.S2. CENP-E and Mps1 are not required for microtubule poison-induced multipolar spindle establishment.

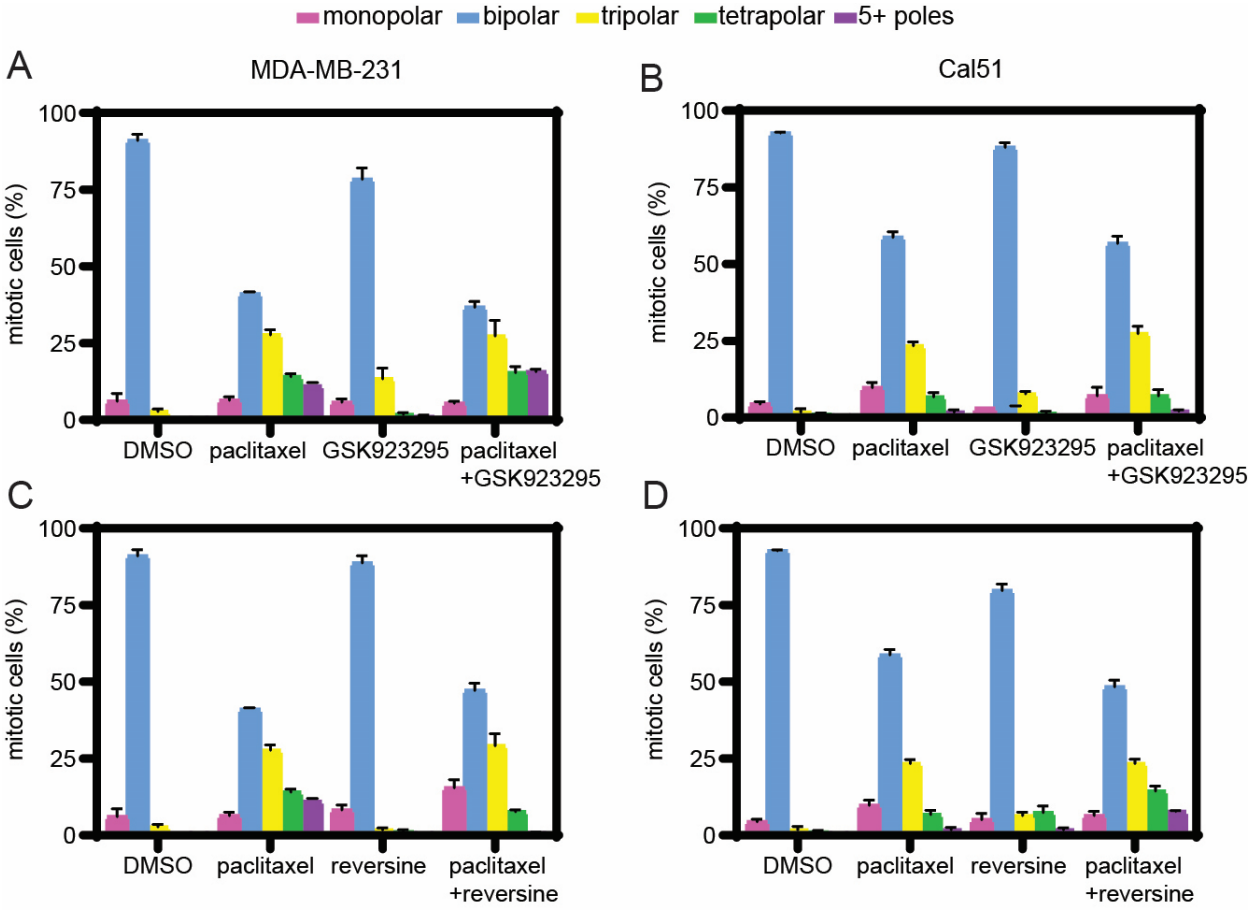

Figure 4.S2. CENP-E and Mps1 are not required for microtubule poison-induced multipolar spindle establishment. A-B) CENP-E is not required for multipolar spindle establishment in paclitaxel. Quantification of mitotic cell spindle polarity in response to paclitaxel, GSK923295, or both in MDA-MB-231 (**A**) or Cal51 cells (**B**). Data represent mean +/- SEM, n≥100 cells in each of three independent replicates. **C-D**) Mps1 is required for multipolar spindle establishment in paclitaxel. Quantification of mitotic cell spindle polarity in response to paclitaxel, reversine, or both in MDA-MB-231 (**C**) or Cal51 cells (**D**). Data represent mean +/- SEM, n≥100 cells in each of three independent replicates.

CHAPTER 5: CONCLUSIONS AND FUTURE DIRECTIONS

The microtubule stabilizing drug paclitaxel is a cornerstone of breast cancer treatment. Paclitaxel entered phase I clinical trials in 1984, and phase II trials the following year. It was trademarked by Bristol Meyers Squibb in 1990 as Taxol (generic name paclitaxel), and since then has become the best-selling anti-cancer drug in history. Despite its long history of clinical use, there is still no clinically used biomarker to determine which patients will experience positive therapeutic effects from paclitaxel treatment. Such a biomarker is urgently need given that only approximately 50% of breast cancer patients treated with paclitaxel respond to therapy. Patients who do not respond to paclitaxel treatment are not only delayed in receiving an effective therapy, but they are also exposed to the potential negative side effects associated with paclitaxel treatment. In addition to nausea and alopecia (hair loss) caused by other chemotherapeutic agents, paclitaxel can also induce potentially life-threatening leukopenia and peripheral neuropathies that can remain permanent even after patients are taken off the drug. The failure to identify a predictive biomarker for paclitaxel response could, in part, be due to an incomplete understanding of paclitaxel's mechanism of cytotoxicity in patients.

For the past three decades, it was widely assumed that paclitaxel caused cell death due to mitotic arrest, as has been observed at high concentrations used in cell culture. We recently showed that intratumoral concentrations after 175 mg/m^2 and 80 mg/m^2 paclitaxel are insufficient to cause mitotic arrest in primary breast cancer patients. Instead, lower clinically relevant concentrations induced multipolar mitotic spindle formation. We found that multipolar spindle maintenance is critical for paclitaxel

to induce the high rates of chromosomal instability necessary for cell death. Increasing multipolar divisions in paclitaxel resulted in improved cytotoxicity. Conversely, decreasing paclitaxel-induced multipolar divisions reduced paclitaxel efficacy. We discovered that multipolar spindle persistence, and not prolonged mitotic duration, correlated with paclitaxel-induced cell death. Moreover, we identified multipolar spindle clustering as a mechanism of paclitaxel resistance. In vitro, we showed that pharmacological and genetic inducers of CIN sensitized cells to paclitaxel. Finally, we found that pre-treatment CIN correlated with taxane response in a cohort of metastatic breast cancer patients. These data support the use of baseline rates of chromosomal instability as a predictive biomarker for paclitaxel response. Identification of agents that increase CIN or exacerbate multipolarity, may be used to improve the clinical utility of paclitaxel.

Due to the fact that multipolar spindle focusing may be a major mechanism of paclitaxel resistance, it is now imperative to identify the mechanisms cells use to cluster paclitaxel-induced multipolar spindles. Previous studies in centrosome amplified cells have identified roles for numerous proteins in centrosome clustering including HSET, dynein, actin, E-cadherin, CEP215, Myb, mitotic checkpoint genes, the augmin complex, Stat3, Stathmin and others (Chavali et al., 2016; Goshima et al., 2007; Konotop et al., 2016; Kwon *et al.*, 2008; Leber et al., 2010; Morris et al., 2017; Quintyne et al., 2005; Rhys *et al.*, 2018; Yang et al., 2008). Future experiments to determine the relative importance of these proteins in focusing paclitaxel-induced multipolar spindles, which do not require centrosome amplification, may reveal proteins with additional value

in predicting response to paclitaxel and lead to the development of pole clustering inhibitors suitable for in vivo use, which are currently unavailable.

While we demonstrated that pre-existing chromosomal instability correlated with taxane response in a metastatic cohort of breast cancer patients, this study was underpowered to validate a predictive biomarker and chromosomal instability did not explain all of the patient-to-patient variation in response. Identification of other factors that play a modifying role in patient response (such as multipolar spindle clustering) would improve a CIN-based biomarker. In the future, more comprehensive measures of cell-to-cell variations in chromosome content, like single cell sequencing, would improve upon our method to measure CIN in patient tumors. Given that we were unable to control for prior treatments, site of biopsy, type of taxane used, and other sources of biologic variation such as breast cancer subtype or hormone receptor status, future studies of a larger homogenous cohort of patients would permit a more robust test of CIN as a predictive biomarker. Single cell sequencing should be performed on samples from our 80 mg/m^2 paclitaxel primary breast cancer patients who have not received prior treatments. It would be interesting to determine if pre-treatment CIN is predictive of response in this cohort.

Our data suggest that subsequent doses of paclitaxel lead to sustained or increased multipolarity, without substantial changes in the mitotic index. However, these data come from a relatively small cohort of patients and additional patients should be analyzed to verify these findings. Recruitment of other patients who consent to additional biopsies after the first dose of paclitaxel (including biopsies after the third and final dose) would also aid in our understanding of how the effects and concentration of

paclitaxel change over time. Observation of surgical samples obtained after paclitaxel treatment, and before AC, may be valuable in understanding how or why some tumors can survive after 12 doses of paclitaxel. These samples should be analyzed for multipolar spindles, mitotic index, and assessed for levels of CIN.

While we found that paclitaxel levels were efficiently cleared in patient plasma, we observed patient-to-patient variability in the ability to clear intratumoral paclitaxel levels. Future experiments are needed to assess the error in these measurements and the potential sources of variability between and within patient biopsies. Due to the fact that we were unable to detect paclitaxel levels in normal tissue, additional care should be also taken to normalize to tumor cellularity when performing bulk intratumoral paclitaxel measurements. It is possible that tumors with reduced cellularity would yield artificially low intratumoral drug levels. MALDI-TOF mass spectrometry to determine paclitaxel distribution with human tumors would also provide insight as to whether our method of bulk biopsy homogenization is problematic. Further, paclitaxel concentration measurements in PBMCs would provide an additional source of data regarding its accumulation in peripheral normal tissue. Finally, the use of LC-MS/MS in the future would provide a more specific and sensitive method to measure paclitaxel levels in patient samples.

Interestingly, we found that low nanomolar doses of other clinically used microtubule poisons including docetaxel, ixabepilone, vinorelbine, and eribulin also induce multipolar spindles, and not mitotic arrest, in breast cancer cell lines. In a small clinical trial of metastatic breast cancer patients, we found that eribulin, vinorelbine, and nab-paclitaxel treatment also induce multipolar mitotic spindles without evidence of

mitotic arrest in the clinical setting, similar to our findings with paclitaxel in primary breast cancer patients. However, a larger cohort of patients is needed to support these findings. Moreover, additional experiments are needed to determine the clinically relevant concentrations for other clinically used microtubule poisons in human tumors. Intracellular accumulation of these drugs over a range of doses needs to be measured in order to recapitulate the clinically relevant range in cells and mice. These data suggest that multipolar spindles may underlie a common mechanism of cytotoxicity for paclitaxel and other clinically used microtubule poisons. Future work is needed to determine if multipolar spindle clustering and pre-existing CIN are relevant mechanisms of resistance and sensitization, respectively, for other drugs belonging to the microtubule poison family.

We determined that Eg5 and Plk1 (to a lesser extent) promote paclitaxel induced multipolar spindle establishment and maintenance. In the future, spindle pole distance measurements from these experiments should be repeated using a three-dimensional (3D) analysis and automated distance measurements between the centroid of each spindle pole (for instance through the use of Imaris software). We also found that multipolar spindles induced by paclitaxel do not require centriole amplification, or on a molecular level, gamma tubulin, centrin or pericentrin. Preliminary data suggest that Plk1 is also required for multipolar spindles induced vinorelbine. However, other experiments are needed to assess the molecular requirements for multipolarity induced by other microtubule poisons. Our evidence also suggested that a low level of centrosome amplification was induced by paclitaxel in Cal51 cells. Preliminary data demonstrated that centrosome amplification was tied to spindle polarity in cell culture.

Tripolar spindles showed a low frequency of centrosome amplification, but it was comparatively more common to find tetrapolar and cells with 5+ spindle poles with too many gamma tubulin foci. However, the correlation between centrosome amplification and spindle polarity was not readily observed in our patient cohort. Timelapse experiments of cells expressing fluorescent tubulin, pericentrin, and centrin would provide more insight into how paclitaxel induces multipolar spindles, and if there is a link between spindle polarity and cellular centrosome number.

Future experiments are also necessary to determine the minimal molecular requirements for microtubule nucleation and spindle pole formation. Our current data suggests that, at the very least, NuMA is required for multipolarity induced by microtubule poisons, given that spindle poles were stained with NuMA in our patient samples. However, experiments performed to assess the role of NuMA in multipolar spindle formation were unsuccessful due to incomplete knock out of NuMA in an inducible CRISPR knock out cell line. Future experiment with a cell line demonstrating complete knock out would permit a more robust test of this hypothesis. Identification of the molecular requirements for multipolar spindles induced by microtubule poisons may allow for the selection of biomarkers whose expression is necessary for the efficacy of these anti-cancer drugs.

We unexpectedly found that multipolar spindles in paclitaxel exhibited time dependency. Reducing mitotic duration reduced multipolar spindles, whereas prolonging mitosis increased multipolarity. Future work aimed at determining whether multipolar spindles induced by other microtubule poisons display temporal requirements is still needed. The exact mechanisms underlying these temporal requirements remain

to be determined, however it is possible that they are linked to time dependent branching microtubule nucleation. In addition to temporal requirements, current literature suggests that there are spatial requirements for spindle pole clustering. Therefore, I propose that there may be a spatiotemporal requirement for microtubule poison-induced multipolar spindle formation and maintenance. It is possible that microtubule poison-induced multipolar spindles start off in close proximity to one another and then move apart over time. In the context of accelerated transit through mitosis, I hypothesize that spindle poles do not have sufficient time to separate from one another, making it more likely that they will cluster together. Future live cell imaging experiments with high temporal and spatial resolution, coupled with automated spindle pole tracking and distance measurements will permit a more robust test of this hypothesis. In conclusion, identification of the cellular and spatiotemporal requirements for multipolarity, and of agents that increase multipolar spindle maintenance and CIN, may improve the clinical utility of paclitaxel and other microtubule poisons.

REFERENCES

1. Alfaro-Aco, R., Thawani, A., and Petry, S. (2020). Biochemical reconstitution of branching microtubule nucleation. Elife *9*. 10.7554/eLife.49797.
2. Bai, R., Nguyen, T.L., Burnett, J.C., Atasoylu, O., Munro, M.H., Pettit, G.R., Smith, A.B., Gussio, R., and Hamel, E. (2011). Interactions of halichondrin B and eribulin with tubulin. J Chem Inf Model *51*, 1393-1404. 10.1021/ci200077t.
3. Baker, D.J., Jeganathan, K.B., Cameron, J.D., Thompson, M., Juneja, S., Kopecka, A., Kumar, R., Jenkins, R.B., de Groen, P.C., Roche, P., and van Deursen, J.M. (2004). BubR1 insufficiency causes early onset of aging-associated phenotypes and infertility in mice. Nat Genet *36*, 744-749.
4. Bakhoum, S.F., Kabeche, L., Murnane, J.P., Zaki, B.I., and Compton, D.A. (2014a). DNA-damage response during mitosis induces whole-chromosome missegregation. Cancer discovery *4*, 1281-1289. 10.1158/2159-8290.CD-14-0403.
5. Bakhoum, S.F., Silkworth, W.T., Nardi, I.K., Nicholson, J.M., Compton, D.A., and Cimini, D. (2014b). The mitotic origin of chromosomal instability. Curr Biol *24*, R148-149. 10.1016/j.cub.2014.01.019.
6. Bakker, B., Taudt, A., Belderbos, M.E., Porubsky, D., Spierings, D.C., de Jong, T.V., Halsema, N., Kazemier, H.G., Hoekstra-Wakker, K., Bradley, A., et al. (2016). Single-cell sequencing reveals karyotype heterogeneity in murine and human malignancies. Genome Biol *17*, 115. 10.1186/s13059-016-0971-7.

7. Barr, F.A., Silljé, H.H., and Nigg, E.A. (2004). Polo-like kinases and the orchestration of cell division. Nat Rev Mol Cell Biol *5*, 429-440. 10.1038/nrm1401.
8. Beck, W.T. (1984). Cellular pharmacology of Vinca alkaloid resistance and its circumvention. Adv Enzyme Regul *22*, 207-227. 10.1016/0065-2571(84)90015-3.
9. Bensch, K.G., and Malawista, S.E. (1968). Microtubule crystals: a new biophysical phenomenon induced by Vinca alkaloids. Nature *218*, 1176-1177. 10.1038/2181176a0.
10. Bensch, K.G., Marantz, R., Wisniewski, H., and Shelanski, M. (1969). Induction in vitro of microtubular crystals by vinca alkaloids. Science *165*, 495-496. 10.1126/science.165.3892.495.
11. Bian, M., Fu, J., Yan, Y., Chen, Q., Yang, C., Shi, Q., Jiang, Q., and Zhang, C. (2010). Short exposure to paclitaxel induces multipolar spindle formation and aneuploidy through promotion of acentrosomal pole assembly. Sci China Life Sci *53*, 1322-1329. 10.1007/s11427-010-4086-1.
12. Bindels, D.S., Haarbosch, L., van Weeren, L., Postma, M., Wiese, K.E., Mastop, M., Aumonier, S., Gotthard, G., Royant, A., Hink, M.A., and Gadella, T.W. (2017). mScarlet: a bright monomeric red fluorescent protein for cellular imaging. Nat Methods *14*, 53-56. 10.1038/nmeth.4074.
13. Birkbak, N.J., Eklund, A.C., Li, Q., McClelland, S.E., Endesfelder, D., Tan, P., Tan, I.B., Richardson, A.L., Szallasi, Z., and Swanton, C. (2011). Paradoxical relationship between chromosomal instability and survival outcome in cancer. Cancer Res *71*, 3447-3452. 10.1158/0008-5472.can-10-3667.

14. Boveri, T. (1902). Ueber mehrpolige Mitosen als Mittel zur Analyse des Zellkerns. Vehr. d. phys. med. Ges. zu Wurzburg, N.F. (available in English translation at: http://8e.devbio.com/article.php?ch=4&id=24) *Bd. 35*.
15. Boveri, T. (1914). The Origin of Malignant Tumors by Theodor Boveri; Translated by Marcella Boveri. Williams and Wilkins, Baltimore, 1929.
16. Budd, G.T., Barlow, W.E., Moore, H.C., Hobday, T.J., Stewart, J.A., Isaacs, C., Salim, M., Cho, J.K., Rinn, K.J., Albain, K.S., et al. (2015). SWOG S0221: a phase III trial comparing chemotherapy schedules in high-risk early-stage breast cancer. J Clin Oncol *33*, 58-64. 10.1200/jco.2014.56.3296.
17. Burkard, M.E., and Weaver, B.A. (2017). Tuning Chromosomal Instability to Optimize Tumor Fitness. Cancer Discov *7*, 134-136. 10.1158/2159-8290.CD-16-1415.
18. Castle, B.T., McCubbin, S., Prahl, L.S., Bernens, J.N., Sept, D., and Odde, D.J. (2017). Mechanisms of kinetic stabilization by the drugs paclitaxel and vinblastine. Mol Biol Cell *28*, 1238-1257. 10.1091/mbc.E16-08-0567.
19. Chavali, P.L., Chandrasekaran, G., Barr, A.R., Tátrai, P., Taylor, C., Papachristou, E.K., Woods, C.G., Chavali, S., and Gergely, F. (2016). A CEP215-HSET complex links centrosomes with spindle poles and drives centrosome clustering in cancer. Nat Commun *7*, 11005. 10.1038/ncomms11005.
20. Chou, T.C. (2010). Drug combination studies and their synergy quantification using the Chou-Talalay method. Cancer Res *70*, 440-446. 10.1158/0008-5472.CAN-09-1947.

21. Chunduri, N.K., and Storchová, Z. (2019). The diverse consequences of aneuploidy. Nature Cell Biology *21*, 54-62. 10.1038/s41556-018-0243-8.
22. Cobham, M.V., and Donovan, D. (2009). Ixabepilone: a new treatment option for the management of taxane-resistant metastatic breast cancer. Cancer Manag Res *1*, 69-77.
23. Compton, D.A., Yen, T.J., and Cleveland, D.W. (1991). Identification of novel centromere/kinetochore-associated proteins using monoclonal antibodies generated against human mitotic chromosome scaffolds. J Cell Biol *112*, 1083-1097. 10.1083/jcb.112.6.1083.
24. Cortes, J., Schöffski, P., and Littlefield, B.A. (2018). Multiple modes of action of eribulin mesylate: Emerging data and clinical implications. Cancer Treat Rev *70*, 190-198. 10.1016/j.ctrv.2018.08.008.
25. Costelloe, C.M., Chuang, H.H., Madewell, J.E., and Ueno, N.T. (2010). Cancer Response Criteria and Bone Metastases: RECIST 1.1, MDA and PERCIST. Journal of Cancer *1*, 80-92. 10.7150/jca.1.80.
26. Crown, J., O'Leary, M., and Ooi, W.S. (2004). Docetaxel and paclitaxel in the treatment of breast cancer: a review of clinical experience. Oncologist *9 Suppl 2*, 24-32. 10.1634/theoncologist.9-suppl_2-24.
27. David, A.F., Roudot, P., Legant, W.R., Betzig, E., Danuser, G., and Gerlich, D.W. (2019). Augmin accumulation on long-lived microtubules drives amplification and kinetochore-directed growth. J Cell Biol *218*, 2150-2168. 10.1083/jcb.201805044.
28. Deeken, J.F., Marshall, J.L., Pishvaian, M.J., Hwang, J., Ahlers, C.M., Clemens, P.L., Parker, S.M., Iacono, L., and LoRusso, P.M. (2014). A phase I study of oral

ixabepilone in patients with advanced solid tumors. Cancer Chemother Pharmacol *73*, 1071-1078. 10.1007/s00280-014-2443-7.

29. Denu, R.A., Zasadil, L.M., Kanugh, C., Laffin, J., Weaver, B.A., and Burkard, M.E. (2016). Centrosome amplification induces high grade features and is prognostic of worse outcomes in breast cancer. BMC Cancer *16*, 47. 10.1186/s12885-016-2083-x.
30. Dhamodharan, R., Jordan, M.A., Thrower, D., Wilson, L., and Wadsworth, P. (1995). Vinblastine suppresses dynamics of individual microtubules in living interphase cells. Mol Biol Cell *6*, 1215-1229. 10.1091/mbc.6.9.1215.
31. Diaz-Rodríguez, E., Sotillo, R., Schvartzman, J.M., and Benezra, R. (2008). Hec1 overexpression hyperactivates the mitotic checkpoint and induces tumor formation in vivo. Proc Natl Acad Sci U S A *105*, 16719-16724. 0803504105 [pii] 10.1073/pnas.0803504105.
32. Dumont, S., and Mitchison, T.J. (2009). Force and length in the mitotic spindle. Current biology : CB 1*9,* R749-R761. 10.1016/j.cub.2009.07.028.
33. Dybdal-Hargreaves, N.F., Risinger, A.L., and Mooberry, S.L. (2015). Eribulin mesylate: mechanism of action of a unique microtubule-targeting agent. Clin Cancer Res 2*1,* 2445-2452. 10.1158/1078-0432.ccr-14-3252.
34. Eisenhauer, E.A., Therasse, P., Bogaerts, J., Schwartz, L.H., Sargent, D., Ford, R., Dancey, J., Arbuck, S., Gwyther, S., Mooney, M., et al. (2009). New response evaluation criteria in solid tumours: revised RECIST guideline (version 1.1). Eur J Cancer 4*5,* 228-247. 10.1016/j.ejca.2008.10.026.

35. Fine, R.L., Chen, J., Balmaceda, C., Bruce, J.N., Huang, M., Desai, M., Sisti, M.B., McKhann, G.M., Goodman, R.R., Bertino, J.S., et al. (2006). Randomized Study of Paclitaxel and Tamoxifen Deposition into Human Brain Tumors: Implications for the Treatment of Metastatic Brain Tumors. Clinical Cancer Research 1*2,* 5770. 10.1158/1078-0432.CCR-05-2356.
36. Fisk, H.A., Mattison, C.P., and Winey, M. (2003). Human Mps1 protein kinase is required for centrosome duplication and normal mitotic progression. Proc Natl Acad Sci U S A 1*00,* 14875-14880. 10.1073/pnas.2434156100.
37. Fisk, H.A., Mattison, C.P., and Winey, M. (2004). A field guide to the Mps1 family of protein kinases. Cell Cycle 3*,* 439-442.
38. Fountzilas, G., Dafni, U., Dimopoulos, M.A., Koutras, A., Skarlos, D., Papakostas, P., Gogas, H., Bafaloukos, D., Kalogera-Fountzila, A., Samantas, E., et al. (2009). A randomized phase III study comparing three anthracycline-free taxane-based regimens, as first line chemotherapy, in metastatic breast cancer: a Hellenic Cooperative Oncology Group study. Breast Cancer Res Treat 1*15,* 87-99. 10.1007/s10549-008-0047-9.
39. Funk, L.C., Wan, J., Ryan, S.D., Kaur, C., Sullivan, R., Roopra, A., and Weaver, B.A. (2020). p53 is not required for cell death and tumor suppression caused by high chromosomal instability. Mol Cancer Res. 10.1158/1541-7786.MCR-20-0488.
40. Funk, L.C., Zasadil, L.M., and Weaver, B.A. (2016). Living in CIN: Mitotic Infidelity and Its Consequences for Tumor Promotion and Suppression. Dev Cell 3*9,* 638-652. 10.1016/j.devcel.2016.10.023.

41. Ganem, N.J., Godinho, S.A., and Pellman, D. (2009). A mechanism linking extra centrosomes to chromosomal instability. Nature 4*60,* 278-282. 10.1038/nature08136.
42. Gidding, C.E., Kellie, S.J., Kamps, W.A., and de Graaf, S.S. (1999). Vincristine revisited. Crit Rev Oncol Hematol 2*9,* 267-287. 10.1016/s1040-8428(98)00023-7.
43. Godek, K.M., Venere, M., Wu, Q., Mills, K.D., Hickey, W.F., Rich, J.N., and Compton, D.A. (2016). Chromosomal Instability Affects the Tumorigenicity of Glioblastoma Tumor-Initiating Cells. Cancer Discov 6*,* 532-545. 10.1158/2159-8290.CD-15-1154.
44. Godinho, S.A., Picone, R., Burute, M., Dagher, R., Su, Y., Leung, C.T., Polyak, K., Brugge, J.S., Théry, M., and Pellman, D. (2014). Oncogene-like induction of cellular invasion from centrosome amplification. Nature 5*10,* 167-171. 10.1038/nature13277.
45. Goel, S., Mita, A.C., Mita, M., Rowinsky, E.K., Chu, Q.S., Wong, N., Desjardins, C., Fang, F., Jansen, M., Shuster, D.E., et al. (2009). A phase I study of eribulin mesylate (E7389), a mechanistically novel inhibitor of microtubule dynamics, in patients with advanced solid malignancies. Clin Cancer Res 1*5,* 4207-4212. 10.1158/1078-0432.CCR-08-2429.
46. Goshima, G., Wollman, R., Goodwin, S.S., Zhang, N., Scholey, J.M., Vale, R.D., and Stuurman, N. (2007). Genes required for mitotic spindle assembly in Drosophila S2 cells. Science 3*16,* 417-421. 10.1126/science.1141314.

47. Gregan, J., Polakova, S., Zhang, L., Tolić-Nørrelykke, I.M., and Cimini, D. (2011). Merotelic kinetochore attachment: causes and effects. Trends in cell biology 2*1,* 374-381. 10.1016/j.tcb.2011.01.003.
48. Habedanck, R., Stierhof, Y.D., Wilkinson, C.J., and Nigg, E.A. (2005). The Polo kinase Plk4 functions in centriole duplication. Nat Cell Biol 7*,* 1140-1146. 10.1038/ncb1320.
49. Hari, M., Yang, H., Zeng, C., Canizales, M., and Cabral, F. (2003). Expression of class III beta-tubulin reduces microtubule assembly and confers resistance to paclitaxel. Cell Motil Cytoskeleton 5*6,* 45-56. 10.1002/cm.10132.
50. Hertz, D.L., Kidwell, K.M., Vangipuram, K., Li, F., Pai, M.P., Burness, M., Griggs, J.J., Schott, A.F., Van Poznak, C., Hayes, D.F., et al. (2018). Paclitaxel Plasma Concentration after the First Infusion Predicts Treatment-Limiting Peripheral Neuropathy. Clin Cancer Res 2*4,* 3602-3610. 10.1158/1078-0432.CCR-18-0656.
51. Hewitt, L., Tighe, A., Santaguida, S., White, A.M., Jones, C.D., Musacchio, A., Green, S., and Taylor, S.S. (2010). Sustained Mps1 activity is required in mitosis to recruit O-Mad2 to the Mad1-C-Mad2 core complex. J Cell Biol 1*90,* 25-34. 10.1083/jcb.201002133.
52. Holland, A.J., Fachinetti, D., Zhu, Q., Bauer, M., Verma, I.M., Nigg, E.A., and Cleveland, D.W. (2012). The autoregulated instability of Polo-like kinase 4 limits centrosome duplication to once per cell cycle. Genes Dev 2*6,* 2684-2689. 10.1101/gad.207027.112.

53. Huang, T.C., and Campbell, T.C. (2012). Comparison of weekly versus every 3 weeks paclitaxel in the treatment of advanced solid tumors: a meta-analysis. Cancer Treat Rev 3*8,* 613-617. 10.1016/j.ctrv.2011.10.008.

54. Ibrahim, N.K., Valero, V., Theriault, R.L., Willey, J., Walters, R.S., Buzdar, A.U., Booser, D.J., and Hortobagyi, G.N. (2000). Phase I study of vinorelbine by 96-hour infusion in advanced metastatic breast cancer. Am J Clin Oncol 2*3,* 117-121.

55. Inwald, E.C., Klinkhammer-Schalke, M., Hofstädter, F., Zeman, F., Koller, M., Gerstenhauer, M., and Ortmann, O. (2013). Ki-67 is a prognostic parameter in breast cancer patients: results of a large population-based cohort of a cancer registry. Breast Cancer Res Treat 1*39,* 539-552. 10.1007/s10549-013-2560-8.

56. Iwanaga, Y., Chi, Y.H., Miyazato, A., Sheleg, S., Haller, K., Peloponese, J.M., Jr., Li, Y., Ward, J.M., Benezra, R., and Jeang, K.T. (2007). Heterozygous deletion of mitotic arrest-deficient protein 1 (MAD1) increases the incidence of tumors in mice. Cancer Res 6*7,* 160-166.

57. Jamal-Hanjani, M., A'Hern, R., Birkbak, N.J., Gorman, P., Grönroos, E., Ngang, S., Nicola, P., Rahman, L., Thanopoulou, E., Kelly, G., et al. (2015). Extreme chromosomal instability forecasts improved outcome in ER-negative breast cancer: a prospective validation cohort study from the TACT trial. Ann Oncol 2*6,* 1340-1346. 10.1093/annonc/mdv178.

58. Janssen, A., Kops, G.J., and Medema, R.H. (2009). Elevating the frequency of chromosome mis-segregation as a strategy to kill tumor cells. Proc Natl Acad Sci U S A 1*06,* 19108-19113.

59. Jemaà, M., Galluzzi, L., Kepp, O., Senovilla, L., Brands, M., Boemer, U., Koppitz, M., Lienau, P., Prechtl, S., Schulze, V., et al. (2013). Characterization of novel MPS1 inhibitors with preclinical anticancer activity. Cell Death Differ 2*0,* 1532-1545. 10.1038/cdd.2013.105.
60. Ji, Z., Gao, H., Jia, L., Li, B., and Yu, H. (2017). A sequential multi-target Mps1 phosphorylation cascade promotes spindle checkpoint signaling. Elife 6. 10.7554/eLife.22513.
61. Jordan, M.A., Thrower, D., and Wilson, L. (1991). Mechanism of inhibition of cell proliferation by Vinca alkaloids. Cancer Res 5*1,* 2212-2222.
62. Jordan, M.A., Toso, R.J., Thrower, D., and Wilson, L. (1993). Mechanism of mitotic block and inhibition of cell proliferation by taxol at low concentrations. Proc Natl Acad Sci U S A 9*0,* 9552-9556.
63. Jordan, M.A., Wendell, K., Gardiner, S., Derry, W.B., Copp, H., and Wilson, L. (1996). Mitotic block induced in HeLa cells by low concentrations of paclitaxel (Taxol) results in abnormal mitotic exit and apoptotic cell death. Cancer Res 5*6,* 816-825.
64. Jordan, M.A., and Wilson, L. (2004). Microtubules as a target for anticancer drugs. Nat Rev Cancer 4*,* 253-265. 10.1038/nrc1317.
65. Kapitein, L.C., Peterman, E.J., Kwok, B.H., Kim, J.H., Kapoor, T.M., and Schmidt, C.F. (2005). The bipolar mitotic kinesin Eg5 moves on both microtubules that it crosslinks. Nature 4*35,* 114-118. 10.1038/nature03503.
66. Kim, Y., Heuser, J.E., Waterman, C.M., and Cleveland, D.W. (2008). CENP-E combines a slow, processive motor and a flexible coiled coil to produce an

essential motile kinetochore tether. J Cell Biol 1*81,* 411-419. 10.1083/jcb.200802189.

67. Kleylein-Sohn, J., Pöllinger, B., Ohmer, M., Hofmann, F., Nigg, E.A., Hemmings, B.A., and Wartmann, M. (2012). Acentrosomal spindle organization renders cancer cells dependent on the kinesin HSET. J Cell Sci 1*25,* 5391-5402. 10.1242/jcs.107474.
68. Komlodi-Pasztor, E., Sackett, D.L., and Fojo, A.T. (2012). Inhibitors Targeting Mitosis: Tales of How Great Drugs against a Promising Target Were Brought Down by a Flawed Rationale. Clinical Cancer Research 1*8,* 51-63. 10.1158/1078-0432.ccr-11-0999.
69. Komlodi-Pasztor, E., Sackett, D.L., and Fojo, T. (2013). Tales of how great drugs were brought down by a flawed rationale--response. Clin Cancer Res 1*9,* 1304. 10.1158/1078-0432.CCR-12-2058.
70. Konotop, G., Bausch, E., Nagai, T., Turchinovich, A., Becker, N., Benner, A., Boutros, M., Mizuno, K., Krämer, A., and Raab, M.S. (2016). Pharmacological Inhibition of Centrosome Clustering by Slingshot-Mediated Cofilin Activation and Actin Cortex Destabilization. Cancer Res 7*6,* 6690-6700. 10.1158/0008-5472.CAN-16-1144.
71. Kops, G.J., Foltz, D.R., and Cleveland, D.W. (2004). Lethality to human cancer cells through massive chromosome loss by inhibition of the mitotic checkpoint. Proc Natl Acad Sci U S A 1*01,* 8699-8704. 10.1073/pnas.0401142101.

72. Kops, G.J., Weaver, B.A., and Cleveland, D.W. (2005). On the road to cancer: aneuploidy and the mitotic checkpoint. Nat Rev Cancer 5*,* 773-785. 10.1038/nrc1714.

73. Koshiba, H., Hosokawa, K., Mori, T., Kubo, A., Watanabe, A., and Honjo, H. (2009). Intravenous paclitaxel is specifically retained in human gynecologic carcinoma tissues in vivo. Int J Gynecol Cancer 1*9,* 484-488. 10.1111/IGC.0b013e3181a130db.

74. Kwon, M., Godinho, S.A., Chandhok, N.S., Ganem, N.J., Azioune, A., Thery, M., and Pellman, D. (2008). Mechanisms to suppress multipolar divisions in cancer cells with extra centrosomes. Genes Dev 2*2,* 2189-2203. 10.1101/gad.1700908.

75. Laucius, C.D., Orr, B., and Compton, D.A. (2019). Chromosomal instability suppresses the growth of K-Ras-induced lung adenomas. Cell Cycle 1*8,* 1702-1713. 10.1080/15384101.2019.1629790.

76. Leber, B., Maier, B., Fuchs, F., Chi, J., Riffel, P., Anderhub, S., Wagner, L., Ho, A.D., Salisbury, J.L., Boutros, M., and Krämer, A. (2010). Proteins required for centrosome clustering in cancer cells. Sci Transl Med 2*,* 33ra38. 10.1126/scitranslmed.3000915.

77. Lee, F.Y., Borzilleri, R., Fairchild, C.R., Kim, S.H., Long, B.H., Reventos-Suarez, C., Vite, G.D., Rose, W.C., and Kramer, R.A. (2001). BMS-247550: a novel epothilone analog with a mode of action similar to paclitaxel but possessing superior antitumor efficacy. Clin Cancer Res 7*,* 1429-1437.

78. Lee, J.J., and Swain, S.M. (2008). The epothilones: translating from the laboratory to the clinic. Clin Cancer Res 1*4,* 1618-1624. 10.1158/1078-0432.CCR-07-2201.

79. Legha, S.S., Tenney, D.M., and Krakoff, I.R. (1986). Phase I study of taxol using a 5-day intermittent schedule. J Clin Oncol 4*,* 762-766. 10.1200/JCO.1986.4.5.762.

80. Lengauer, C., Kinzler, K.W., and Vogelstein, B. (1997). Genetic instability in colorectal cancers. Nature 3*86,* 623-627. 10.1038/386623a0.

81. Leonard, G.D., Fojo, T., and Bates, S.E. (2003). The role of ABC transporters in clinical practice. Oncologist 8*,* 411-424. 10.1634/theoncologist.8-5-411.

82. Lera, R.F., and Burkard, M.E. (2012). High mitotic activity of Polo-like kinase 1 is required for chromosome segregation and genomic integrity in human epithelial cells. J Biol Chem 2*87,* 42812-42825. 10.1074/jbc.M112.412544.

83. Logarinho, E., Maffini, S., Barisic, M., Marques, A., Toso, A., Meraldi, P., and Maiato, H. (2012). CLASPs prevent irreversible multipolarity by ensuring spindle-pole resistance to traction forces during chromosome alignment. Nat Cell Biol 1*4,* 295-303. 10.1038/ncb2423.

84. Lynch, A.R., Arp, N.L., Zhou, A.S., Weaver, B.A., and Burkard, M.E. (2021). Quantifying chromosomal instability from intratumoral karyotype diversity using agent-based modeling and Bayesian inference. bioRxiv, 2021.2004.2026.441466. 10.1101/2021.04.26.441466.

85. Maiato, H., and Logarinho, E. (2014). Mitotic spindle multipolarity without centrosome amplification. Nat Cell Biol 1*6,* 386-394.

86. Maliga, Z., Kapoor, T.M., and Mitchison, T.J. (2002). Evidence that monastrol is an allosteric inhibitor of the mitotic kinesin Eg5. Chem Biol 9*,* 989-996.

87. Malureanu, L., Jeganathan, K.B., Jin, F., Baker, D.J., van Ree, J.H., Gullon, O., Chen, Z., Henley, J.R., and van Deursen, J.M. (2010). Cdc20 hypomorphic mice fail to counteract de novo synthesis of cyclin B1 in mitosis. J Cell Biol 1*91,* 313-329. jcb.201003090 [pii] 10.1083/jcb.201003090.

88. Markman, M. (2003). Managing taxane toxicities. Support Care Cancer 11*,* 144-147. 10.1007/s00520-002-0405-9.

89. McEwen, B.F., Chan, G.K., Zubrowski, B., Savoian, M.S., Sauer, M.T., and Yen, T.J. (2001). CENP-E is essential for reliable bioriented spindle attachment, but chromosome alignment can be achieved via redundant mechanisms in mammalian cells. Mol Biol Cell 12*,* 2776-2789. 10.1091/mbc.12.9.2776.

90. McIntosh, J.R. (2016). Mitosis. Cold Spring Harbor perspectives in biology 8, a023218. 10.1101/cshperspect.a023218.

91. Mechetner, E., Kyshtoobayeva, A., Zonis, S., Kim, H., Stroup, R., Garcia, R., Parker, R.J., and Fruehauf, J.P. (1998). Levels of multidrug resistance (MDR1) P-glycoprotein expression by human breast cancer correlate with in vitro resistance to taxol and doxorubicin. Clin Cancer Res 4, 389-398.

92. Mehta, R.R., Graves, J.M., Hart, G.D., Shilkaitis, A., and Gupta, T.K. (1993). Growth and metastasis of human breast carcinomas with Matrigel in athymic mice. Breast Cancer Research and Treatment 25*,* 65-71. 10.1007/BF00662402.

93. Michel, L.S., Liberal, V., Chatterjee, A., Kirchwegger, R., Pasche, B., Gerald, W., Dobles, M., Sorger, P.K., Murty, V.V., and Benezra, R. (2001). MAD2 haplo-

insufficiency causes premature anaphase and chromosome instability in mammalian cells. Nature 40*9,* 355-359.

94. Milas, L., Hunter, N.R., Kurdoglu, B., Mason, K.A., Meyn, R.E., Stephens, L.C., and Peters, L.J. (1995). Kinetics of mitotic arrest and apoptosis in murine mammary and ovarian tumors treated with taxol. Cancer Chemother Pharmacol 35*,* 297-303. 10.1007/BF00689448.
95. Milross, C.G., Mason, K.A., Hunter, N.R., Chung, W.K., Peters, L.J., and Milas, L. (1996). Relationship of mitotic arrest and apoptosis to antitumor effect of paclitaxel. J Natl Cancer Inst 88*,* 1308-1314. 10.1093/jnci/88.18.1308.
96. Mitchison, T., and Kirschner, M. (1984). Dynamic instability of microtubule growth. Nature 31*2,* 237-242. 10.1038/312237a0.
97. Mori, T., Kinoshita, Y., Watanabe, A., Yamaguchi, T., Hosokawa, K., and Honjo, H. (2006). Retention of paclitaxel in cancer cells for 1 week in vivo and in vitro. Cancer Chemother Pharmacol 58*,* 665-672. 10.1007/s00280-006-0209-6.
98. Morris, E.J., Kawamura, E., Gillespie, J.A., Balgi, A., Kannan, N., Muller, W.J., Roberge, M., and Dedhar, S. (2017). Stat3 regulates centrosome clustering in cancer cells via Stathmin/PLK1. Nature Communications 8, 15289. 10.1038/ncomms15289.
99. Moudi, M., Go, R., Yien, C.Y., and Nazre, M. (2013). Vinca alkaloids. Int J Prev Med 4, 1231-1235.
100. Na, G.C., and Timasheff, S.N. (1982). In vitro vinblastine-induced tubulin paracrystals. J Biol Chem 25*7,* 10387-10391.

101. Nettles, J.H., Li, H., Cornett, B., Krahn, J.M., Snyder, J.P., and Downing, K.H. (2004). The binding mode of epothilone A on alpha,beta-tubulin by electron crystallography. Science 30*5,* 866-869. 10.1126/science.1099190.

102. Ngan, V.K., Bellman, K., Hill, B.T., Wilson, L., and Jordan, M.A. (2001). Mechanism of mitotic block and inhibition of cell proliferation by the semisynthetic Vinca alkaloids vinorelbine and its newer derivative vinflunine. Mol Pharmacol 60*,* 225-232. 10.1124/mol.60.1.225.

103. Nogales, E., Wolf, S.G., Khan, I.A., Ludueña, R.F., and Downing, K.H. (1995). Structure of tubulin at 6.5 A and location of the taxol-binding site. Nature 37*5,* 424-427. 10.1038/375424a0.

104. Orecchioni, S., Talarico, G., Labanca, V., Calleri, A., Mancuso, P., and Bertolini, F. (2018). Vinorelbine, cyclophosphamide and 5-FU effects on the circulating and intratumoural landscape of immune cells improve anti-PD-L1 efficacy in preclinical models of breast cancer and lymphoma. British Journal of Cancer 11*8,* 1329-1336. 10.1038/s41416-018-0076-z.

105. Perez, E.A. (2009). Microtubule inhibitors: Differentiating tubulin-inhibiting agents based on mechanisms of action, clinical activity, and resistance. Molecular Cancer Therapeutics 8, 2086. 10.1158/1535-7163.MCT-09-0366.

106. Petry, S., Groen, A.C., Ishihara, K., Mitchison, T.J., and Vale, R.D. (2013). Branching microtubule nucleation in Xenopus egg extracts mediated by augmin and TPX2. Cell 15*2,* 768-777. 10.1016/j.cell.2012.12.044.

107. Prosser, S.L., and Pelletier, L. (2017). Mitotic spindle assembly in animal cells: a fine balancing act. Nature Reviews Molecular Cell Biology 18*,* 187-201. 10.1038/nrm.2016.162.

108. Qin, R.S., Zhang, Z.H., Zhu, N.P., Chen, F., Guo, Q., Hu, H.W., Fu, S.Z., Liu, S.S., Chen, Y., Fan, J., and Han, Y.W. (2018). Enhanced antitumor and anti-angiogenic effects of metronomic Vinorelbine combined with Endostar on Lewis lung carcinoma. BMC Cancer 18*,* 967. 10.1186/s12885-018-4738-2.

109. Quasthoff, S., and Hartung, H.P. (2002). Chemotherapy-induced peripheral neuropathy. J Neurol 24*9,* 9-17. 10.1007/pl00007853.

110. Quintyne, N.J., Reing, J.E., Hoffelder, D.R., Gollin, S.M., and Saunders, W.S. (2005). Spindle multipolarity is prevented by centrosomal clustering. Science 307*,* 127-129. 10.1126/science.1104905.

111. Ranganathan, S., McCauley, R.A., Dexter, D.W., and Hudes, G.R. (2001). Modulation of endogenous beta-tubulin isotype expression as a result of human beta(III)cDNA transfection into prostate carcinoma cells. Br J Cancer 85*,* 735-740. 10.1054/bjoc.2001.1956.

112. Rhys, A.D., Monteiro, P., Smith, C., Vaghela, M., Arnandis, T., Kato, T., Leitinger, B., Sahai, E., McAinsh, A., Charras, G., and Godinho, S.A. (2018). Loss of E-cadherin provides tolerance to centrosome amplification in epithelial cancer cells. J Cell Biol 217*,* 195-209. 10.1083/jcb.201704102.

113. Rodrigues-Ferreira, S., Nehlig, A., Moindjie, H., Monchecourt, C., Seiler, C., Marangoni, E., Chateau-Joubert, S., Dujaric, M.-E., Servant, N., Asselain, B., et al. (2019). Improving breast cancer sensitivity to paclitaxel by increasing

aneuploidy. Proceedings of the National Academy of Sciences 116, 23691-23697. 10.1073/pnas.1910824116.

114. Roque, D.M., Bellone, S., Buza, N., Romani, C., Cocco, E., Bignotti, E., Ravaggi, A., Rutherford, T.J., Schwartz, P.E., Pecorelli, S., and Santin, A.D. (2013). Class III β-tubulin overexpression in ovarian clear cell and serous carcinoma as a maker for poor overall survival after platinum/taxane chemotherapy and sensitivity to patupilone. Am J Obstet Gynecol 209, 62.e61-69. 10.1016/j.ajog.2013.04.017.

115. Rosell, R., Scagliotti, G., Danenberg, K.D., Lord, R.V., Bepler, G., Novello, S., Cooc, J., Crinò, L., Sánchez, J.J., Taron, M., et al. (2003). Transcripts in pretreatment biopsies from a three-arm randomized trial in metastatic non-small-cell lung cancer. Oncogene 22, 3548-3553. 10.1038/sj.onc.1206419.

116. Rowald, K., Mantovan, M., Passos, J., Buccitelli, C., Mardin, B.R., Korbel, J.O., Jechlinger, M., and Sotillo, R. (2016). Negative Selection and Chromosome Instability Induced by Mad2 Overexpression Delay Breast Cancer but Facilitate Oncogene-Independent Outgrowth. Cell Rep 15, 2679-2691. 10.1016/j.celrep.2016.05.048.

117. Roylance, R., Endesfelder, D., Gorman, P., Burrell, R.A., Sander, J., Tomlinson, I., Hanby, A.M., Speirs, V., Richardson, A.L., Birkbak, N.J., et al. (2011). Relationship of extreme chromosomal instability with long-term survival in a retrospective analysis of primary breast cancer. Cancer Epidemiol Biomarkers Prev 20, 2183-2194. 10.1158/1055-9965.epi-11-0343.

118. Rugo, H.S., Barry, W.T., Moreno-Aspitia, A., Lyss, A.P., Cirrincione, C., Leung, E., Mayer, E.L., Naughton, M., Toppmeyer, D., Carey, L.A., et al. (2015). Randomized Phase III Trial of Paclitaxel Once Per Week Compared With Nanoparticle Albumin-Bound Nab-Paclitaxel Once Per Week or Ixabepilone With Bevacizumab As First-Line Chemotherapy for Locally Recurrent or Metastatic Breast Cancer: CALGB 40502/NCCTG N063H (Alliance). Journal of Clinical Oncology 33*,* 2361-2369. 10.1200/jco.2014.59.5298.

119. Rutledge, S.D., Douglas, T.A., Nicholson, J.M., Vila-Casadesús, M., Kantzler, C.L., Wangsa, D., Barroso-Vilares, M., Kale, S.D., Logarinho, E., and Cimini, D. (2016). Selective advantage of trisomic human cells cultured in non-standard conditions. Sci Rep 6, 22828. 10.1038/srep22828.

120. Ryan, S.D., Britigan, E.M., Zasadil, L.M., Witte, K., Audhya, A., Roopra, A., and Weaver, B.A. (2012). Up-regulation of the mitotic checkpoint component Mad1 causes chromosomal instability and resistance to microtubule poisons. Proc Natl Acad Sci U S A 10*9,* E2205-2214. 10.1073/pnas.1201911109.

121. Samuels, B.L., Hollis, D.R., Rosner, G.L., Trump, D.L., Shapiro, C.L., Vogelzang, N.J., and Schilsky, R.L. (1997). Modulation of vinblastine resistance in metastatic renal cell carcinoma with cyclosporine A or tamoxifen: a cancer and leukemia group B study. Clin Cancer Res 3, 1977-1984.

122. Santaguida, S., Tighe, A., D'Alise, A.M., Taylor, S.S., and Musacchio, A. (2010). Dissecting the role of MPS1 in chromosome biorientation and the spindle checkpoint through the small molecule inhibitor reversine. J Cell Biol 19*0,* 73-87. 10.1083/jcb.201001036.

123. Santamaria, A., Wang, B., Elowe, S., Malik, R., Zhang, F., Bauer, M., Schmidt, A., Silljé, H.H., Körner, R., and Nigg, E.A. (2011). The Plk1-dependent phosphoproteome of the early mitotic spindle. Mol Cell Proteomics 10*,* M110.004457. 10.1074/mcp.M110.004457.

124. Sapkota, H., Wren, J.D., and Gorbsky, G.J. (2020). CSAG1 maintains the integrity of the mitotic centrosome in cells with defective p53. J Cell Sci 13*3.* 10.1242/jcs.239723.

125. Schaar, B.T., Chan, G.K., Maddox, P., Salmon, E.D., and Yen, T.J. (1997). CENP-E function at kinetochores is essential for chromosome alignment. J Cell Biol 13*9,* 1373-1382.

126. Schiff, P.B., Fant, J., and Horwitz, S.B. (1979). Promotion of microtubule assembly in vitro by taxol. Nature 27*7,* 665-667. 10.1038/277665a0.

127. Schiff, P.B., and Horwitz, S.B. (1980). Taxol stabilizes microtubules in mouse fibroblast cells. Proc Natl Acad Sci U S A 77*,* 1561-1565.

128. Selmecki, A.M., Dulmage, K., Cowen, L.E., Anderson, J.B., and Berman, J. (2009). Acquisition of aneuploidy provides increased fitness during the evolution of antifungal drug resistance. PLoS Genet 5, e1000705. 10.1371/journal.pgen.1000705.

129. Shetty, N., and Gupta, S. (2014). Eribulin drug review. South Asian J Cancer 3, 57-59. 10.4103/2278-330X.126527.

130. Silk, A.D., Zasadil, L.M., Holland, A.J., Vitre, B., Cleveland, D.W., and Weaver, B.A. (2013). Chromosome missegregation rate predicts whether

aneuploidy will promote or suppress tumors. Proc Natl Acad Sci U S A 11*0,* E4134-4141. 10.1073/pnas.1317042110.

131. Singh, A., Denu, R.A., Wolfe, S.K., Sperger, J.M., Schehr, J., Witkowsky, T., Esbona, K., Chappell, R.J., Weaver, B.A., Burkard, M.E., and Lang, J.M. (2020). Centrosome amplification is a frequent event in circulating tumor cells from subjects with metastatic breast cancer. Mol Oncol. 10.1002/1878-0261.12687.

132. Smith, E., Hégarat, N., Vesely, C., Roseboom, I., Larch, C., Streicher, H., Straatman, K., Flynn, H., Skehel, M., Hirota, T., et al. (2011). Differential control of Eg5-dependent centrosome separation by Plk1 and Cdk1. The EMBO journal 30*,* 2233-2245. 10.1038/emboj.2011.120.

133. Steegmaier, M., Hoffmann, M., Baum, A., Lénárt, P., Petronczki, M., Krssák, M., Gürtler, U., Garin-Chesa, P., Lieb, S., Quant, J., et al. (2007). BI 2536, a potent and selective inhibitor of polo-like kinase 1, inhibits tumor growth in vivo. Curr Biol 17*,* 316-322. 10.1016/j.cub.2006.12.037.

134. Storchova, Z., and Pellman, D. (2004). From polyploidy to aneuploidy, genome instability and cancer. Nat Rev Mol Cell Biol 5, 45-54. 10.1038/nrm1276.

135. Stucke, V.M., Silljé, H.H., Arnaud, L., and Nigg, E.A. (2002). Human Mps1 kinase is required for the spindle assembly checkpoint but not for centrosome duplication. EMBO J 21*,* 1723-1732. 10.1093/emboj/21.7.1723.

136. Sweeney, M.J., Boder, G.B., Cullinan, G.J., Culp, H.W., Daniels, W.D., Dyke, R.W., Gerzon, K., McMahon, R.E., Nelson, R.L., Poore, G.A., and Todd,

G.C. (1978). Antitumor activity of deacetyl vinblastine amide sulfate (vindesine) in rodents and mitotic accumulation studies in culture. Cancer Res 38*,* 2886-2891.

137. Symmans, W.F., Volm, M.D., Shapiro, R.L., Perkins, A.B., Kim, A.Y., Demaria, S., Yee, H.T., McMullen, H., Oratz, R., Klein, P., et al. (2000). Paclitaxel-induced apoptosis and mitotic arrest assessed by serial fine-needle aspiration: implications for early prediction of breast cancer response to neoadjuvant treatment. Clin Cancer Res 6, 4610-4617.

138. Thompson, S.L., and Compton, D.A. (2008). Examining the link between chromosomal instability and aneuploidy in human cells. J Cell Biol 18*0,* 665-672. 10.1083/jcb.200712029.

139. Toppmeyer, D., Seidman, A.D., Pollak, M., Russell, C., Tkaczuk, K., Verma, S., Overmoyer, B., Garg, V., Ette, E., Harding, M.W., and Demetri, G.D. (2002). Safety and efficacy of the multidrug resistance inhibitor Incel (biricodar; VX-710) in combination with paclitaxel for advanced breast cancer refractory to paclitaxel. Clin Cancer Res 8, 670-678.

140. Tsuruo, T., Inaba, M., Tashiro, T., Yamori, T., Ohnishi, Y., Ashizawa, T., Sakai, T., Kobayashi, S., and Gomi, K. (1994). Evaluation of antitumor activity of navelbine (vinorelbine ditartrate) against human breast carcinoma xenografts based on its pharmacokinetics in nude mice. Anticancer Drugs 5, 634-640. 10.1097/00001813-199412000-00004.

141. Tucker, R.W., Owellen, R.J., and Harris, S.B. (1977). Correlation of cytotoxicity and mitotic spindle dissolution by vinblastine in mammalian cells. Cancer Res 37*,* 4346-4351.

142. Urruticoechea, A., Smith, I.E., and Dowsett, M. (2005). Proliferation marker Ki-67 in early breast cancer. J Clin Oncol 23*,* 7212-7220. 10.1200/JCO.2005.07.501.

143. Vahdat, L.T., Garcia, A.A., Vogel, C., Pellegrino, C., Lindquist, D.L., Iannotti, N., Gopalakrishna, P., and Sparano, J.A. (2013). Eribulin mesylate versus ixabepilone in patients with metastatic breast cancer: a randomized Phase II study comparing the incidence of peripheral neuropathy. Breast Cancer Res Treat 14*0,* 341-351. 10.1007/s10549-013-2574-2.

144. van Ree, J.H., Nam, H.J., Jeganathan, K.B., Kanakkanthara, A., and van Deursen, J.M. (2016). Pten regulates spindle pole movement through Dlg1-mediated recruitment of Eg5 to centrosomes. Nat Cell Biol 18*,* 814-821. 10.1038/ncb3369.

145. Wan, J., Block, S., Scribano, C.M., Thiry, R., Esbona, K., Audhya, A., and Weaver, B.A. (2019). Mad1 destabilizes p53 by preventing PML from sequestering MDM2. Nat Commun 10*,* 1540. 10.1038/s41467-019-09471-9.

146. Wang, G., Jiang, Q., and Zhang, C. (2014). The role of mitotic kinases in coupling the centrosome cycle with the assembly of the mitotic spindle. J Cell Sci 127*,* 4111-4122. 10.1242/jcs.151753.

147. Waters, J.C., Chen, R.H., Murray, A.W., and Salmon, E.D. (1998). Localization of Mad2 to kinetochores depends on microtubule attachment, not tension. J Cell Biol 14*1,* 1181-1191.

148. Watts, C.A., Richards, F.M., Bender, A., Bond, P.J., Korb, O., Kern, O., Riddick, M., Owen, P., Myers, R.M., Raff, J., et al. (2013). Design, synthesis, and

biological evaluation of an allosteric inhibitor of HSET that targets cancer cells with supernumerary centrosomes. Chem Biol 20*,* 1399-1410. 10.1016/j.chembiol.2013.09.012.

149. Weaver, B.A. (2014). How Taxol/paclitaxel kills cancer cells. Mol Biol Cell 25*,* 2677-2681. 10.1091/mbc.E14-04-0916.

150. Weaver, B.A., Silk, A.D., Montagna, C., Verdier-Pinard, P., and Cleveland, D.W. (2007). Aneuploidy acts both oncogenically and as a tumor suppressor. Cancer Cell 11*,* 25-36. 10.1016/j.ccr.2006.12.003.

151. Wengner, A.M., Siemeister, G., Koppitz, M., Schulze, V., Kosemund, D., Klar, U., Stoeckigt, D., Neuhaus, R., Lienau, P., Bader, B., et al. (2016). Novel Mps1 Kinase Inhibitors with Potent Antitumor Activity. Mol Cancer Ther 15*,* 583-592. 10.1158/1535-7163.MCT-15-0500.

152. Wiernik, P.H., Schwartz, E.L., Strauman, J.J., Dutcher, J.P., Lipton, R.B., and Paietta, E. (1987). Phase I clinical and pharmacokinetic study of taxol. Cancer Res 47*,* 2486-2493.

153. Wilhelm, T., Olziersky, A.M., Harry, D., De Sousa, F., Vassal, H., Eskat, A., and Meraldi, P. (2019). Mild replication stress causes chromosome mis-segregation via premature centriole disengagement. Nat Commun 10*,* 3585. 10.1038/s41467-019-11584-0.

154. Wood, K.W., Lad, L., Luo, L., Qian, X., Knight, S.D., Nevins, N., Brejc, K., Sutton, D., Gilmartin, A.G., Chua, P.R., et al. (2010). Antitumor activity of an allosteric inhibitor of centromere-associated protein-E. Proc Natl Acad Sci U S A 107*,* 5839-5844. 10.1073/pnas.0915068107.

155. Yang, Z., Loncarek, J., Khodjakov, A., and Rieder, C.L. (2008). Extra centrosomes and/or chromosomes prolong mitosis in human cells. Nat Cell Biol 10, 748-751. 10.1038/ncb1738.

156. Yao, X., Abrieu, A., Zheng, Y., Sullivan, K.F., and Cleveland, D.W. (2000). CENP-E forms a link between attachment of spindle microtubules to kinetochores and the mitotic checkpoint. Nat Cell Biol 2, 484-491. 10.1038/35019518.

157. Yvon, A.M., Wadsworth, P., and Jordan, M.A. (1999). Taxol suppresses dynamics of individual microtubules in living human tumor cells. Mol Biol Cell 10, 947-959.

158. Zaheed, M., Wilcken, N., Willson, M.L., O'Connell, D.L., and Goodwin, A. (2019). Sequencing of anthracyclines and taxanes in neoadjuvant and adjuvant therapy for early breast cancer. Cochrane Database Syst Rev 2, Cd012873. 10.1002/14651858.CD012873.pub2.

159. Zasadil, L.M., Andersen, K.A., Yeum, D., Rocque, G.B., Wilke, L.G., Tevaarwerk, A.J., Raines, R.T., Burkard, M.E., and Weaver, B.A. (2014). Cytotoxicity of paclitaxel in breast cancer is due to chromosome missegregation on multipolar spindles. Sci Transl Med 6, 229ra243. 10.1126/scitranslmed.3007965.

160. Zasadil, L.M., Britigan, E.M., and Weaver, B.A. (2013). 2n or not 2n: Aneuploidy, polyploidy and chromosomal instability in primary and tumor cells. Semin Cell Dev Biol 24, 370-379. 10.1016/j.semcdb.2013.02.001.